LA-7101-T
Thesis

UC-34a
Issued: January 1978

Investigation of Uranium Plasma Emission from 1050 to 6000 Å

Joseph Michael Mack, Jr.

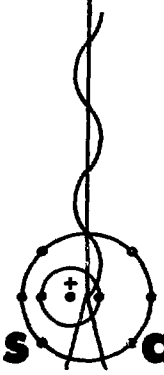

los alamos
scientific laboratory
of the University of California
LOS ALAMOS, NEW MEXICO 87545

An Affirmative Action/Equal Opportunity Employer

UNITED STATES
DEPARTMENT OF ENERGY
CONTRACT W-7405-ENG. 36

TABLE OF CONTENTS

Abstract of Thesis Presented to the Graduate Council
of the University of Florida in Partial Fulfillment of the Requirements
for the Degree of Doctor of Philosophy

INVESTIGATION OF URANIUM PLASMA EMISSION FROM 1050 TO 6000 Å

By

Joseph Michael Mack, Jr.

December 1977 ✓

Chairman: Dr. Richard T. Schneider
Major Department: Nuclear Engineering Sciences

Absolute emission coefficient measurements on arc-generated uranium plasmas in local thermodynamic equilibrium are described for a wavelength bandwidth of 1050 to 6000 Å. Low- and high-pressure arcs were investigated for their emission properties, characteristic temperatures and uranium partial pressures. Temperatures from 5500 to 8000 K and uranium partial pressures from 0.001 to 0.01 atm were found at the arc centerline. The new emission data are compared with other similar experimental results and to existing theoretical calculations. The effects of cold-layer UF_6 photoabsorption on uranium plasma emission characteristics are established for UF_6 molecular densities ranging from 1.0×10^{16} to 1.0×10^{17} cm^{-3} and layer thickness from 1.0 to 5.0 cm.

Ab Initio atomic structure calculations were made using relativistic Hartree exchange wavefunctions, from which oscillator strength distributions were computed for transition arrays of interest. These calculations give supporting evidence as to the credibility of the measured emission at various wavelengths, particularly in the vacuum ultraviolet. It is suggested that a consistent picture as to the nature of uranium plasma emission, at these plasma conditions, emerges and the capability now exists to successfully compute major emission features of uranium and other complex atomic systems.

I. INTRODUCTION

With the advent of the nuclear age and the subsequent strong trend toward development of uranium-based technology, research priorities concerning the nature of the uranium atom have acquired substantially increased importance. Initial involvement in metallurgical and nucleonic properties was largely due to the apparent need for weapon fabrication and later some aspects of reactor technology. By 1947 a new area of interest was the study of uranium plasmas at high temperature (6 keV),[1] for a physical understanding of energy release caused by nuclear detonations. This was the first significant attempt to model the uranium atom using a quantum and statistical mechanical basis from which was extracted thermodynamic and optical information. Eventually, interest was generated in lower temperature (0.5 → 5 eV) uranium plasmas because of the potential usefulness of plasma core reactors as a means for space propulsion and possibly as an energy source for MHD power generation.[2-4] More recently, worldwide need for uranium isotope enrichment using laser processes[5-12] has opened a new and significant area which is stimulating much basic research of the uranium atom. Uranium plasma research is also influencing the development of nuclear-pumped laser systems. This particular program has had some recent breakthroughs[13,14] which will likely increase the research momentum on the study of neutral and once-ionized uranium.

An accurate theoretical model of the uranium atom would represent a monumental step in understanding complex atomic systems. The mathematical description of many-electron atoms has been attempted using several

methods imbedded with various approximations.[15-17] In many situations, experimental results are available to substantiate theory or at least to raise questions about the validity of certain aspects of theoretical treatment. Currently, there is little conclusive theoretical-experimental validation of the atomic properties of uranium and uranium plasmas. However, there is a significant effort under way by Steinhaus et al.[18,19] to establish experimentally the energy levels of neutral and once-ionized (UI and UII) uranium. This effort evolved from work by Schuurmans[20] and Kiess et al.[21] in 1946. With subsequent improvement in optics, spectroscopic techniques, and atomic structure calculations, confidence is increasing in energy-level definition but progress is slow.

The specific emission coefficient $\varepsilon_\lambda(T,P)$ characterizes the light emission from a volume element of plasma. It is defined as the amount of energy emitted per unit time, from a given volume, into a specified solid angle and wavelength interval. It can be composed of continuous and/or discrete components, both of which are strong functions of plasma temperature and density (pressure) of the radiating species. The formulation of an adequate theoretical model of the uranium atom can be strongly assisted (perhaps out of necessity) by obtaining from experiment detailed knowledge of the uranium emission coefficient. Because calculation of such a property (for uranium) is impossible without a model that suffers from several approximations, experimental verfication through emission coefficient measurement is needed. This thesis reports on an experiment designed to measure the specific emission coefficient of a uranium plasma and to relate these data to state-of-the-art theoretical predictions.

Miller[22] and Martency et al.[23] have acquired emission coefficient data from UF_6 shock-tube and radio-frequency induction-heated Ar-UF_6 plasmas, respectively. Uranium plasma emission coefficients obtained from UF_6 discharges present distinct impurity problems, potentially resulting in distorted emission coefficient wavelength dependence. A dc uranium arc was chosen as the light source for the present experiment to reduce plasma impurities and provide a steady-state, less contaminated plasma to determine its emission properties. The wavelength bandwidth considered is from 1050 Å to an upper limit of 6000 Å. The emission data are then compared to similar data generated by other research groups. Also included is a comparison to theoretical emission coefficient predictions. In summary, this effort was conceived to establish a unified picture of the progress made over the past few years concerning the experimental and theoretical investigations characterizing uranium plasma emission.

Chapter II describes the plasma diagnostics necessary for the determination of basic plasma properties such as temperature, particle densities, and radiation. Particular attention is given to the application of such diagnostics to uranium plasmas. Uranium arc plasma generation and arc stability are discussed in Chapter III. Also examined are the various methods of data acquisition and intensity calibration applied in the course of this investigation. Chapters IV and V indicate the emission measurements for uranium plasmas at two distinct arc conditions. Brief descriptions and comparisons of other similar experiments are given amoung these, the present effort, and theoretical predictions. In Chapter VI theoretical models of the uranium atom are critically considered. A comparison is made between emission peak locations of the

present results to theoretically predicted locations for the higher temperature arc plasma. A discussion of the major points of this overall effort then concludes this study.

II. PLASMA THEORY AND DIAGNOSTICS

Plasma temperature and density diagnostics are based on the assumption that relevant information can be extracted from theoretical descriptions of microscopic plasma processes. Generally, plasma constituents exhibit balance between the population and depopulation of neutral and/or ionic energy levels. This implies that for every excitation event (to use an example) there is a corresponding de-excitation, not necessarily brought about by the inverse excitation process. Plasma particles that are excited and de-excited by the same mechanism demonstrate detailed balancing. Arc plasmas are usually considered to be collision-dominated in the sense that e^--atom collisions cause most of the excitations and de-excitations. However, radiative de-excitation can also be important as indicated by strong photon output. Therefore, arc plasmas are rarely characterized by detailed balancing, and various approximations such as local thermodynamic equilibrium (LTE) and partical LTE[24] must be used.

II-1. Equilibration Considerations

Griem[25] has developed criteria that indicate which equilibrium state applies to a given plasma. Most of these tests set limits on the dominance (or lack thereof) of collisional rates over radiative rates. Griem developed the following criterion for complete LTE in a hydrogen-like system:

$$n_e \geq 9 \times 10^{17} \left(\frac{\Delta E_{0,1}}{Z^2 E_H} \right)^3 \left(\frac{kT_e}{Z^2 E_H} \right)^{1/2} Z^7 \qquad \text{(II-1)}$$

Where n_e = electron density (cm^{-3}),

Z = net plasma charge (Z=1 for neutral; Z=2 for singly ionized),

$\Delta E_{0,1}$ = energy (eV) of 1st excited state with respect to the ground state,

kT_e = thermal energy of plasma electrons (eV), and

E_H = ionization potential of hydrogen (eV).

This criterion estimates the lower limit of electron density required to maintain a hydrogenic system in complete LTE. A hydrogenic system is usually characterized by a large energy gap between the ground state and first excited level, and successively smaller energy separations between levels as continuum is approached. Hydrogen (and helium) is also one of the more difficult elements to bring into LTE because of its relatively high-lying first excitation level. Thus, hydrogen can usually serve as an upper-limit estimation for the validity of LTE for more complex systems. However, the electron density criterion offered by Eq. (II-1) is <u>not</u> directly applicable to the uranium system because the known energy-level description of the uranium atom (or ion) simply does not fit the hydrogenic picture. In fact, the first excitation levels of UI and UII are ≃ 0.077 eV (UI) and 0.03 eV (UII), which, for singly ionized uranium at 8500 K, implies $n_e \geq 3.9 \times 10^9$ cm^{-3}. This is well below any reasonable values for n_e basically because of the strong dependence on $\Delta E_{0,1}$ which has a very small value for neutral and once-ionized uranium. Applied to hydrogen at 8500 K, $n_e \geq 8.8 \times 10^{16}$ cm^{-3}, this limiting value for n_e is probably too restrictive for the uranium system. Griem,[26] McWhirter,[27] and

Wilson[23] have developed a test which depends on the energy level structure of a specific atomic system, thus reducing the necessity of assuming hydrogen-like characteristics. This criterion (hereafter called the ladder criterion) is more applicable to complex systems.

The ladder criterion presumes that the most difficult level to populate will form the largest energy gap ascending the energy level diagram. Existence of LTE in an optically thin collision-dominated plasma is tested by

$$n_e \geq C\, T_e^{1/2}\, (E_k - E_i)^3 \quad , \tag{II-2}$$

where $C = 1.6 \times 10^{12}$ (McWhirter[27]).

The electron temperature T_e has units of K; the largest energy gap in eV for the atom under study is $(E_k - E_i)$. Equation (II-2) is not sufficient for LTE because e^- relaxation time, e^--atom relaxation time, and atom relaxation time must dominate whatever other transient phenomena occur in the plasma. Most stable steady-state arcs satisfy these relaxation requirements.

To apply Eq. (II-2) to a uranium plasma it is necessary to define the largest energy-level gap found in its level diagram. Complete tabulation of this information is unavailable, but a representative gap width may be defined by examination of the work by Steinhaus et al.[18,19] and Blaise and Radziemski.[29] Considering neutral uranium (UI), the 620.323 cm^{-1} - 3800.829 cm^{-1} levels provide the largest gap (~ 3130 cm^{-1}). This implies an electron density of 7.2×10^{12} cm^{-3} at 5500 K. Similarly for singly ionized uranium (UII), the largest gap is about 2126 cm^{-1} (2294.70 - 4420.87).[30] Assuming an electron temperature of 10 000 K (UII), the corresponding electron density

limit is then 2.93 x 10^{12} cm^{-3}. If partial LTE is assumed, the largest energy gap need only be defined above the thermal energy limit.

In conclusion, although there is no feasible way to determine accurately the LTE limits on electron density for atomic and once-ionized uranium, reasonable estimates can be obtained using Eqs. (II-1) and (II-2).

II-2. Plasma Radiation

Many factors affect the net photon output from a plasma. Optical depth and absorption are the most important. In many laboratory plasmas, photons emitted from the plasma central region may be absorbed en route to the outer boundary. The degree of trapping implies an optical depth, $\tau_\nu(x)$, which is simply the effective absorption coefficient integral $\kappa_\nu(x)$ over a given homogeneous plasma depth X.* The relation between the intensity $I_\nu(x)$ and energy emitted as a function of the line-of-sight depth into the plasma is governed by Eq. (II-3), the equation of radiative transfer.

$$\frac{dI_\nu(x)}{d\tau_\nu(x)} = I_\nu(x) - \frac{\varepsilon_\nu(x)}{\kappa_\nu(x)} \quad . \tag{II-3}$$

The specific emission coefficient, $\varepsilon_\nu(x)$, (energy/volume-wavelength-time-solid angle) and $\varepsilon_\nu(x)/\kappa_\nu(x)$ is the source function of radiation (energy/area-wavelength-time-solid angle). The source function for an LTE plasma is equivalent to the Planck function.

---

*In this sense X connotes a homogeneous plasma depth, and the subscript ν implies that there is a spectral dependence to τ and κ.

The general solution to the equation of radiative transfer is

$$I_\nu(x) = I_\nu(o)\, e^{-\tau_\nu(x)} + \int_0^x R_\nu(T)\, \kappa'_\nu(x')\, e^{-\tau_\nu(x')}\, dx' \,, \quad \text{(II-4)}$$

where $I_\nu(x)$ = observed intensity at X, ν (energy/area-time-solid angle-wavelength,

$I_\nu(o)$ = intensity of background source (if there is one) at ν,

$B_\nu(T)$ = Planck function at T, ν (energy/area-time-solid angle-wavelength),

$\kappa'_\nu(x')$ = effective absorption coefficient (length^{-1}) at x', ν, and

$\varepsilon_\nu(x')$ = specific emission coefficient at x', ν (energy/volume-time-solid angle-wavelength).

In Eq. (II-4), a situation is possible where <u>all</u> emitted photons transport beyond the outer plasma boundary, that is, if $\tau_\nu(x) \to o$. Then the observed intensity is simply the emission coefficient integral over the line-of-sight depth, provided the plasma is homogeneous. This plasma is designated optically thin. The other extreme would be $\tau_\nu(x) \to \infty$; here all emitted photons are trapped within the outer plasma boundary, and then the plasma radiates as a surface where $I_\nu \to B_\nu$. This plasma is designated optically thick and exhibits a blackbody spectral distribution of radiation.

Generally, in relating the concept of optical depth to arc plasmas, the line-of-sight depth and the effective absorption coefficient must be determined. Usually the line-of-sight depth will be quite small (for arcs), making the effective absorption coefficient <u>the</u> important quantity. Unless the plasma pressure is 50 atmospheres or

greater (dense arc plasmas), the only significant absorption will be located (on the wavelength scale) at some of the spectral line centers, usually formed in the lower energy levels. In many cases for low- and intermediate-density plasmas, the effective absorption coefficient will be small for most wavelengths.

Line, recombination, and continuum radiation are three basic radiation types occurring in an arc plasma. Line radiation is usually associated with relatively low temperatures, i.e., 4 000 K-15 000 K; recombination and continuum radiation can be substantial when the characteristic plasma temperature is > 15 000 K. Detailed treatments of recombination and continuum radiation are given by Cooper.[31]

Spontaneous emission and stimulated emission result in line radiation. Stimulated emission (often thought of as negative absorption) is a difficult item to isolate and therefore, is usually defined as an effective absorption coefficient for any plasma as shown by:

$$\kappa'_{\nu}(x) = \kappa'_{L_{\nu}}(x) + \kappa_{C_{\nu}}(x) \qquad \text{(II-5a)}$$

$$\kappa'_{L_{\nu}}(x) = \kappa_{L_{\nu}}(x) - \kappa_{SE_{\nu}}(x) \quad , \qquad \text{(II-5b)}$$

where κ'_{ν} = total (measured) effective absorption coefficient at x, ν cm^{-1} ,

$\kappa'_{L_{\nu}}(x)$ = total effective line absorption coefficient at x, ν,

$\kappa_{L_{\nu}}(x)$ = line absorption coefficient at x, ν,

$\kappa_{C_{\nu}}(x)$ = total continuum absorption coefficient at x, ν, and

$\kappa_{SE_\nu}(x)$ = negative absorption coefficient caused by stimulated emission at x, ν.

Thus, $\kappa_{SE_\nu}(x)$ represents an effective decrease in $\kappa_\nu(x)$. If an energy absorption transition by a bound electron of an atom is considered, where u ⇒ upper level and ℓ ⇒ lower level, the description of line absorption at a given frequency is given by

$$\kappa_{K_\nu}(x) = \frac{h\nu_{\ell \to u}}{c} n_\ell B_{\ell \to u} \phi_\kappa(\nu) , \qquad \text{(II-6)}$$

where $\nu_{\ell \to u}$ = the frequency of the transition (s^{-1}),

n_ℓ = population density of the lower state (cm^{-3}),

$B_{\ell \to u}$ = Einstein's probability for absorption (cm/g),

$\phi_\kappa(\nu)$ = absorption line-shape function with

$$\int_{line} \phi_\kappa(\nu)\, d\nu = 1, \text{ and}$$

X = line-of-sight distance into plasma.

Similarly, the line emission coefficient for a homogeneous plasma at frequency ν is described by

$$\varepsilon_{L_\nu}(x) = \frac{h\nu_{u \to \ell}}{4\pi} n_u A_{u \to \ell} \phi_\varepsilon(\nu) , \qquad \text{(II-7)}$$

where $\varepsilon_{L_\nu}(x)$ is the specific line emission coefficient at ν and plasma depth x. Actually, a continuum emission coefficient should also be considered for completeness, but this is not included here because of its small (or inextractable) contribution. The population density (cm^{-3}) of the spontaneous upper level transition and Einstein probability for such a transition are given by n_u and $A_{u \to \ell}$(s^{-1}), respectively. The normalized line-shape function is indicated by $\phi_\varepsilon(\nu)$, such that

$\int_{line} \phi_\varepsilon(\nu)d\nu = 1$. The line intensity $I_\nu(x)$ from such a transition would simply be determined by multiplying the line emission coefficient by the appropriate LOS plasma depth through a constant emission zone.

Arc plasmas are inherently inhomogeneous to varying degrees. Free-burning arcs usually exist with significant temperature gradients along the major part of an approximately cylindrical arc column radius, which results in radially varying intensities. Therefore, the emission coefficient will also have a radial dependence that must be extracted by unfolding methods applied to observed intensities. Many wall-stabilized arcs have less severe temperature gradients, with the exception of that region approaching the wall.[32-37] This implies the possibility of an approximately homogeneous nature in temperature and density in the major part of the cylindrical arc plasma in the radial direction. Although a relatively constant temperature profile does not assure homogeneous density and emission profiles, it can be a strong indicator.

II-3. Emission Coefficient Determination

The geometry of inhomogeneous optically thin arc plasmas is approximated by a number of concentric zones about the vertical axis, as shown in Fig. II-1. Each zone is assumed to display constant emission which is a function of a single temperature and density for that zone. The intensity at a given location along the arc chord is the sum of emission contributions for each zone intercepted by a LOS ray passing through the geometry. The emission coefficient must then be unfolded from the measured integrated intensities by the familiar Abel transform. The analytical form of the transform equations[38] is

$$I(y) = 2\int_0^x \varepsilon(r)dx = 2\int_y^{r_0} \frac{\varepsilon(r)rdr}{\sqrt{r^2-y^2}} \text{ , and} \qquad \text{(II-8a)}$$

$$\varepsilon(r) = -\frac{1}{\pi}\int_r^{r_0} \frac{I'(y)dy}{\sqrt{y^2-r^2}} \text{ .} \qquad \text{(II-8b)}$$

The geometrical relations are developed using Fig. II-1.

There are two common approaches used in solving Eqs. (II-8a) and (II-8b) for $\varepsilon(r)$. The first is by fitting an appropriate polynomial to the experimental intensities, differentiating, and using Eq. (II-8b) to obtain $\varepsilon(r)$. The details of such a method are given in Ref. 39. The second method approximates the integrals with sums and extracts the desired information numerically. The numerical form of Eq. (II-8a) is given by

$$I_i^T(y) = 2\sum_j \varepsilon_j(r)\, \ell_{ij} \text{ .} \qquad \text{(II-9)}$$

In Fig. II-1, the i^{th} LOS in the j^{th} concentric ring is defined by the length coefficients, ℓ_{ij}, and $\varepsilon_j(r)$ represents the average emission coefficient for the j^{th} ring. Equation (II-9) results in a system of simultaneous linear equations for each $\varepsilon_j(r)$, $I_j^T(y)$, which can be solved by matrix inversion to obtain the $\varepsilon_j(r)$ vector.

When the plasma under investigation has significant intensity gradients, a number of rings (as many as 40) may be necessary to approximate adequately the intensity profile and allow computation of emission coefficients within acceptable error. Each ring requires a corresponding intensity determination, which may be too difficult to obtain, depending on plasma stability. However, too many subdivisions may cause

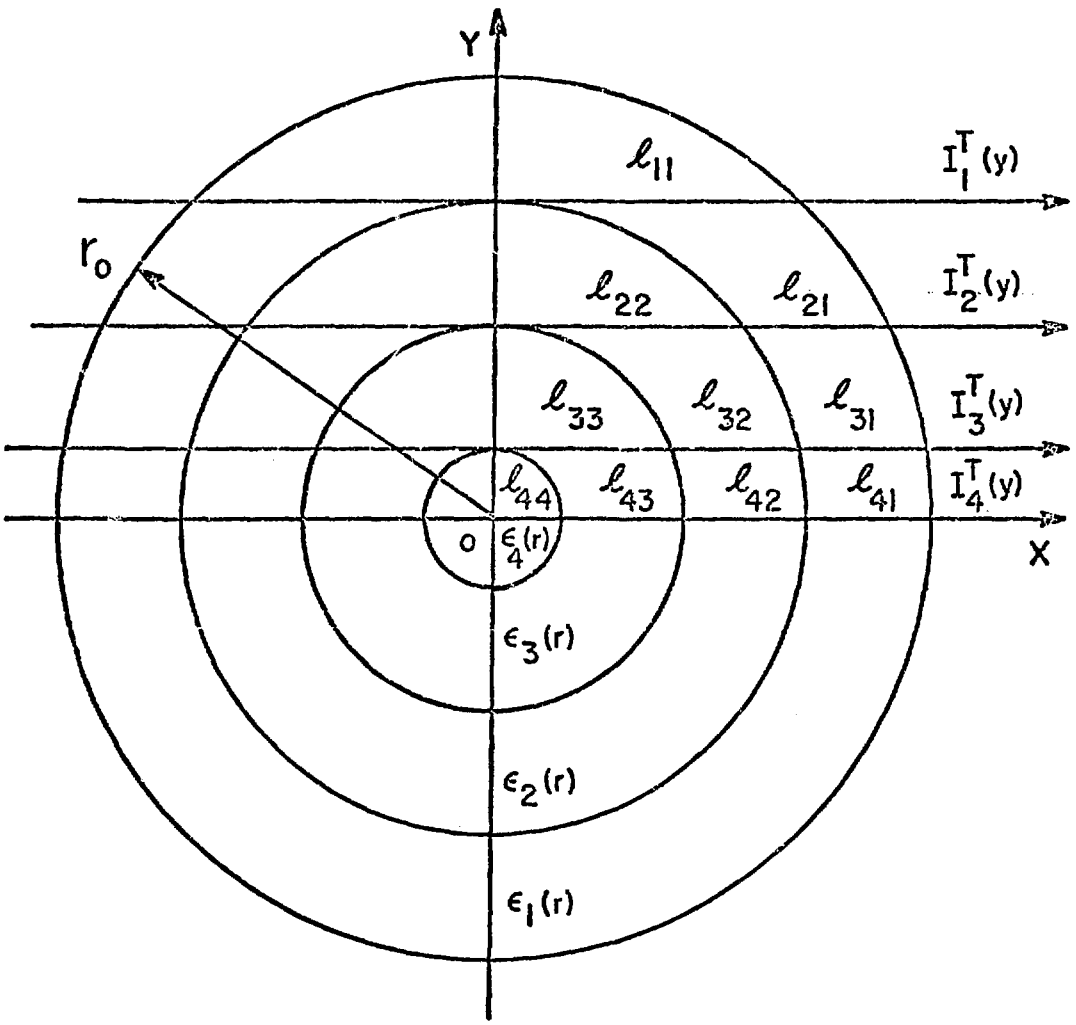

Fig. II-1. Zonal division of a cylindrically symmetric plasma.

oscillations in the unfolding process if an exceptionally smooth intensity profile is not available. Substantial error (20 → 30%) on the intensity profile measurement (especially for the outermost ring) will be propagated to the central zone and will yield a poor estimate of its emission value. For this situation, too many rings will introduce large oscillations and an unacceptable error propagation. Obviously, there is an optimum number of rings depending upon the overall intensity profile shape and the experimental error value, particularly at the outermost ring.

Many studies have dealt with various techniques to implement the inversion[40-43] but these primarily address algorithmic problems (interpolation, smoothings, etc). Kock,[44] Nestor,[42] and Bockasten[43] address error propagation by using numerical methods for inversion. These analyses imply that the correct number of subdivisions is a direct function of the experimental error in the outermost zone as well as the shape of the intensity profile.[44] When error in the outer zones approaches 20% or more, four or five zones may define the limiting accuracy.

To relate these considerations to the inversion of the wall-stabilized uranium arc intensity data, a four-ring numerical unfolding scheme was chosen because of time limitations involved in acquiring zonal intensity data for more than four zones, and the experimental error associated with the outermost zonal intensity was ∿ +25%. When this error is considered with a 10% calibration error and an estimate of error for using only four rings, the total error estimate of central zone emission coefficients ranges from 28 → 36%.

II-4. Plasma Temperature

Many techniques used for temperature diagnostics were developed by Griem,[23] Hefferlin,[45] and Lochte-Holtgreven.[46] The following discussion considers only those temperature diagnostics applied to a uranium arc plasma, including the Boltzmann plot, norm temperature, relative norm temperature, and the modified brightness-emissivity methods.

A. Boltzmann Plot Method

The integrated* line intensity for a homogeneous, optically thin plasma into a depth x is

$$I_\nu = \frac{h\nu_{u\to\ell}}{4\pi} A_{u\to\ell} n_u \ell . \qquad \text{(II-10)}$$

If the plasma is in complete LTE and inhomogeneous, $n_u(T)$ is determined by the Boltzmann factor yielding

$$I_\nu = \frac{h\nu_{u\to\ell}}{4\pi} \frac{g_u}{Z(T)} A_{u\to\ell} n_o(T) e^{-(E_u/kT)} \ell_{ij} , \qquad \text{(II-11)}$$

where T = excitation temperature (K) ,

$A_{u\to\ell}$ = transition propability (seconds^{-1}) ,

$\nu_{u\to\ell}$ = transition frequency ,

g_u = statistical weight of the upper level ,

$n_o(T)$ = ground state population density of a particular ionization state (#/cm^3) ,

$Z(T)$ = partition function ,

E_u = energy of upper level (eV), and

ℓ_{ij} = ring depth of zone of assumed constant emission (Fig. II-1).

*Integrated in this sense means integration over the line-shape function $\int_{line} \phi_\varepsilon(\nu)d\nu$ has already been performed.

Taking the natural log of both sides of Eq. (II-11) and rearranging terms yield an equation analogous to that of a straight line:

$$\ln\left\{\frac{\nu_{u\to\ell}\, I_\nu}{g_u\, A_{u\to\ell}}\right\} = \ln\left\{\frac{h\, n_o(T)\rho_{ij}}{4\pi Z(T)}\right\} - \left\{\frac{1}{kT}\right\} E_{um} \,. \qquad \text{(II-12)}$$

If for two or more spectral lines, ln (constant * $I_\nu)_m$ is plotted against E_{um} ("m" refers to a particular transition), the resultant slope of the curve will approximate -1/kT. If I_ν is measured in absolute units, the ordinate intercept also determines the LTE ground state number density for that species.

Equation (II-12) was developed considering complete LTE and can be modified for use with less restrictive equilibrium concepts. When partial LTE is assumed, the Boltzmann plot method for complete LTE is modified to yield

$$\ln\left\{\frac{\nu_{u\to\ell}\, I_\nu}{g_u\, A_{u\to\ell}}\right\} = \ln\left\{\frac{h\, n_\ell \rho_{ij}}{4\pi g_\ell}\right\} - \left\{\frac{1}{kT}\right\} (E_u - E_\ell) \,, \qquad \text{(II-13)}$$

where: E_ℓ = energy level of lower energy, and

g_ℓ = lower level statistical weight.

The essential difference between Eq. (II-12) and Eq. (II-13) is that the intercept term no longer defines the true ground-state density in partial LTE.

Application of the Boltzmann plot technique for relative or absolute temperature determination requires the following conditions:

(1) at least partial LTE must exist in an optically thin plasma,

(2) many transitions should be used,

(3) these spectral lines should have a correspondingly significant energy-level separation, and

(4) this technique can be used for inhomogeneous plasmas, but the intensity data ideally should first be spatially resolved to express the emission coefficient as a function of plasma radius (in cylindrical geometry). If there is no spatial resolution the computed temperature will be an approximate value, but in many instances it will yield a good estimate of an average arc temperature. The accuracy of these temperatures is governed by intensity measurement and uncertainty in atomic constants. The largest source of error for uranium plasmas is usually caused by the uncertainty of gA values which can be as much as 50%. Only in extreme cases will the average centerline temperature deviate by more than 20% from the true centerline temperature.

To apply this method to uranium plasmas (or any method dependent on gA values), availability of well-defined spectral lines is severely limited. These lines must meet the previously mentioned requirements and be locatable with the instrumentation to be used. Application of the Boltzmann plot method to uranium plasmas is straightforward in principle; but practically speaking, a very tedious task strongly dependent on spectrograph resolution, line identification, and availability of relevant constants.

B. Norm-Temperature Method

If the equilibrium emission $\varepsilon_\nu(T)$ of a transition in a specified ionic state is plotted against temperature, and if the temperature is high enough, the resultant curve will be peaked at the norm-temperature T_n, defined on an emission-vs-temperature plot as the temperature

at which $d\varepsilon_\nu(T)/dT = \varepsilon'_\nu(T) = 0$. The norm temperature can then be used to estimate the characteristic plasma temperature. First, it is necessary to determine which ionization state corresponds to identified emission lines generated by the plasma. Then $\varepsilon_\nu(T)$ is computed for a spectral line known to be from the dominant ionic stage by using appropriate equilibrium relations. Then $\varepsilon'_\nu(T) = 0$ is determined, thus defining T_n. The maximum temperature of an equilibrium plasma emitting a line in a particular dominant ionic state can be on the order of T_n, which is indicative of the energy necessary to ionize the plasma to that state.

Obvious disadvantages of such a method are that T_n is only an estimate of the characteristic plasma temperature, and while transition probabilities need not be known, the Saha equation must be solved to obtain the neutral and ionic number densities, thereby requiring LTE. The primary advantages are that only spectral line is necessary and that this method can easily be adapted to the relative norm-temperature method.

C. Relative Temperature Method

The relative temperature method is an extension (in many cases) of the norm-temperature method in that the norm-temperature can be used as a reference plasma temperature and temperatures at other spatial locations related to it. It can be used for plasmas which have cylindrical geometry with radial temperature profiles $T(r)$ and at least one defined temperature such as T_n. If this is the case, the resultant emission profile $\varepsilon_\nu(r)$ pertaining to a specific transition can be similar to that shown in Fig. II-2; one point on the desired temperature profile $T(r)$ is defined by $\varepsilon_\nu(r_0)$ and T_n. From equilibrium relations, ratios of $\varepsilon_\nu(r_0)/\varepsilon_\nu(r_i)$ may be computed and the corresponding $T(r_i)$ determined.

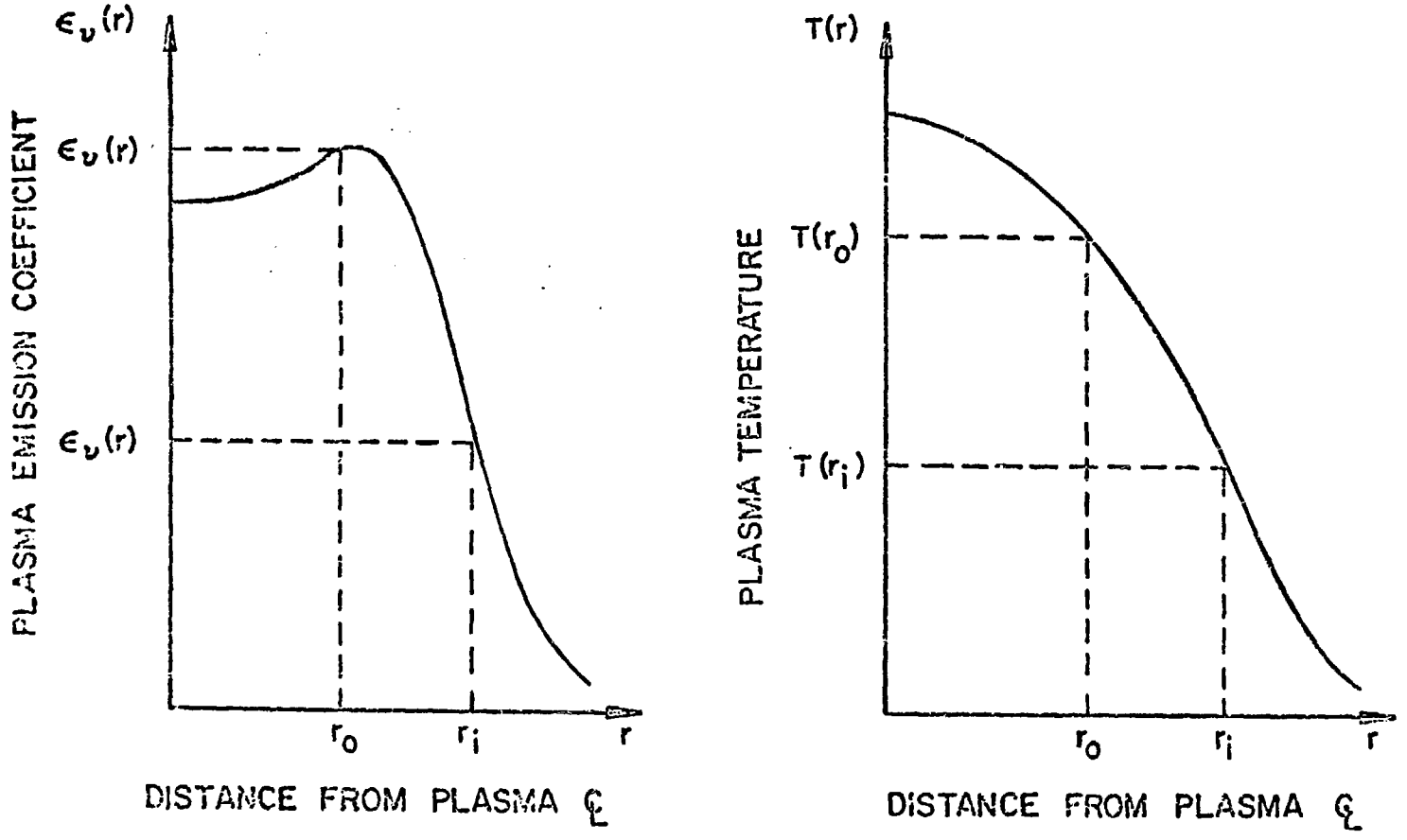

Fig. II-2. Plasma emission-temperature profile.

$$\frac{\varepsilon_\nu(r_i)}{\varepsilon_\nu(r_o)} = \frac{Z[T(r_o)]}{Z[T(r_i)]} \frac{n_T(r_i)}{nT(r_o)} \exp\left\{ -\left[\frac{E_u}{k}\right]\left(\frac{1}{T(r_i)} - \frac{1}{T(r_o)}\right)\right\} . \qquad \text{(II-14)}$$

Any temperature on $T(r_i)$, determined by other independent methods, will suffice for $T(r_o)$.

The relative temperature method is particularly straightforward when dealing with the norm-temperature situation. Transition probabilities are not needed, but the temperature dependence of partition function should be considered. Only one transition need be used, thus eliminating any calibration procedures. This method is very attractive for use with spectroscopically complex plasmas because it is independent of gA values.

D. Modified Brightness-Emissivity Method

Temperature measurement methods previously discussed require the assumption of negligible absorption or an optically thin plasma. If certain spectral lines emitted by a thin plasma have measurable absorption (say at the spectral-line centers), temperature may be determined using spectral-line absorption as a basis.

The brightness-emissivity method (BEM)* adapts the radiative-transfer equation (Eq. (II-3)] solution to a homogeneous LTE absorbing plasma.[46,47] The following equations form the basis for this method.

$$\begin{aligned} I_\nu^T(x) &= I_\nu^S(x)\, e^{-\tau_\nu(x)} + I_\nu^P(x) \\ I^T(x) &= I^S(o)\, e^{-\tau_\nu(x)} + B_\nu^P(T)\left[1 - e^{-\tau_\nu(x)}\right] \qquad \text{(II-15)} \\ I_\nu^T(x) &= I_\nu^S(o)\, e^{-\tau_\nu(x)} + B^P(T)\, \epsilon_\nu , \end{aligned}$$

*Emissivity, as considered in this instance, is the ratio of the plasma intensity to the Planck intensity at a specified temperature and wavelength.

where ϵ_ν = emissivity,

x = LOS plasma depth,

$I_\nu^T(x)$ = total observed intensity at (ν, x),

$I_\nu^S(x)$ = total external source intensity without absorption at (ν, x),

$I_\nu^S(0)$ = total external source intensity without absorption at ν, $x = 0$ (the plasma boundary), and

$B_\nu^P(T)$ = Planck function indicative of the brightness temperature of the plasma.

The known quantities $I_\nu^T(x)$, $I_\nu^S(x)$, $\tau_\nu(x)$, and ϵ_ν allow determination of the plasma brightness temperature using the Planck function for the plasma.

The primary disadvantage of the BEM is lack of applicability to inhomogeneous plasmas such as those formed with arcs. Usher and Campbell[48] have adapted the BEM to the homogeneous case. The modified BEM differs from the BEM in that an unfolding scheme resolves the absorption coefficient and temperature profiles spatially.

The absorption coefficient of a spectral line is determined by a constant intensity background source and measurement of the wavelength attenuation as the line passes through the plasma. If the inhomogeneous plasma is composed of homogeneous rings (similar to Fig. II-1), an unfolding technique[47] can be used to calculate the average line-center absorption coefficient, $\bar{\kappa}_i'(\lambda)$, for each ring from

$$\bar{\kappa}_i'(\lambda) = \frac{1}{\ell_{ii}} \left\{ \frac{1}{2} \ln \left[\frac{V_S}{V_i^T - V_i^P} \right] - \sum_{j=1}^{i-1} \bar{\kappa}_j' \ell_{ij} \right\} . \qquad \text{(II-16)}$$

Voltage signals V_S, V_i^T, and V_i^P are from a photomultiplier tube for the i^{th} LOS position. The voltages indicate background source intensity, total attenuated intensity, and plasma intensity, in that order. The ℓ_{ij} in Eq. (II-16) represents the length segments in the j^{th} ring along the i^{th} LOS position as shown in Fig. II-1. Figure II-3 shows a typical oscillogram of the photomultiplier output related to Eq. (II-16). The background source of known characteristics (Xenon flashtube) is flashed on the line-center of interest as shown on the upper trace. The lower trace shows the flashtube signal spread in time to facilitate intensity voltage measurement. The oscillograms are recorded at different chordal positions of the plasma and Eq. (II-16) is used to determine the line-center absorption profile across the radial dimension of an assumed cylindrically symmetrical arc.

The temperature is determined by an extension of the brightness-emissivity method to the inhomogeneous case. The technique uses measured voltages and calculated line-absorption values. The temperature method requires that the background source temperature (or equivalently, the intensity) be known. The average temperature in the j^{th} ring of the plasma is determined from

$$T_j = \frac{C_2}{\lambda} \left\{ \ln \left[1 + \frac{B_S}{B_j} \left(e^{C_2/\lambda T_b} - 1 \right) \right] \right\}^{-1} . \qquad \text{(II-17)}$$

The Planck functions B_S and B_j represent intensities of the background source and the j^{th} plasma ring at wavelength λ, and T_b is the brightness temperature of the background source. The B_j's are calculated using the measured voltages and the computed plasma absorption profile. The complicated expression for B_j is found in Ref. 47.

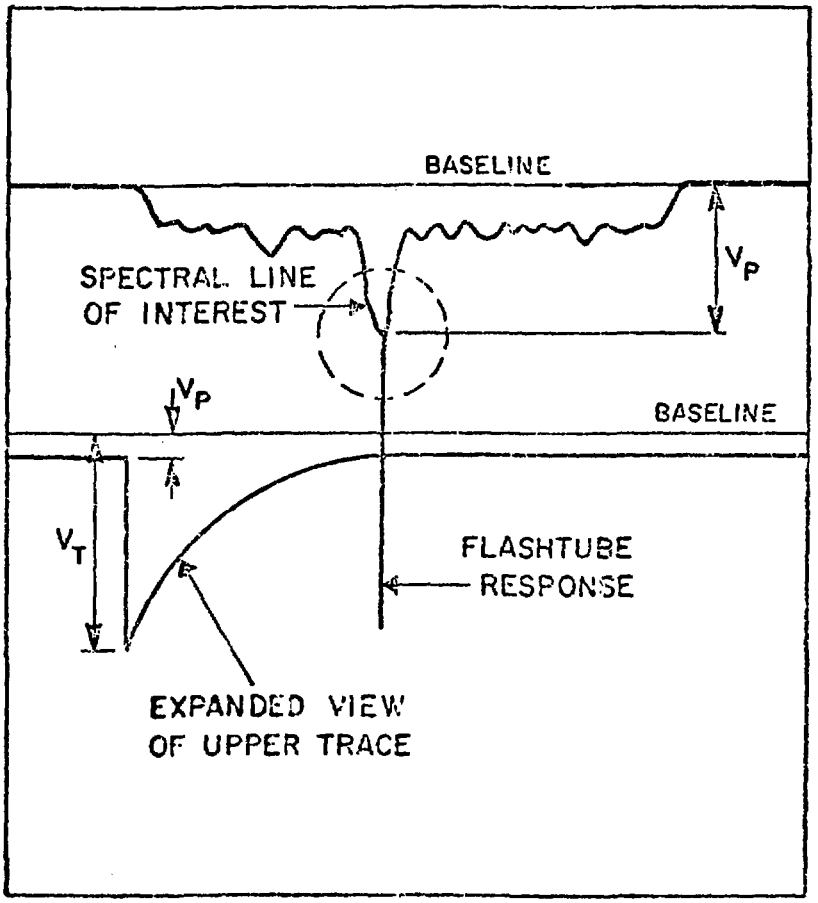

Fig. II-3. Oscillogram of photomultiplier output.

There is very little available information about atomic properties of uranium. This information would be useful when performing plasma temperature diagnostics on spectroscopically complex elements; however, the modified BEM is particularly effective for use with uranium plasmas because it is independent of these constants. Because this technique deals adequately with plasma inhomogeneities, it is suitable for application to arc plasmas. Implementation of the method is cumbersome because it means a long-duration ($\sim$ minutes) steady-state plasma, a well-defined standard background source and its associated circuitry to provide a rather elaborate data acquisition sequence.

II-5. Density Measurements

To define plasma pressure, total or partial, it is necessary to determine ground-state population densities for all ionization stages in the plasma. The equation of state (in conjunction with Dalton's law of partial pressure) for each plasma component is then used to define a total pressure. A substantial effort is involved in establishing population densities. The determinations must rely on an accurate atomic description of the plasma constituents and precise intensity calibration. Griem[25] states that even in an optimum situation it is often impossible to reduce density error below 30%. Therefore, most plasma density determinations are order-of-magnitude estimates.

Two density diagnostics, which were applied to the uranium arc plasma, are described in the following sections: absolute line intensity and pressure-temperature correlation (PTC).

A. Absolute Line Intensity Method

The integrated line intensity for a transition from level u to level ℓ is given by Eq. (II-10). Equation (II-10) applies to a line

emitted from a homegeneous optically thin LTE plasma. Modification to an absorbing plasma requires compensation (build-up) along the entire line-shape profile. Obtaining absorption build-up factors at many points along the line profile may not be possible because of line-wing overlap, especially in plasmas displaying complex spectra where isolated lines may not exist. Fortunately, absorption in many arc plasmas tends to be concentrated at spectral-line centers (on the wavelength scale). Therefore, an absorption coefficient determined at the spectral-line center approximates, to a usually acceptable degree, the maximum absorption coefficient taken over the entire line profile. This remains a good approximation as long as the spectral line exhibits a sharp profile. Using the above as a basis, absorption build-up may be incorporated into the line-intensity equation by the following:

$$I^{a}_{\nu_{total}} = \frac{h\nu_{u\to\ell}}{4\pi} \frac{G_u}{Z} A_u \quad n_o \, e^{-E_u/kT_e} \, \ell_{ij} \, \gamma \, , \qquad \text{(II-18)}$$

where γ represents a dimensionless absorption build-up factor.

The variables in Eq. (II-18) are the intensity, the excitation temperature, and the ground-state number density. Clearly, to find n_o for a homogeneous plasma, absolute intensity units must be known and excitation temperature must be determined by an independent method. For an inhomogeneous plasma, unfolding should be performed, or the calculated number density would indicate an approximate value. The absorption build-up is determined experimentally, but this factor will be insignificant where the plasma is optically thin.

It is difficult to apply this method to plasmas emitting complex spectra to obtain precise values of n_o. In addition to uncertainties

associated with inadequately defined atomic constants, there are problems in defining the integrated-line intensity $I^a_{\nu_{total}}$ in absolute units for a specific transition. Many practical considerations in the measurement of $I^a_{\nu_{total}}$ are discussed in Ref. 36, but procedures for spectral-line-wing overlap in complex spectra are especially interesting.

Uranium spectra show no isolated line structure; therefore, we must find the peak magnitude and FWHM that can be used to define a corresponding Voigt profile,[49] a theoretical representation of the actual line profile including wings. This area can be calculated analytically to yield a good estimate of the integrated spectral-line intensity.

B. Pressure-Temperature Correlation (PTC) Technique

Partial pressure estimates of plasma constituents can be based a pseudoanalytic approach such as the PTC technique.[50,51] This method uses a temperature profile correlation between experimentally determined and calculated temperature profiles. The experimental profile is typically established by the Boltzmann plot method, whereas the calculated profiles are computed using the relative (norm) temperature method. Calculations of radiation specie number densities and, hence, partial pressures are inherent to the computed profiles. A family of calculated temperature profiles is generated to be parametric in the plasma total pressure. Because the experimental profile is an independent measurement, intersection of this curve with that of the calculated profiles implies (with the aid of the Saha equation) a plasma number density and partial pressure.

This method has the uncertainties found in applying the relative (norm) temperature method (Sec. II.4C) as well as experimental inaccuracies inherent in the Boltzmann plot technique (Sec. II.4A).

*Full-width at half maximum of peak intensity value.

Uranium plasma number densities, as determined by the absolute-line method, are often uncertain. Pressure-temperature correlation removes some of this uncertainty and furnishes supporting evidence to experimentally determined densities.

III. URANIUM PLASMA EXPERIMENT HARDWARE

III-1. Uranium Plasma Generation

For this investigation uranium plasma was generated by a direct-current uranium arc constructed by Randol[51] at the University of Florida. Many original features were retained; system details are in Ref. 51. There have been some important changes to the original system which will be described in this report.

A. Uranium Plasma Containment Cell

Figure III-1 shows the uranium plasma containment vessel. The stainless steel vessel is designed to withstand safely cover-gas pressure to 100 atmospheres. It can also be operated in the vacuum mode down to at least 300 torr. Contact is made between the tungsten cathode and uranium anode by remote movement of the cathode with a pneumatic electrode-drive cylinder. Both electrodes are water-cooled. The gas distribution head can give directional flow to the incoming cover-gas near the arc electrodes. .The viewport windows are sealed from both sides for pressure or vacuum operation. The gas inlets also serve as the pumping ports when an evacuated chamber is desired.

B. Segmented Assembly

Within the containment vessel, fastened to the headplate, are several annular water-cooled copper segments (disks). The disks are arranged concentrically around the anode-cathode configuration for arc wall-stabilization. Figure III-2 shows the segmented assembly with its orientation to the electrode configuration. The arc column length is

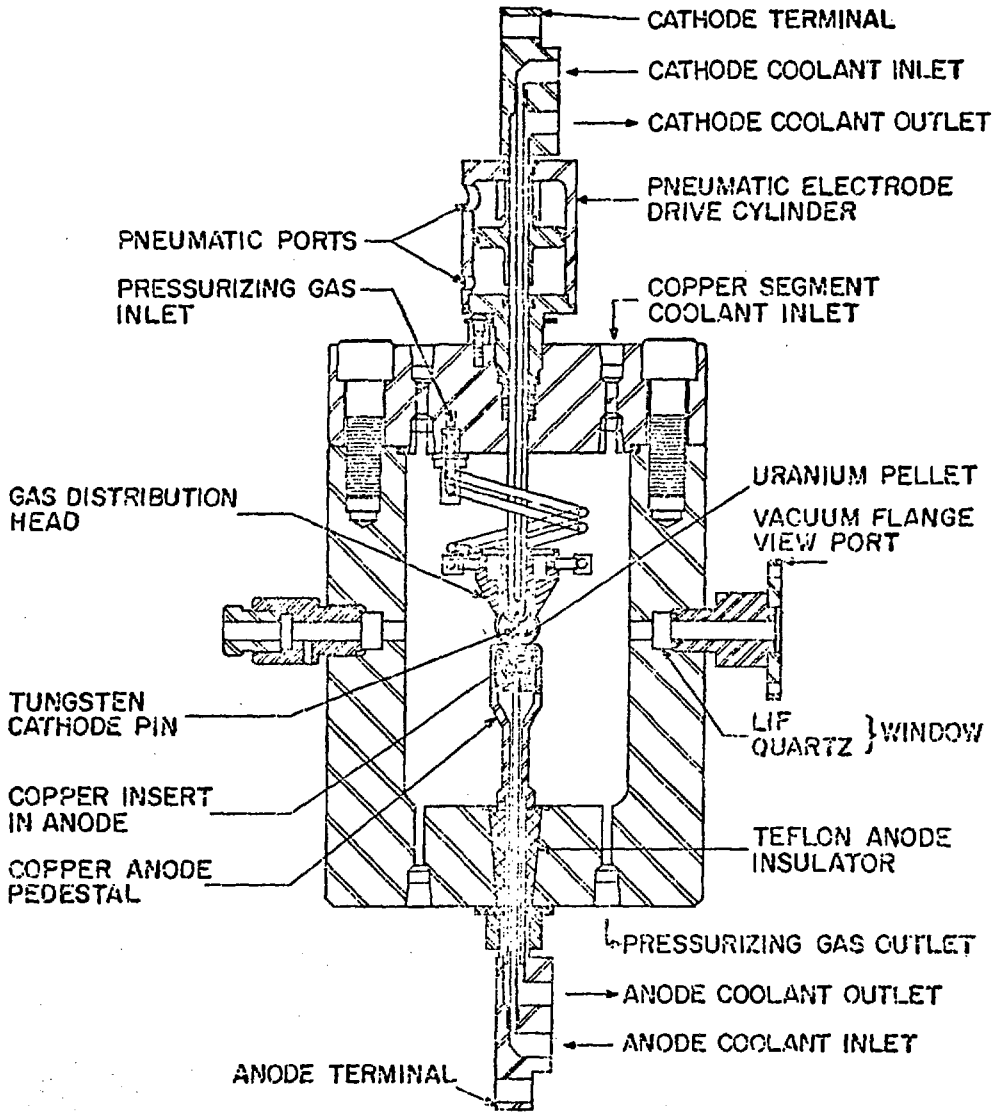

Fig. III-1. Uranium plasma containment cell.

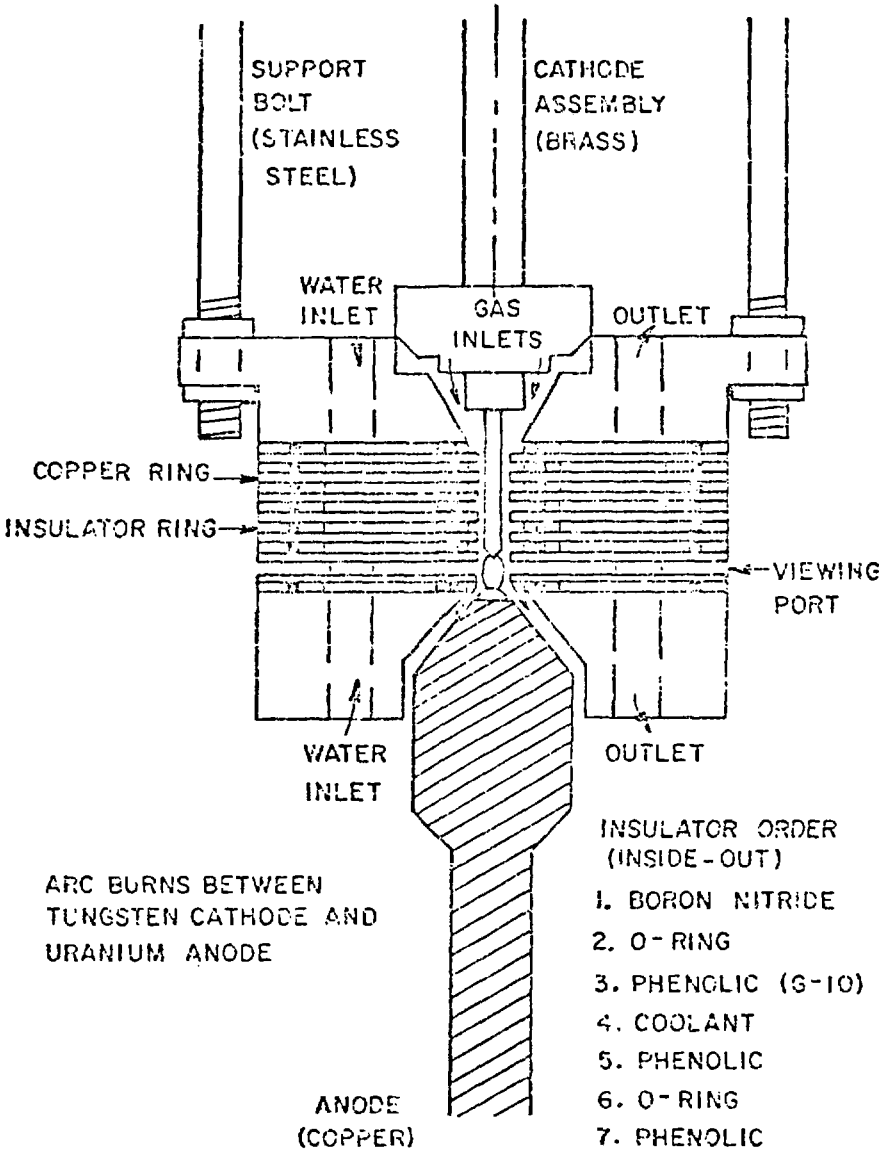

Fig. III-2. Uranium arc device segmented assembly.

shown undersized, and the plasma column was actually in contact with several of the water-cooled disks. The segmented assembly also acts as thermal shield for the pressure seals and as an effective particle shield to lessen deposition on the viewport window.

C. Pressure System

A schematic representation of the pressure system, designed for flexibility of regulation from 0-2000 psi, is shown in Fig. III-3. Adequate cell exhaust filtering removes uranium which might escape to the atmosphere. The vent on the downstream side of the cell or the roughing pump on the upstream side provides particulate venting. The high-pressure gas supply is isolated for safety in case of electrical power failure. A high-pressure solenoid valve, normally closed, prohibits gas flow unless the solenoid is energized.

D. Coolant System

Enough coolant must be supplied to the segmented assembly, anode, and ballast resistor. The cathode is primarily convection-cooled by the surrounding segmented assembly. The 60-psi water-line pressure provides adequate cooling for an arc power input of at least 100 watts; however, a centrifugal pump provides more flow if necessary. These features are shown in Fig. III-4.

E. Power Supply System

Two 650 A, 120 V dc, diesel motor generators arranged in a series are used as the primary source of electrical power for arc operation. They can be operated remotely or at the generator controls as a continuously adjustable voltage supply. Current through the arc circuit is limited by air- and water-cooled ballast resistors. The fuse limit is 300 A, 250 V. Current is adjusted for a given set of electrodes

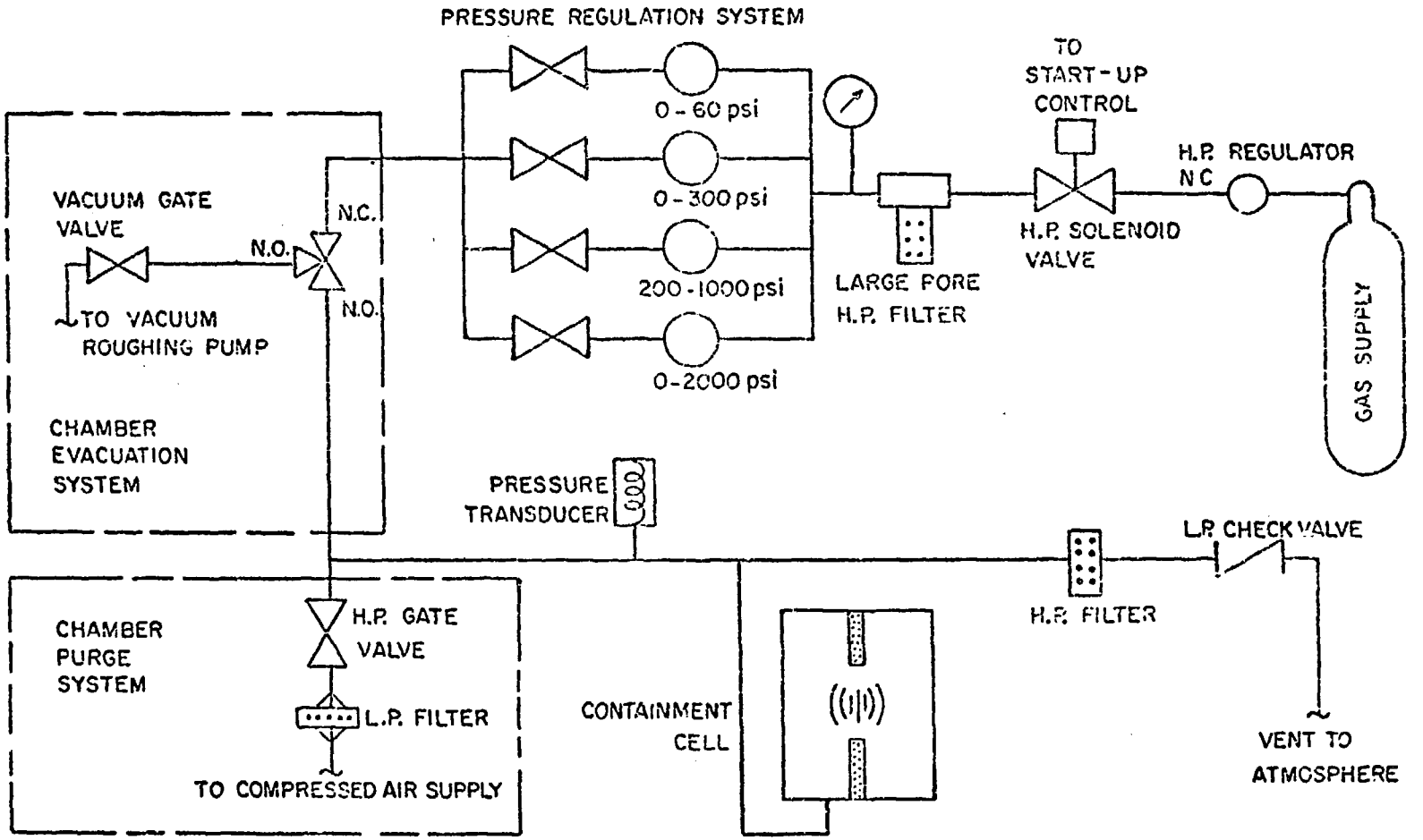

Fig. III-3 Pressure system schematic.

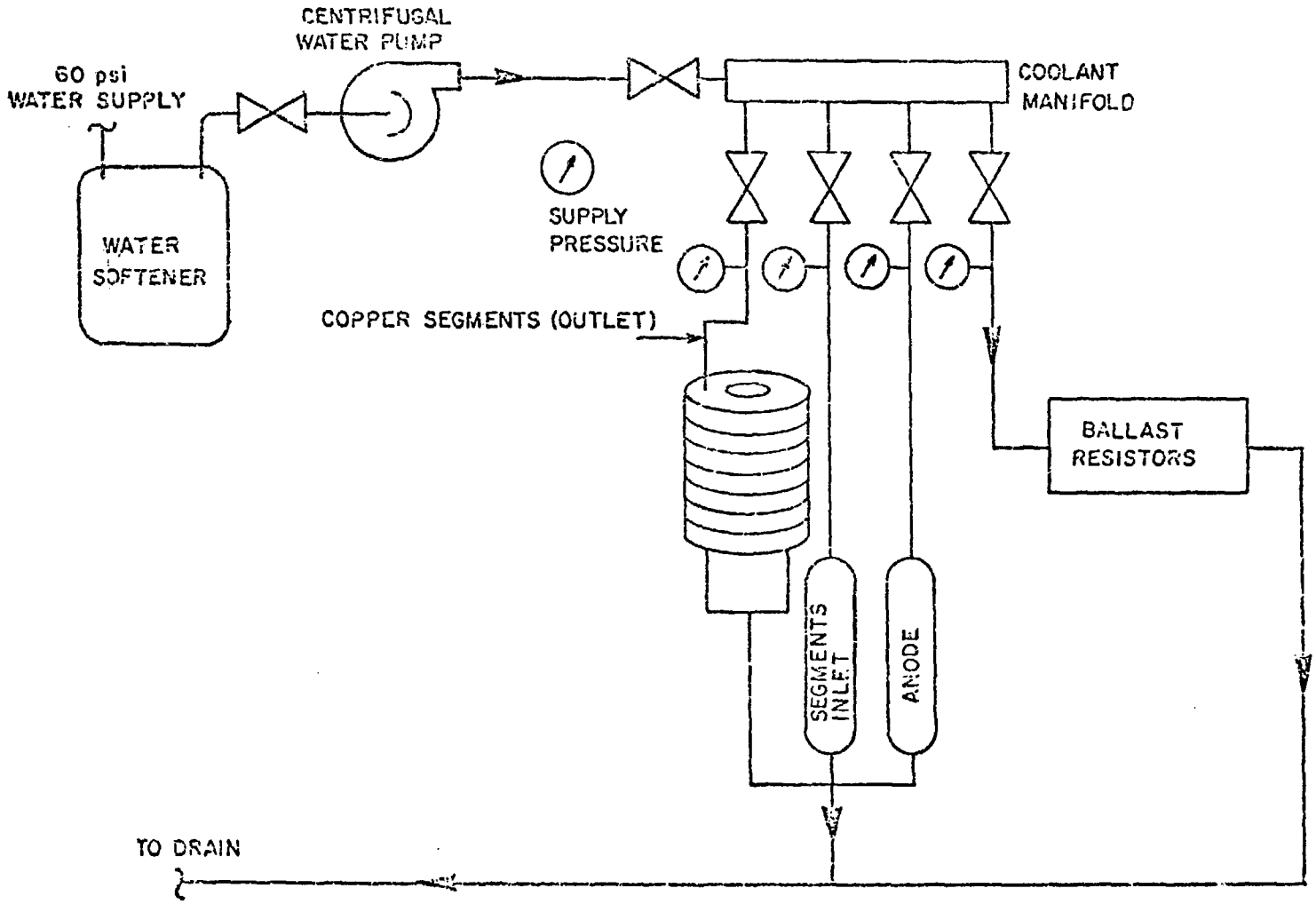

Fig. III-4. Coolant system schematic.

during arc operation by parallel switching of air-cooled resistors into or out of the circuit. Typically, this operating point was 50 A, 20 V. The uranium arc circuitry is shown in Fig. III-5. Current-voltage monitoring is accomplished on a continuous basis by Honeywell stripchart recorders (not shown on Fig. III-5).

III-2. Uranium Plasma Stability

Construction of a dc uranium arc was not difficult; however, development of a stable dc uranium arc which would allow photoelectric diagnostics demanded extensive effort. For spectroscopic measurements, this particular uranium plasma was required to be very stable for density-temperature measurements and marginally stable for emission measurements. Arc current, i_c, was used as a stability yardstick. Marginally stable implied average i_c changes $\leq$ -10% over the entire length of data collecting time with a maximum of $\pm$ 5% for instantaneous i_c changes. Temperature-density stability is indicated by similar average i_c limits and by instantaneous variation of $i_c \leq 2\%$. The University of Florida uranium arc evolved from a free-burning arc to a rather sophisticated wall-stabilized arc (Fig. III-6). A brief account of the development toward increased arc stability follows.

A. Free-Burning Arc

For simplicity, a free-burning arc under a static helium cover gas was used (Fig. III-6A). Unfortunately, motion of the anode and cathode spots was inherent in its operation, and this caused unacceptable movement of the arc column as well as current-voltage fluctuations. There is no agreement among arc physicists as to the reasons for these spot movements; however, bibliographical information can be obtained from Ref. 46. Many techniques were applied to reduce these instabilities,

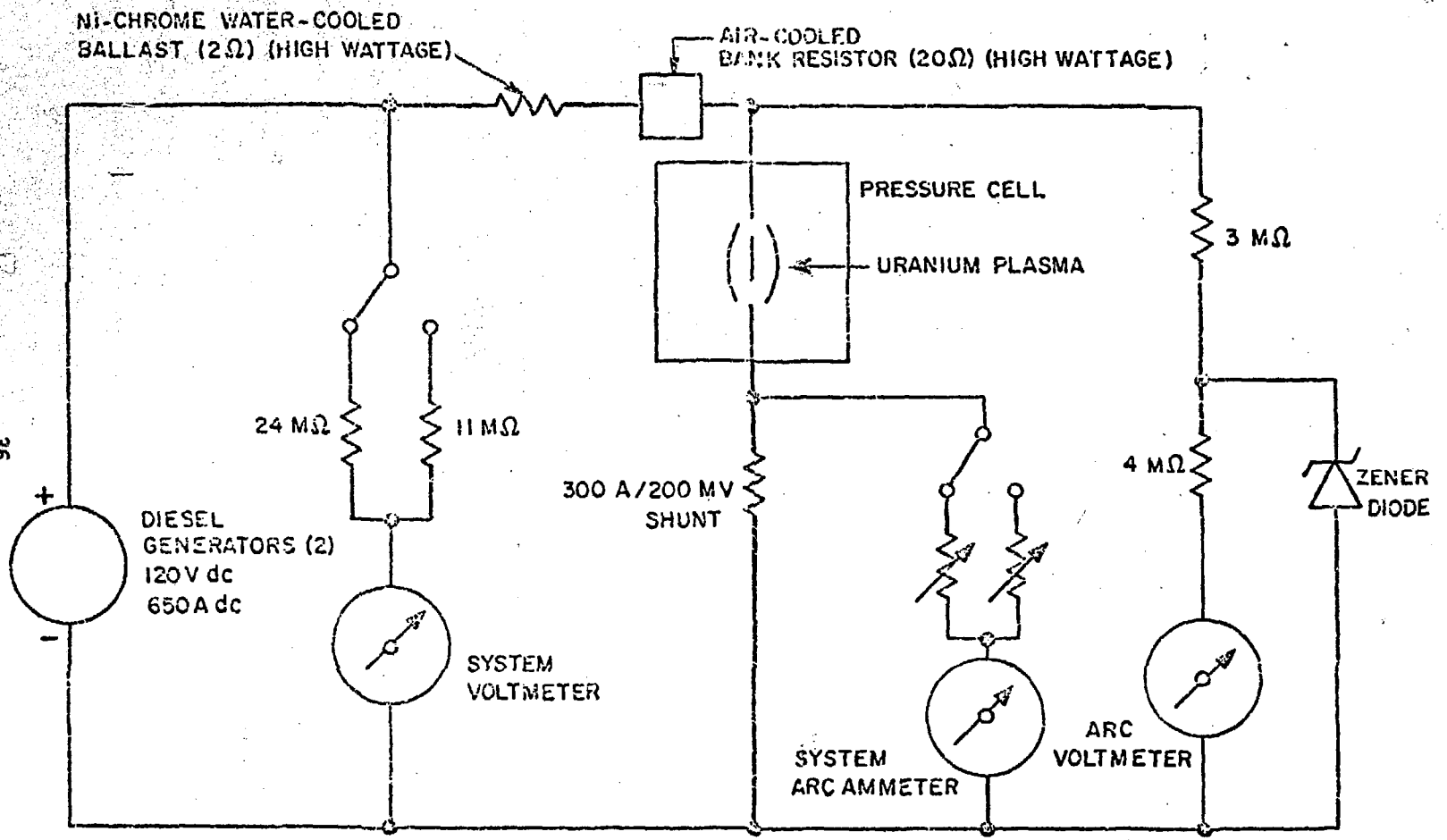

Fig. III-5. Uranium arc electrical schematic.

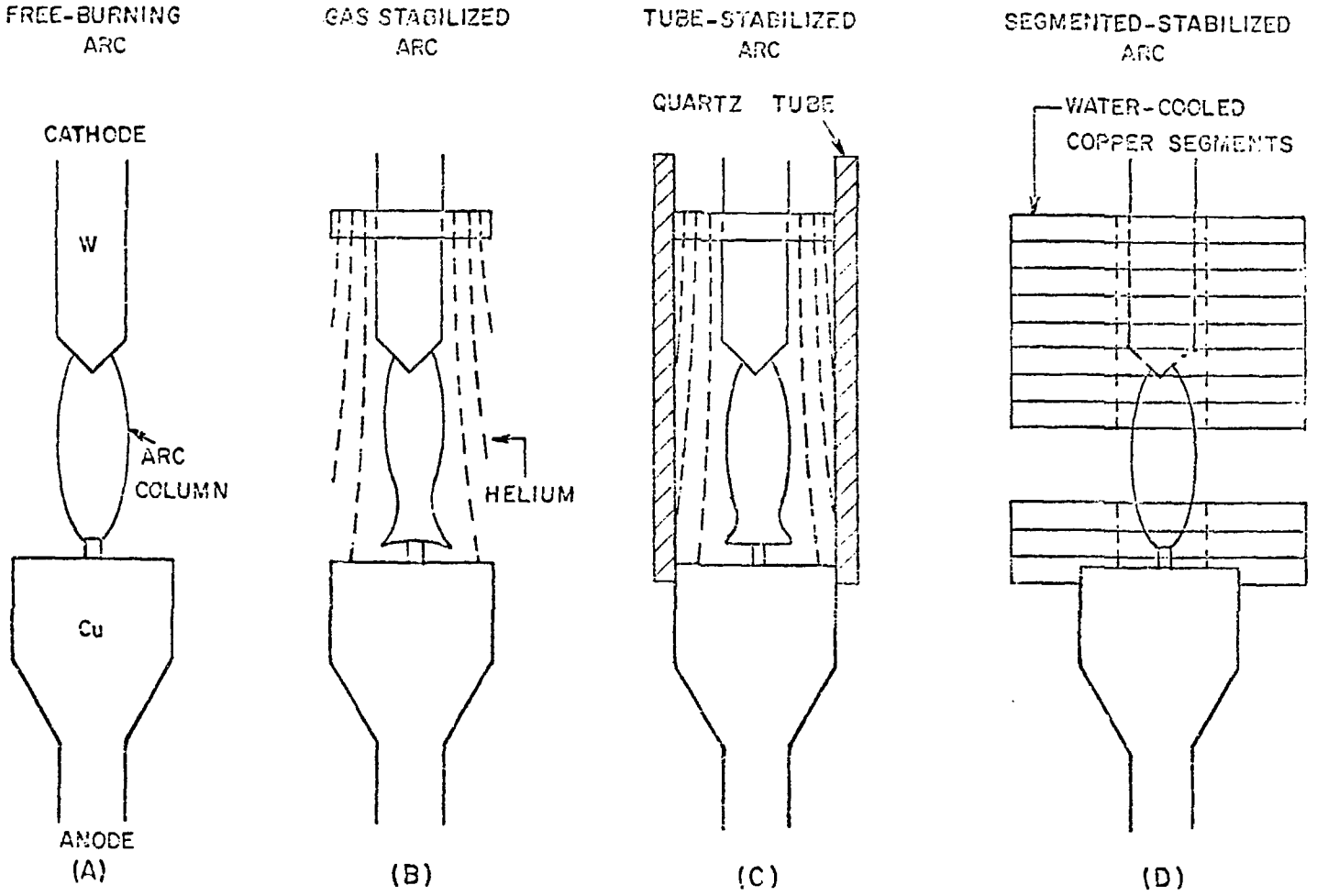

Fig. III-6. Uranium arc configurations.

such as sharply pointed and polished electrodes, changes in arc gap, changes in electrode diameter, and different cooling rates, but all were inadequate.

B. Gas-Stabilized Arc

Next, a gas distribution head was used to localize large-scale movement of the arc column (Fig. III-6B), and cover gas (helium) was directed downward from the gas head the length of the arc column. The flow contact with the anode caused a divergence of the cover gas at the uranium pellet and a bell-shaped cover-gas flow pattern formed. The cover-gas flow boundary formed the "wall" needed for arc-column localization.

C. Tube-Stabilized Arc

Stabilization was enhanced by forced containment of helium gas flow along the arc column (Fig. III-6C). A quartz tube was placed concentrically with the electrode vertical axis and helium was forced the length of the quartz tube. The restricted flow greatly reduced the helium turbulence and its effect on the outer and inner arc column. However, within five munutes of run time significant particle deposition coated the quartz tube causing unpredictable intensity attenuation and prohibiting long-duration (photoelectric) measurements.

D. Segmented-Stabilized Arc

The segmented assembly (Figs. III-2 and III-6D) replaced the quartz tube from the previous case and reduced the deposit problem at the viewport. The vacuum (low-pressure) segmented arc provided stability for photo-electric intensity, temperature, and density measurements, while the high-pressure segmented arc exhibited marginal stability acceptable only for photo-electric intensity measurements. The

segmented-arc configuration was the final step attempted in the quest for superior arc stability. Even with marginal stability at higher pressures, this system was employed for most of the experiments reported here.

III-3. Data Acquisition

Spectroscopic diagnostics required detection and analysis of radiation emitted by the uranium arc plasma. The experimental effort of this research was composed of two broadly defined categories.

(1) the measurement of intensity (emission), and

(2) diagnostics for temperature-density determination.

Figure III-7 illustrates necessary components for simultaneous measurements of intensity (to 2500 Å), temperature, and low-pressure arc density. Intensity measurements which extended into the vacuum uv were performed using a third spectrograph (McPherson Model 218, not shown) designed specifically for use at low wavelengths. Temperature and density for a high-pressure arc were inferred from photographic spectral analysis completed by Randol[51] and Mack[52] using a free-burning arc at similar I-V conditions. Details are in Chapter V.

A. Spectral Line Profile and Absorption Data for the Low-Pressure Arc

The modified BEM (Sec. II-4D) was used to determine the line-center absorption coefficient and characteristic plasma temperature for the low-pressure arc. The background source was a xenon flashtube (EGG FX-12-25). The firing and delay schematic is in Fig. III-8. Flashtube calibration information follows in Sec. III-3C.

Figure III-7 shows the sequence which established line absorption, temperature, and density: the beam splitter passed part of the arc radiation to S_1. A rotating refractor plate (quartz) in conjunction

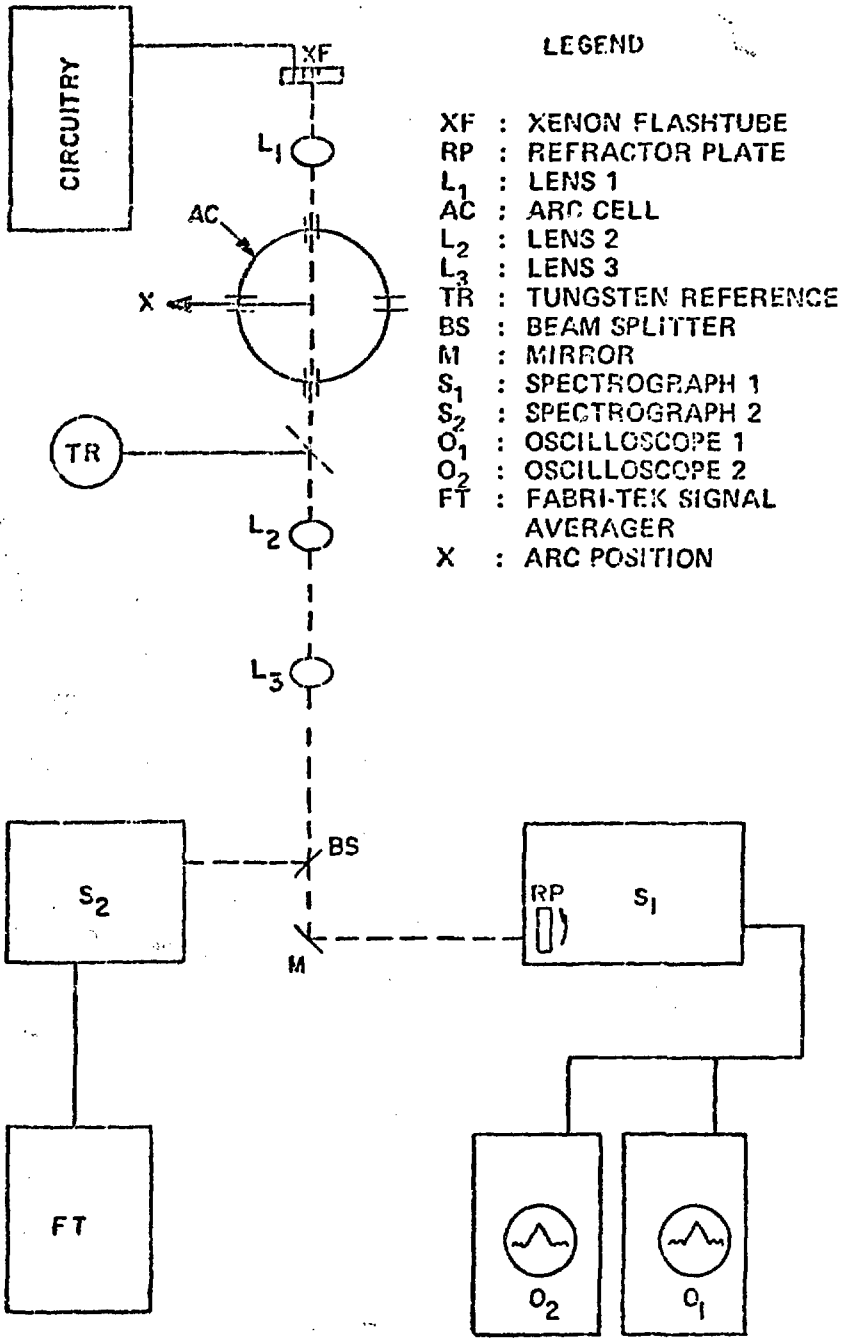

Fig. III-7. Simultaneous data acquisition system.

with spectrograph (S_1) used as monochrometer, swept a particular line of interest across the exit slit plane of S_1. An RCA 1P28 phototube placed behind the S_1 exit slit responded to the spectral line as it moved past. That line profile was recorded by oscilloscopes by O_1 and O_2. At the instant the sweep reached the central wavelength of the line profile, the xenon flashtube triggered. This enabled the flashlamp radiation to be superimposed on a specific spectral line center (Fig. II-3). Flashtube timing was accomplished by electronic delay circuitry shown in Fig. III-8. The ground-state particle density was determined from the line profile of oscillograms O_2 with the absolute line method; line center absorption and the plasma temperature were determined from oscillograms O_1.

B. Photoelectric Intensity Data

Photoelectric intensity measurements were made from 2000 Å - 5500 Å for the low-pressure uranium arc and from 1050 Å - 6000 Å for the helium-uranium (high-pressure) arc. Intensity of the low-pressure uranium arc as a function of wavelength in the visible and near uv were recorded by using part of the data acquisition system shown in Fig. III-2. A scanning spectrograph S_2 received arc radiation reflected from the front surface of a beam-splitter. The phototube response was monitored and stored digitally by a signal-averager [a time-averaging digitizer that integrates (smooths) small random input voltage (arc) fluctuations] which resulted in very reproducible arc intensity traces as a function of wavelength. Four memory areas within the signal-averager were used for storage of the spectral intensity $I_\lambda(x)$, where x is a particular LOS position in an arc traverse. A four-point Abel unfolding for spatial resolution of the arc intensities was performed

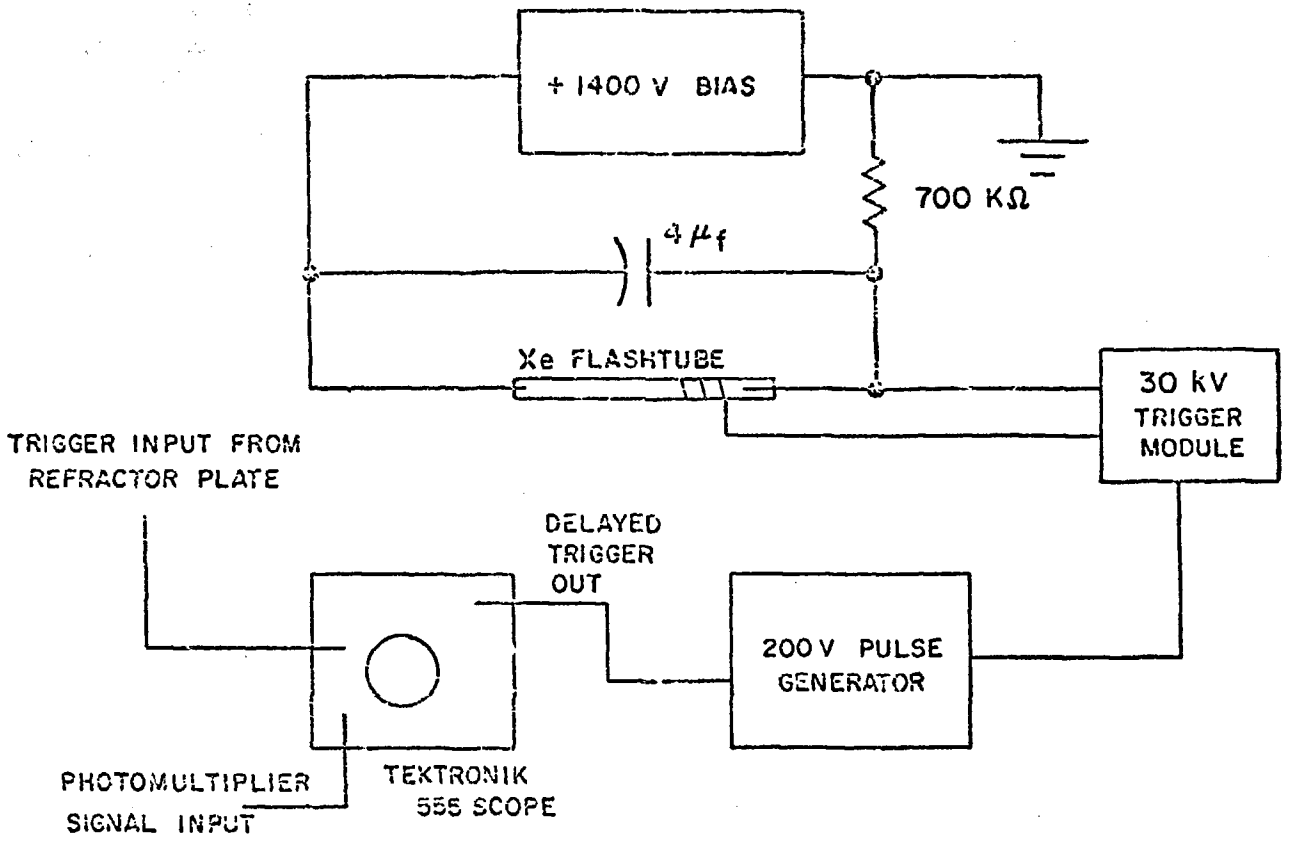

Fig. III-8. Xenon flashtube - firing and delay schematic.

to obtain the spectral emission coefficient $\varepsilon_\lambda(r)$, where r is the radial distance from the arc center. The limited arc stability duration prevented more than four acceptable LOS intensity measurements. Oscilloscope O_2 was used to trigger the signal-averager sweep at the desired wavelength. Ultraviolet transmission through the optical system was carefully investigated to be certain that no glass was present and to study the system attenuation properties. The 2537 Å Hg spectral line generated by a very stable mercury discharge was chosen for these purposes. The line was transmitted with negligible attenuation and contamination signals produced by internal reflections within the spectrograph S_2 were removed with baffles.

The photomultiplier used with S_2 was an EMI-9514 with a sodium salicylate window which acted as wavelength shifter from the ultraviolet to the visible. The phototube-sodium salicylate combination greatly improved the system wavelength sensitivity to ultraviolet and vacuum ultraviolet radiation. Sodium salicylate was ideal for use in the uv and vacuum uv because it possesses a nearly constant quantum efficiency from 500 Å to ~ 3300 Å.[53] The fluorescent radiation spectral distribution maximum is 4300 Å and 10% of the maximum at 3800 Å and 5300 Å,[46,53,54] which conforms to the maximum wavelength response of many photomultipliers.

For vacuum uv intensity detection the McPherson (Model 218) spectrograph designed to be responsive at wavelengths in the vacuum uv was used in conjunction with the photomultiplier signal-averager system previously described. This particular spectrograph contained magnesium fluoride-coated (Al + MgF_2) optics, a 2400-groove/mm grating blased for 1500 Å, and a vacuum capability of at least 0.001 μ. The vacuum uv

region is reported only for the helium-uranium arc plasma because of its relatively higher temperature and correspondingly stronger emission in this wavelength region. The low-pressure arc did not have noticeable emission in this wavelength region.

In some instances, it was physically impossible to interchange the source with a reference standard at the same location; therefore, we used a symmetric arrangement of the calibration and uranium sources in which the light-path attenuation for either source was identical. We eliminated unwanted stray radiation from within the spectrograph, which is particularly critical in the vacuum uv where the signal detection is difficult. Many intensity-wavelength scans were taken below 2000 Å with a deuterium lamp (Oriel, C-42-72-12) in several orientations after each helium-uranium arc run to insure optimal signal transmission. These signals were carefully checked to minimize higher order contamination and internal reflections.

C. Intensity Calibration

For radiation calibration in the visible and near-uv wavelength regions, the tungsten lamp and the positive crater of a carbon arc as standards are adequate; however, these sources are unacceptable for lower wavelengths because of the weak intensities below 2500 Å.[55] In fact, below 2500 Å there are few commercially available standard calibration sources. LTE hydrogen discharges (fill gas is either hydrogen or deuterium) are the best potential sources, but they require extensive investigation for their own respective properties. The theoretical description of the hydrogen atom is essentially complete, and once the electron densities are known, the intensities are computed and cross-checked by experiment to provide calibration information for

such a discharge. Therefore, two calibration sources were used: a tungsten lamp for the visible and near uv, and a deuterium discharge for the uv and vacuum uv.

Two tungsten filament lamps made by the Eppley Company were used for intensity calibration in the visible and near uv. One was calibrated by the NBS and designated the "standard lamp"; the second served as a "reference lamp." The reference lamp was used as the experiment standard but periodically cross-calibrated to the standard lamp. The calibration curve for the standard lamp is given in Fig. III-9. The associated accuracy of the values was stated to be ±10%.[56]

A deuterium discharge was used to calibrate intensities below 2500 Å. The lamp had a suprasil fused-silica window with a 50% transmission point at about 1750 Å, and a calibration point at 1662 Å was the apparent lower wavelength limit. Figures III-10 and III-11 show the wavelength dependence of the spectral radiance at two current modes. The absolute intensities as calibrated from this lamp carry a ±10% uncertainty,[57] verified by cross-check of the deuterium lamp intensity against the tungsten filament standard at four different wavelengths above 2500 Å. The percentage difference between the quoted deuterium intensities and the cross-checked intensities was always within the uncertainty limits. The percentage difference tended to increase toward the lower wavelengths and the calibration points below 2000 Å are associated with an unknown maximum uncertainty less than ±10% up to 1750 Å. The last deuterium calibration point resides at 1662 Å as dictated by the fused-silica window cutoff of the discharge lamp. The 1662 Å calibration point is below the fused-silica 50% transmission wavelength of 1750 Å and is quite uncertain.[57] Calibration for intensity data to the

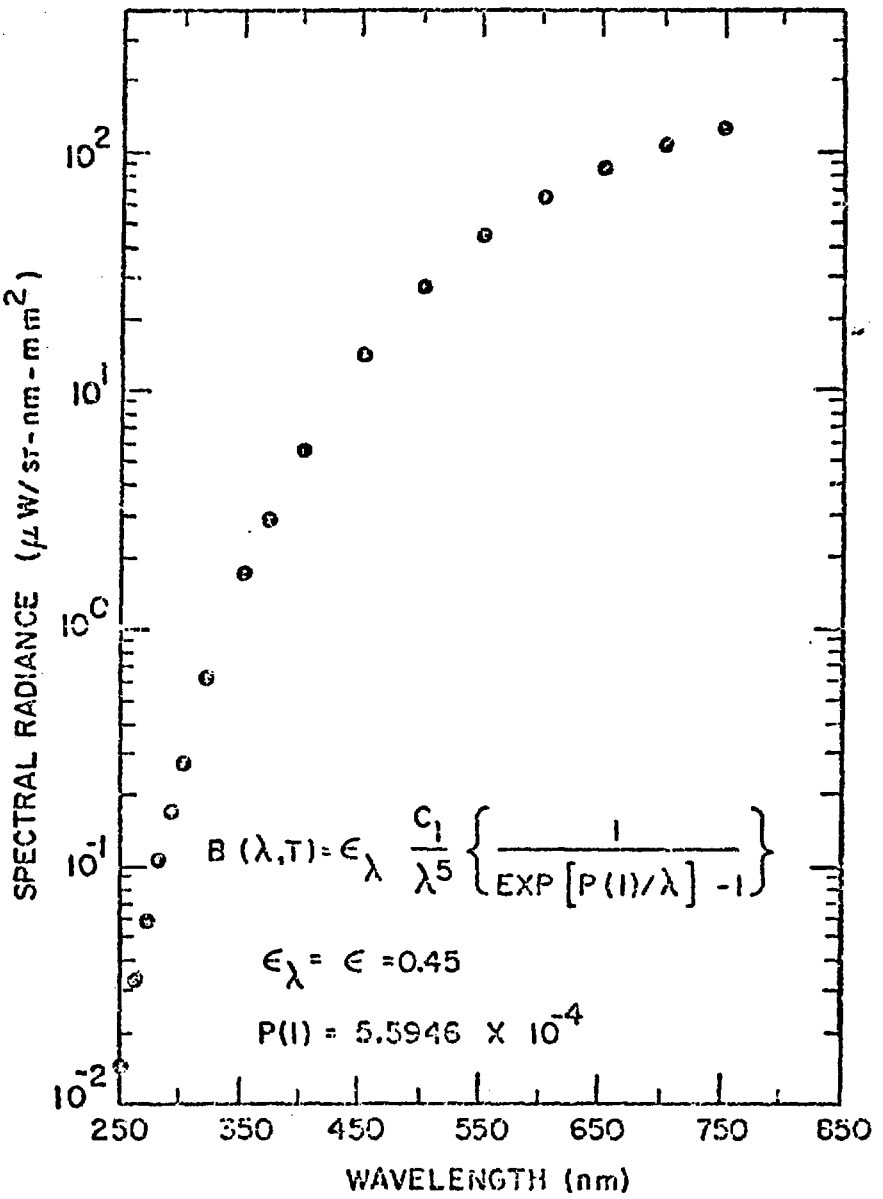

Fig. III-9. NBS tungsten standard lamp calibration, (EPUV-1148)--35 amperes.

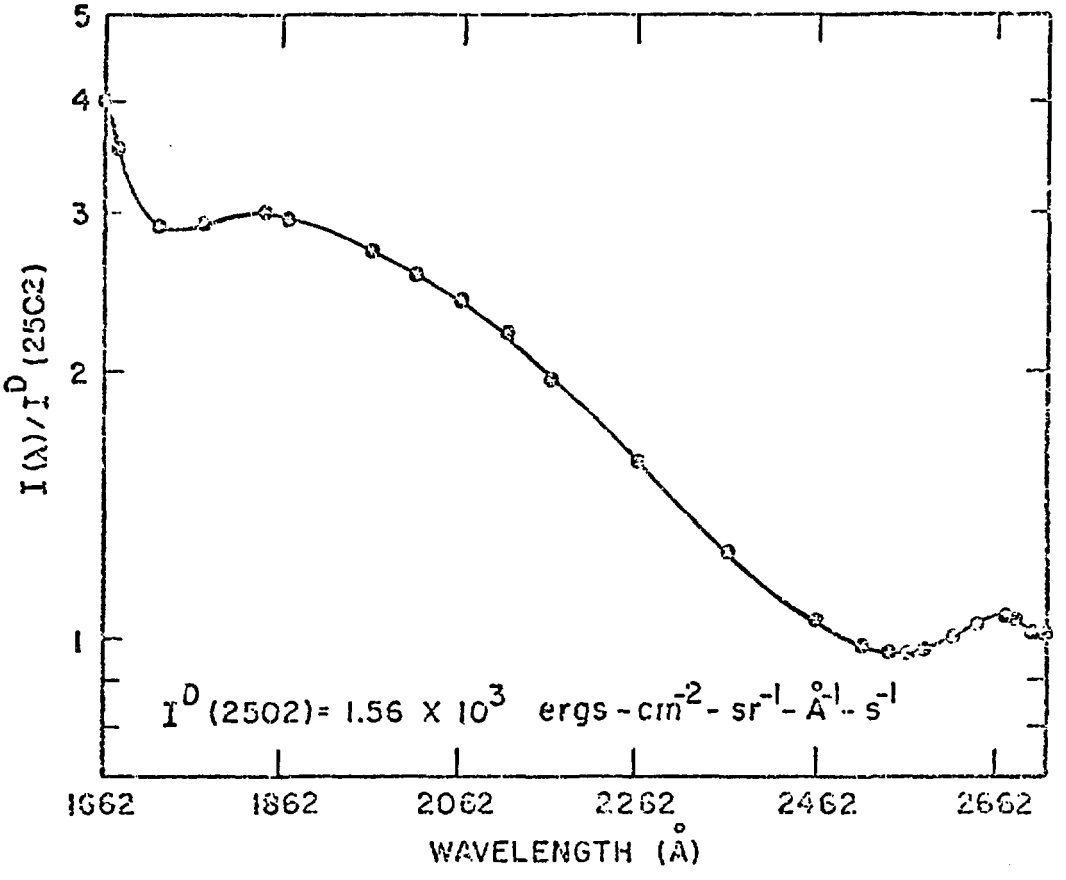

Fig. III-10. Deuterium lamp calibration curve, Kern lamp at 300 ma.

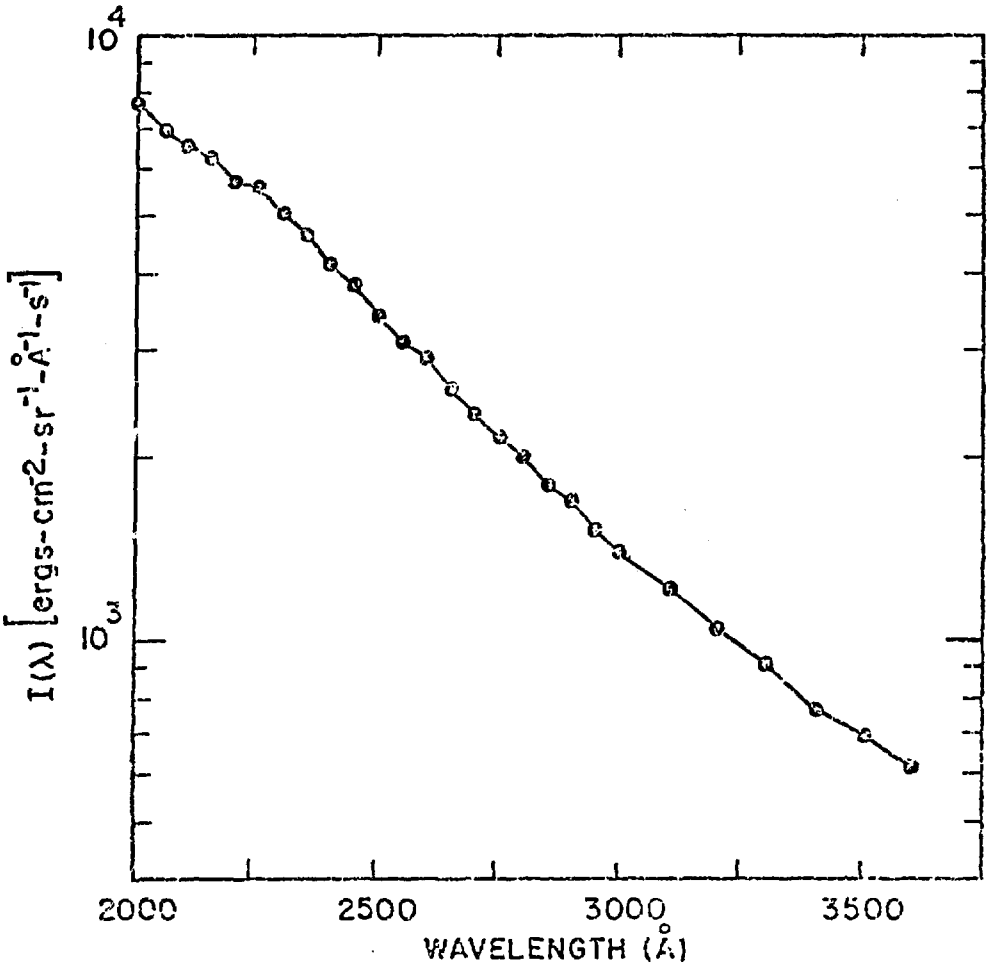

Fig. III-11. NBS deuterium lamp calibration curve, Oriel lamp at 315 ma.

LiF cutoff (1050 Å) called for an approach which did not require explicit standard calibration points at the lower wavelengths.

The branching-ratio technique was considered for absolute intensity calibration in the vacuum uv and it is based on the intensity partition of at least two spontaneous optically thin transitions with a common upper level.[58,59] The intensity ratios of these two lines is a strict function of the transition-probability ratio and independent of plasma inhomogeneities and LTE. To apply this technique in the vaccum uv, one transition must appear in the visible and the other in the vacuum uv. This method is sound provided isolated spectral lines exist and well-defined transition probabilities are used. The application of branching-ratio calibration to uranium spectra fails in both respects.

Back-extrapolation calibration (BEC), an approximate technique, was used. Helium-uranium arc intensity data were collected in bandwidths 900 Å → 1750 Å → 4300 Å. Intensities above 1750 Å were calibrated against the deuterium discharge and tungsten standard; whereas arc intensities at wavelengths below 1750 Å were assigned absolute units by BEC. (Intensity signals from the low-pressure uranium arc required calibration down to 2500 Å which was done with the tungsten standard.)

Intensity calibration using a standard source is essentially a system response comparison of (in this case a spectrograph-photomultiplier combination) a known photon flux to a photon flux of an unknown source. The absolute intensity of the unknown is then related to that of the standard by:

$$I_{ARC}(\lambda) = I_{STD}(\lambda) \frac{\phi_{STD}(\lambda)}{\phi_{ARC}(\lambda)} \frac{V_{ARC}(\lambda)}{V_{STD}(\lambda)} , \qquad \text{(III-1)}$$

where $I_{ARC}(\lambda)$ = arc intensity [ergs/cm^2-sec-Å-str] at λ,

$I_{STD}(\lambda)$ = standard source intensity [ergs/cm^2-sec-Å-str] at λ,

$\phi_{STD}(\lambda)$ = optical path reduction factor (%) for the standard source at λ,

$\phi_{ARC}(\lambda)$ = optical path reduction factor (%) for the uncalibrated source at λ,

$V_{STD}(\lambda)$ = response signal (volts) of optical system to standard photon flux at λ, and

$V_{ARC}(\lambda)$ = response signal (volts of optical system to uncalibrated photon flux at λ.

If the standard and uncalibrated sources are in identical orientations, the optical path reduction ratio $\phi_{STD}(\lambda)/\phi_{ARC}(\lambda)$ will cancel. The system response will inherently be accounted for in the $V_{ARC}(\lambda)$ and $V_{STD}(\lambda)$ signals. Equation (III-1) is valid as long as $I_{STD}(\lambda)$ is known, in this case to the 1750 Å cutoff of the deuterium lamp fused-silica window. To apply Eq. (III-1) to wavelengths less than 1750 Å, a system response below 1750 Å for the standard source intensity as a function of wavelength must be assumed.

The wavelength dependence of system response below 1750 Å was assumed flat and equal to 1.0, which implies that the combined effect of the incident (to the optical system) photon flux on transmittance caused by losses in all of the intercepted optical elements is negligible. This is categorically not the case. However, such a tactic provides a straightforward approach to a conservative estimate of the correct absolute intensities. Relating this idea to Eq. (III-1), a unique intensity implies a unique system voltage with no wavelength dependence. Knowing the absolute intensity of the standard and its

corresponding voltage at 1750 Å in addition to the arc intensity system response voltage for all wavelengths of interest below 1750 Å, the absolute arc intensity may be estimated by solving:

$$I_{ARC}(\lambda) \simeq \frac{I_{STD}(1750\ \text{Å})\ V_{ARC}(\lambda)}{V_{STD}(1750\ \text{Å})} \quad . \tag{III-2}$$

$V_{ARC}(\lambda)$ retains the system response to the arc intensity, but the wavelength dependence of the system response to the standard intensity cannot be recorded because of the window cutoff. Therefore, assuming the negligible optical loss, the arc intensities are underestimated by the composite optical loss factors and whatever molecular absorption is present.

Whenever an approximation is applied, as was the case with the intensity calibration in the vacuum uv, an indication of uncertainty is valuable. In this investigation the uncertainty was a function of the attenuation of photon flux incident on the optical elements of the system composed of a 10-mm LiF window, two spectrograph mirrors, the sodium-salicylate phototube window, and the grating. (The spectrograph mirrors and grating were Al-MgF_2 coated). A composite wavelength-dependent transmission curve can be constructed if transmission/reflectance data for each optical component are available. This total curve can then weight the appropriate system response voltage, thereby recovering (to a first approximation) the photon losses as the field passes through the optical system.

Reflectance-wavelength information is available in the literature[60,61] for coated and uncoated optics as is transmission data for LiF.[62,63] The grating efficiencies for the McPherson 2400-groove/mm

grating blazed at 1500 Å (Al-MgF_2 coated) were furnished by Quartz et al.[64] Table III-1 is a compilation of the relevant information which allows construction of a composite system transmission curve. These data provide an approximation of intensity calibration error (using back-extrapolation) based on system optical losses. The quantum efficiency of the sodium salicylate phototube window was assumed to be approximately unity[65] with a constant wavelength dependence.[53,65,66]

The composite efficiencies of Table III-1 indicate that back-calibration intensity values can be in error at the longer wavelengths (1750 Å) by a factor of 6 and more toward shorter wavelengths. A calibrated "signal" detected below 1200 Å is suspect because of the sharp LiF cutoff near 1200 Å as shown by Table III-1.

Use of the xenon flashtube for temperature-absorption diagnostics required a calibration for dependence of brightness temperature on wavelength. This was accomplished by comparison (at a desired wavelength) of the system response to the xenon discharge and to an NBS-calibrated tungsten-filament lamp.[67] A xenon lamp brightness temperature of 6745 K ± 100 K was established in a wavelength range of 3600 Å → 5400 Å.

TABLE III-1

VACUUM UV SYSTEM RESPONSE

λ[A]	Grating Efficiency[a]	Al+MgF_2 Mirror Reflectance[b]	Reflectance Mirrors	LiF Transmittance[c]	Composite Transmission	Composite Buildup[d]
1050	0.06	0.30	0.09	0.10	0.00054	1852
1100	0.06	0.49	0.2401	0.20	0.00288	347
1200	0.32	0.78	0.6084	0.40	0.08709	12
1250	0.37	0.82	0.6724	0.55	0.1368	7.3
1300	0.40	0.82	0.6724	0.60	0.1614	6.2
1400	0.36	0.80	0.64	0.76	0.175	5.7
1500	0.43	0.78	0.6084	0.75	0.1962	5.1
1600	0.35	0.76	0.5776	0.80	0.1617	6.1
1700	0.32	0.76	0.5776	0.86	0.1589	6.3
1800	0.31	0.81	0.6561	0.87	0.1769	5.7
1900	0.30	0.83	0.6889	0.88	0.1818	5.5
2000	0.30	0.83	0.6889	0.89	0.1839	5.4

[a] Ref. 64

[b] Ref. 60, 61

[c] Ref. 62

[d] Build-up factors indicate the multipliers necessary to account for losses at a specified wavelength to increase the detected signal to its no-loss value.

IV. LOW-PRESSURE URANIUM ARC DATA REDUCTION

IV-1. Spectral analysis

Spectra emitted by the low-pressure uranium arc plasma (∿ 300 torr) were identified manually and by computer.[68] They exhibited a mixture of atomic (UI) and singly ionized (UII) uranium line structure, but dominated by atomic uranium emission lines. For diagnostic purposes the 3653.21 Å and 3659.16 Å UI emission lines were used. The 3653.21 Å line is reported[69] to have upper and lower levels at 31 166 cm^{-1} and 3801 cm^{-1}, respectively. It was selected primarily because of its relatively high-lying lower and upper levels, which enhanced the possibility of evaluating energy states populated above the thermal limit if partial LTE existed. The 3659.16 Å line was chosen for the same diagnostic purposes (temperature and density measurements) as the 3653.16 Å line. Its transition is between levels 27 941 cm^{-1} and 620 cm^{-1}.[69] The first excited level of atomic uranium is 620 cm^{-1} and it would be less likely to meet LTE criteria. A comparison of temperature-density diagnostics using the lines with two distinctly different lower levels served as one useful indicator of the validity of LTE assumptions. While energy level was a prime line-choice factor, the spectral lines were also selected on a basis of wavelength, relative isolation (from the other nearby lines), identification certainty, and availability of transition probabilities for transitions considered.

IV-2. Temperature Measurement

The electron temperature was measured by the modified brightness-emissivity method (Sec. II.4). First, it was necessary to obtain line-center absorption coefficients as a function of arc radius by applying flashtube absorption diagnostics (Sec. III.3A). Line-center absorption profiles using the 3653.21 Å and 3659.16 Å UI transitions are shown in Fig. IV-1 and represent absorption measurements taken during the best conditions of arc stability and flashtube firing. The two reported profiles indicate maximum absorption at the arc center which is usually the region of maximum temperature.

Uncertainty in absorption coefficient values was both numerical and experimental. The unfolding scheme converting $\kappa_0(x) \rightarrow \kappa_0(r)$[47] was responsible for the numerical uncertainty, and the accuracy of the oscillogram voltages defined the primary experimental error (κ_0 indicates the line-center absorption coefficient). The oscillograms contained recorded voltages representing the flashlamp intensity attenuated by the plasma as well as the true plasma intensity. The plasma voltage uncertainty was mainly caused by arc intensity change which fell within +2% during data collection. Flashlamp attenuation uncertainty resulted from arc intensity fluctuation, flashlamp intensity variation, and arc cell viewport attenuation.

Since the flashlamp was located behind the arc cell, its light output passed through two viewport windows in the segmented assembly (Figs. III-1 and III-2); whereas the arc photon field passed through only one on its path to the detector. During arc operation, deposits occurred on both viewports; line-center absorption of the light emitted by the flashlamp was recorded photoelectrically at four points from the arc

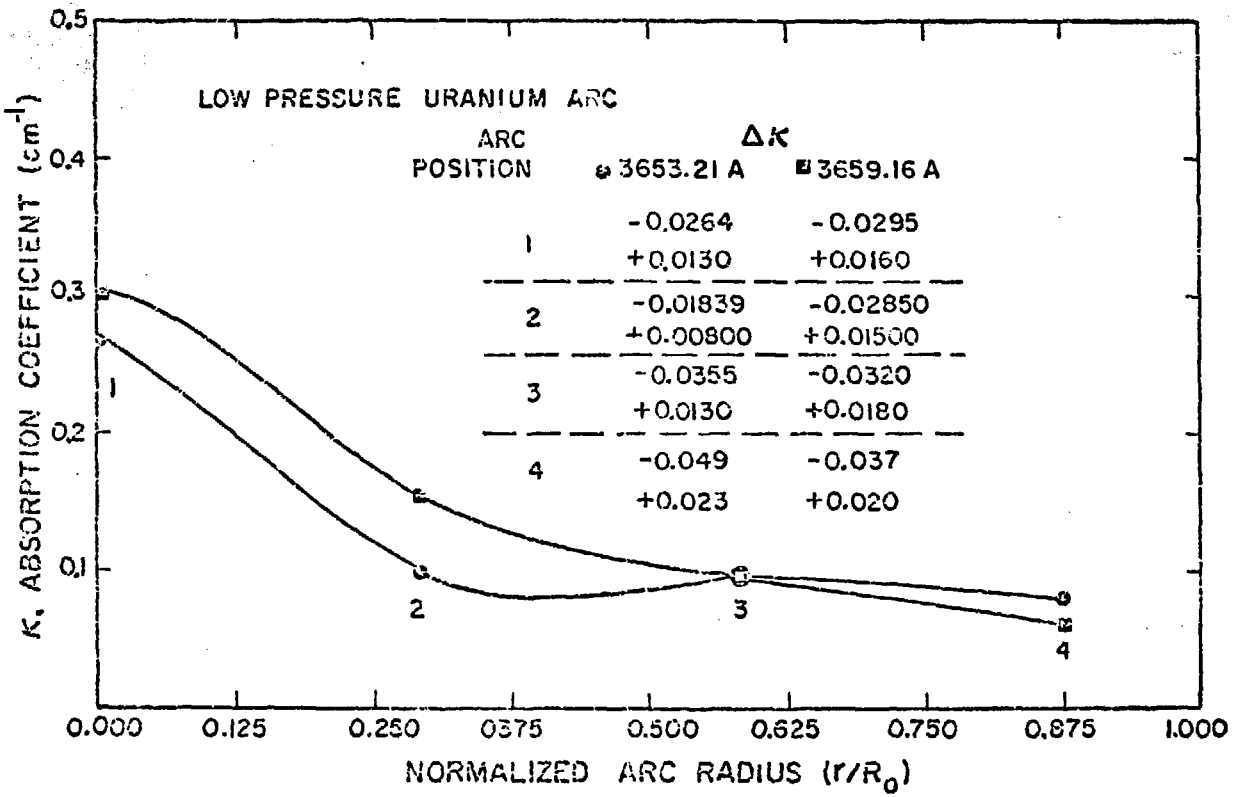

Fig. IV-1. Line-center absorption coefficient profile.

center outward, thus the values at further distance from the arc center were more uncertain. Usher[47] has considered all of these possible contributions to absorption profile uncertainty. Using an argon arc with the same experimental apparatus as this uranium arc, Usher[47] found a fairly constant absorption profile uncertainty across the arc. This was not true of the uranium arc because the viewport deposition problems resulted in a larger absorption coefficient uncertainty as outer regions of the arc were approached. The flashlamp intensity was degraded because its radiation field passed through two viewpoints (as opposed to one for the arc plasma emission), resulting in overestimates of the true absorption coefficient values at all points along the arc radius. Error analysis showed that these estimated uncertainties were $\sim$ 10% at the centerline to $\sim$ 62% at the outer point.

The apparent uncertainties of radial absorption coefficients influenced the temperature computation uncertainty. Again, the error analysis of Usher[47] was used to obtain temperature uncertainties. Figure IV-2 illustrates the radial temperature dependence for the low-pressure arc plasma. The uncertainty limits generally increase as the arc center is approached. If we consider that the uncertainty calculated for the outer radial location is propagated to the central locations, it is possible that the innermost temperature will have an associated uncertainty greater than that of the outermost temperature value. Therefore, while the outermost temperature had the largest experimental error, the central temperature had the largest total error. Several temperature profiles were determined using both transitions (3653.21 Å, 3659.19 Å), and Fig. IV-2 shows results for each transition. The 3653 Å diagnosis typically showed a very reproducible

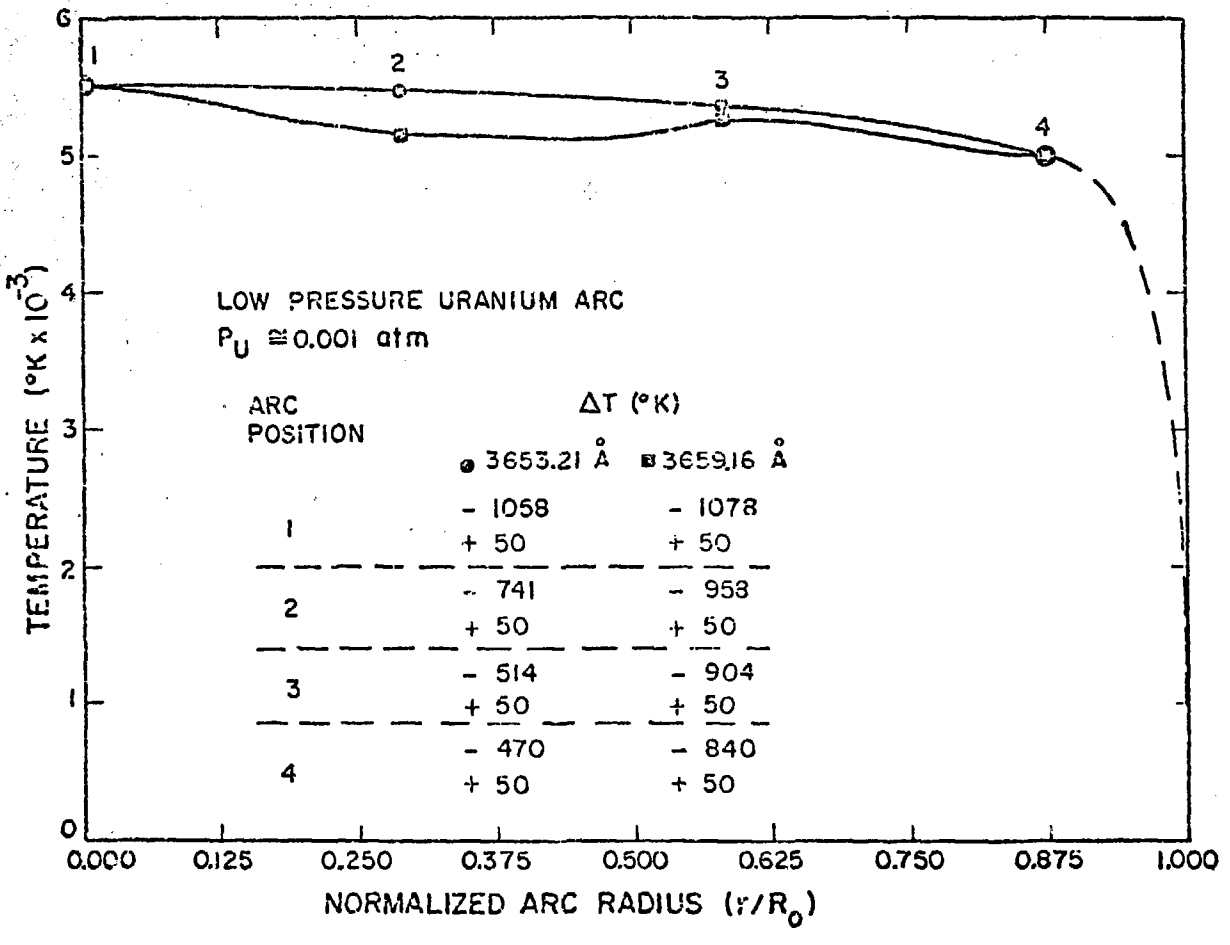

Fig. IV-2. Low-pressure uranium arc temperature profile.

temperature profile; whereas the 3659 Å transition indicated less reproducibility. The profiles from both transitions compared rather well and offered supporting evidence for the existence of LTE conditions within the bulk of the arc column down to fairly low-lying levels.

Of particular interest is the rather flat radial temperature dependence. There have been numerous flat temperature profiles reported for various wall-stabilized arc plasmas.[32-38] Plasma confinement using a cooler material wall generally results in a reduction of the temperature gradient from the arc center toward the wall. In many cases, conduction loss is not the only contributor to the profile curvature. Conductive heat transfer along the arc temperature gradient to the wall and radiative transfer losses, which are strongly dependent on the plasma conditions and type of radiating species, account for most of the energy loss from an arc. That a flat temperature profile in wall-stabilized arcs can be realized is substantiated in the literature and not in controversy; at issue is the rationalization of such a temperature profile for a wall-stabilized uranium arc which is measured by this investigation.

The temperature profile for wall-stabilized arcs must be consistent with the energy-balance equation given by

$$\sigma E^2 = \nabla \cdot F_C + \nabla \cdot F_R \quad , \qquad \text{(IV-1)}$$

where σ = electrical conductivity,

E = electric field,

F_C = conduction flux density, and

F_R = radiation flux density.

The implication is that the electrical energy input to a steady-state arc plasma balances the radiation and conduction losses (convection being neglected). Conduction loss is governed by the temperature profile gradient; whereas, radiative losses are defined by the equation of radiative transfer, Eq. (II-3).

Temperature profile curvature will be a function of the relative magnitude of the conduction or radiation loss terms. If radiation effects are negligible, conduction becomes the dominant loss mechanism, resulting in an approximately parabolic temperature profile with a comparatively high central temperature as shown in Fig. IV-3.[34] When radiation losses become important, the central temperature is generally lowered and the profile shape flattened. Also included in Fig. IV-3 are the effects of self-absorption on the temperature profile. In general, having zero absorption implies a smaller central temperature caused by the larger radiation loss term. A flatter profile also results because most of the curvature is caused by conduction near the wall. When absorption is included, the result is an increase in central temperature and more radial curvature. The curvature of the profile at the arc center is typically controlled by radiation losses, while at the arc boundary such curvature is usually controlled by conduction losses.

Several parameters affect the magnitude of conduction and radiation loss terms. Generally, wall-stabilized arcs exhibit high radiation losses at higher pressures, greater temperatures, smaller radii, and at greater emission density of the dominant radiating plasma constituent.[34,35,70,71] The current and pressure of the low-pressure uranium arc would indicate that the temperature profile shape would

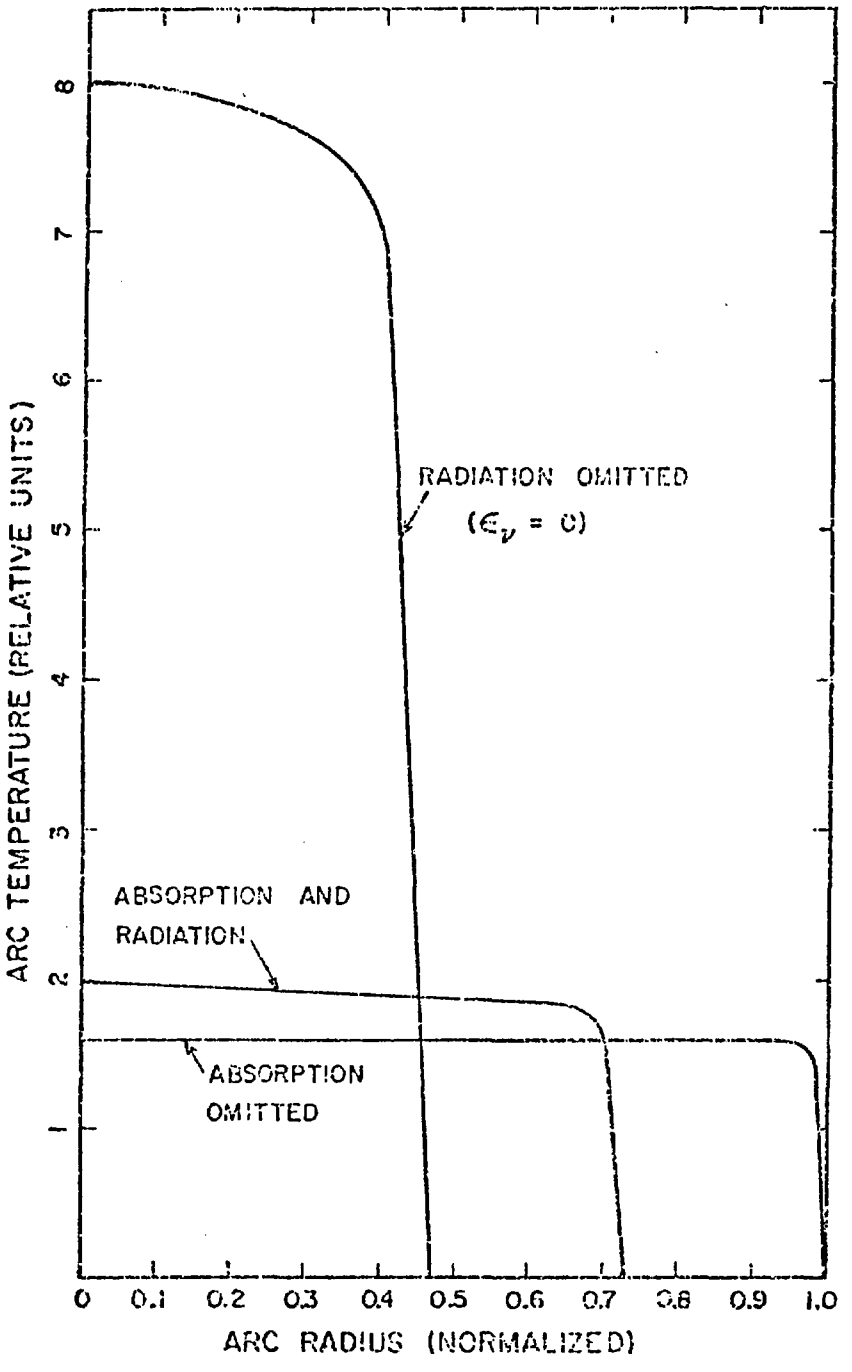

Fig. IV-3. Effect of radiation on arc profile.

not be highly flattened except for the significant radiation flux loss produced by such a dense emitter as uranium. The striking lack of temperature profile curvature (till the arc boundary is approached) can be reasonably attributed to the dense core radiation characteristic of excited uranium in a wall-stabilized configuration.[72] Shumaker[73] has shown that nitrogen and argon wall-stabilized arcs operating at similar current, voltage, and pressure conditions produced temperature profile shapes of different degrees of curvature. The radiating species with the denser characteristic radiation (argon) produced the flatter temperature profile.

From LTE considerations the normal temperature (Sec. II.4B) for several UI transitions was calculated to be about 5000 K at 0.001 atm uranium pressure. The 5500 K measured temperature indicated a mixture of UI and UII radiating species with UI dominating, which was consistent with the spectral analysis. (See Appendix A for Saha equation number density and normal temperature curves). The probability that partial LTE exists also implies that the gas temperature differs from the electron temperature--magnitude of difference is questionable. This problem has been studied by Gurevich[74] who used mercury and argon discharges at total pressures from 0.1 to 1 atm. Their technique essentially monitors the distinct cooling of the electrons to the gas temperature and subsequent general cooling of the plasma. The intensity output tracks the cooling and can be followed with a scope-phototube combination. The method is sensitive to electron-gas temperature differentials as small as 0.5%. The conclusions are that the temperature differential is a strong function of total (and electron) pressure and weak function of arc current. The extrapolated temperature differential

for the present arc could be as much as 100 K to 200 K because of the partial LTE state arc plasma.

IV-3. Density Measurement

The ground-state particle density (UI) for the low-pressure uranium arc was determined by the absolute line method (Sec. II.5A). This method involved the shape definition of the desired spectral line, its absolute intensity calibration, an independent temperature measurement, and uncertainty estimation. The exact line profile could not be defined because of the large line-overlap characteristic of uranium spectra. A Voigt analysis[49] was used to approximate the line area of the same lines (3653 Å, 3659 Å) used for the temperature measurements. Because these data were taken simultaneously with the intensity-wavelength information, significant temporal fluctuation should be common to all and treatment of fluctuation was unnecessary. Line intensity calibration was performed with a tungsten-filament NBS-calibrated lamp. No attempt was made to establish a radial density profile because associated errors negated the effort. Line-center absorption was also accounted for by appropriate build-up factors. The calibrated UI ground-state density for the low-pressure uranium arc was $\sim 7 \times 10^{14}$ cm^{-3}. This value is an order-of-magnitude estimate of an approximate density radially through the arc column. Assuming uncertainties in spectral line area, gA, and temperatures of ±15, ±50, and ±20%, respectively, resulted in a density range of $1.28 \times 10^{14} \rightarrow 7.89 \times 10^{15}$ cm^{-3}. This indicated, from Saha analysis, that a nominal value for the uranium total pressure, rounded to the nearest integral logarithmic pressure, would be $\simeq$ 0.001 atm (1.3×10^{15} cm^{-3}).

The electron density, n_e, for the low-pressure uranium arc will generally follow the curve for singly ionized uranium. Saha equation calculations of n_e for a plasma with a total uranium pressure of 0.001 atm, T = 5500 K, predicts $n_e \simeq 6 \times 10^{14}$ cm^{-3}. This is well within the LTE ladder criterion of 3.8×10^{11} cm^{-3} established in Sec. II.1. Measurement of the electron density by an independent technique such as a line broadening analysis was too uncertain, primarily because uranium lines lacked isolation and definition. Therefore, this effort was abandoned and no direct experimental evidence of the magnitude of the electron density was obtained. However, similar work of Voigt[75] on a 5500 K uranium arc reported n_e to be $\sim 5 \times 10^{13}$ cm^{-3}. This substantiated the assumption of n_e large enough for the present arc to be characterized by at least partial LTE nearly at the ground level.

One of the more subtle aspects of this density determination was the implicit assumption of complete LTE. Strictly speaking, this is very difficult to realize, and one usually resorts to a commitment of partial LTE. If partial LTE is valid, an exact density measurement (using a diagnostic method which relies upon complete LTE, such as the absolute line method) is not possible, and any attempt will be in error because of this apparent conflict. The magnitude of this error can be calculated for hydrogen and estimated for helium. Unfortunately, for the case of uranium only a qualitative description of error direction is valid.[76,77]

The effect of the complete LTE assumption when there is only partial LTE can be understood by considering the population densities of a simple energy level diagram as illustrated in Fig. IV-4.

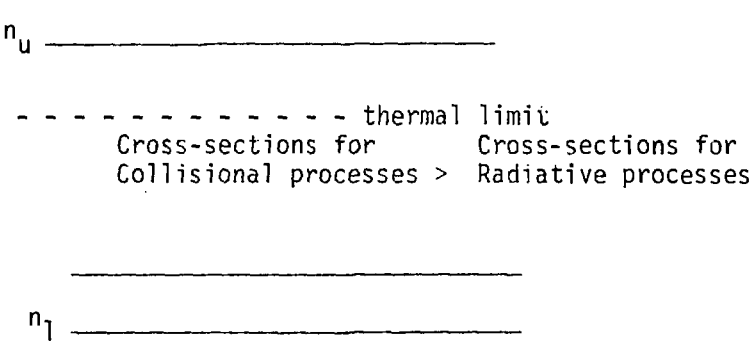

Fig. IV-4. Energy-level diagram with thermal limit.

When complete LTE exists, the population density of each level is defined by the Boltzmann Factor, $n_u/n_o \propto \exp[-E_u/kT]$. However, if partial LTE prevails, the population of levels below a thermal limit are influenced by radiative de-excitation from upper levels and self-absorption, particularly with transitions terminating at the ground level. Detailed definition of level population for uranium is virtually impossible, but in most cases one can argue that if partial LTE holds, the levels below the thermal limit will be over-populated. Thus, by assuming partial LTE and using complete LTE relations to determine the ground-state density, an underestimate results, probably proportional to some function of the thermal limit height above the ground level. The thermal limit in the uranium system cannot be well established; but from LTE criteria applied to the low-pressure uranium arc (Sec. II.1), it is likely to be close to ground level. If the thermal limit is close to ground level, the error incurred by using complete LTE relations to determine the ground-state population is "small." Because this is an order-of-magnitude measurement, such error is most likely to be insignificant at these temperatures and pressures.

IV-4. Emission Coefficient Determination

Spectral analysis of radiation structure emitted by the low-pressure uranium arc plasma indicated a preponderance of known UI line spectra mixed with some identifiable UII structure. The species-mix ratio is not available because of uncertainties involved in line identification on uranium spectra. However, at the maximum temperature of 5500 K a Saha ratio of n_{UII}/n_{UI} can approach 1.0, and cooler arc regions will be weighted toward larger values of n_{UI}.

Intensity from the low-pressure arc was observed at four equally spaced arc positions. Details of data acquisition are in Sec. III.3B. The spectrograph used for this study was a Hilger-Ingis (Model S05-10000) modified to a rapid-scan capability (1.28 s from 2000 to 6000 Å). A 1200-grooves/mm grating was used with a blaze angle of 17.2° corresponding to a wavelength of 5490 Å in the first order. Intensity calibration was performed using a tungsten-filament NBS-calibrated standard.

Preliminary experiments indicated a rapid decrease of arc intensity below 3500 Å and very little signal at wavelengths less than 2500 Å. Steinhaus et al.[18,19] also indicates little structure between 2000 and 2500 Å for UI. We decided that emission from this particular arc plasma below 2000 Å would be relatively insignificant, and the effort required to detect potential vacuum uv emission was not justified for this plasma.

The calibrated arc intensity-wavelength data is plotted in Fig. IV-5. Four similar sets of intensity data were generated for each arc burn; the data plotted in Fig. IV-5 corresponds to the central arc region only. The data acquisition method (signal averaging) produced

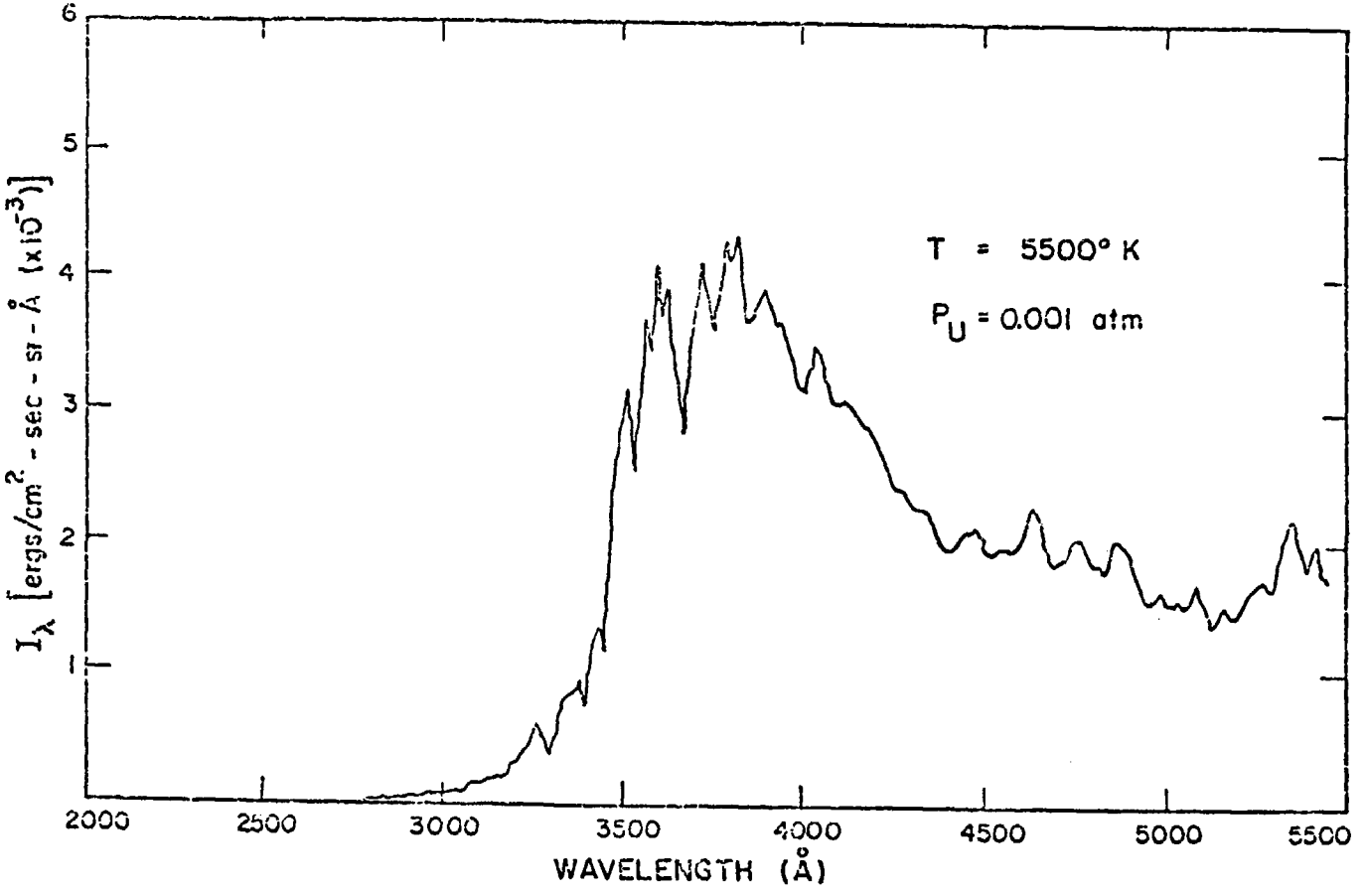

Fig. IV-5. Low pressure uranium arc calibrated intensity.

very reproducible intensity-wavelength data sets; only major arc intensity fluctuations could not be removed. When these major fluctuations occurred the data were discarded, thus, the data plotted in Fig. IV-5 is in error by the intensity uncertainty of the standard tungsten lamp calibration source, which is approximately ±10%.[55] The calibration of uranium plasma intensity was done using the "Plasma Source Calibration Program."[78] However, intensity data sets taken in the outer arc regions are in error by as much as +12 to 20% because deposition on the viewport interfered with the optical path from the plasma source to the spectrograph entrance slit.

The four intensity-wavelength data sets were spatially resolved by a four-point numerical Abel unfolding after averaging over 100 Å bandwidths. The results for this emission coefficient calculation in the central arc location are shown in Fig. IV-6. Error sources in these data are attributed to the absolute intensity calibration, viewport deposition, and four-point spatial resolution. The calibration and deposition errors have already been mentioned and are carried over to the emission coefficient determination. Spatial resolution error is much more difficult to address. It is composed of error caused by propagation of experimental uncertainties and the high probability of using a non-optimal zone number for the unfolding (statistical error).

Experimental error propagation through the inversion process was estimated by unfolding the data with and without such error included. The statistical error was estimated by relying on the analysis of Kock and Richter,[44] based on the form of the intensity profile, number of rings chosen, smoothness of profile, and maximum outer-zone experimental error. An exact match did not exist and extrapolation was

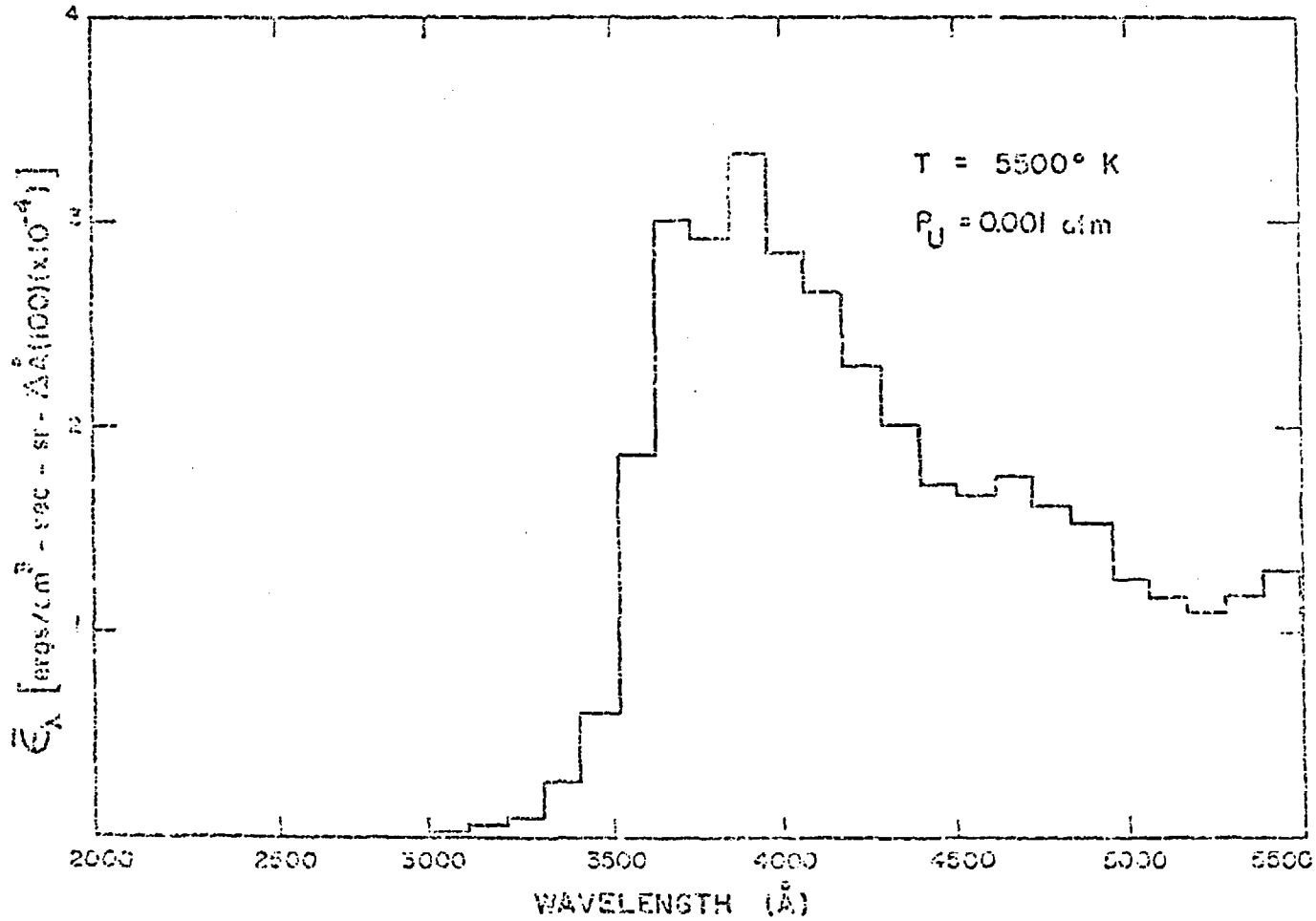

Fig. IV-6. Low-pressure uranium arc emission coefficient averaged over 100 angstrom intervals.

applied. Following the above approach, the error for the central zone emission coefficient shown in Fig. IV-6 should fall within -14% to +23%.

Credibility of the shape and location of the important features on the wavelength scale is questionable; unfortunately, there are no other data recorded at the same conditions for comparison. However, comparison data exist[18,19,79] for qualitative assessment of credibility.

Krascella[79] tried to approximate the intensity-wavelength distribution of an Argon-UF_6 system at temperatures varying from 5000 to 9000 K. Level populations were calculated through equilibrium relations, whereas partition functions, atomic constants, and observed line location were extracted primarily from Corliss and Bozman.[69] Using this information the possible integrated line intensities were computed and averaged over 100-Å bandwidths. This semiempirical technique lacks information about important quantities such as statistical weights, accurate transition probabilities, uncertain UF_6 decomposition schemes, and offers very incomplete uranium line structure tables. However, this work was valuable in establishing observable spectral distribution of electromagnetic radiation from uranium plasmas at various conditions and was useful for comparison to our results even though Krascella estimates had gaps. The comparison at least substantiated a trend in the emission coefficient shape. No comparison was made between absolute values because of the diversity in systems.

A comparison is shown in Fig. IV-7 where the Krascella data were shifted in magnitude to be superimposed upon our results which follow the shape trend shown by Krascella. The irregularities in the Krascella data (caused by the lack of experimental line data in the gap regions) are expected and do not detract from the conclusion that the

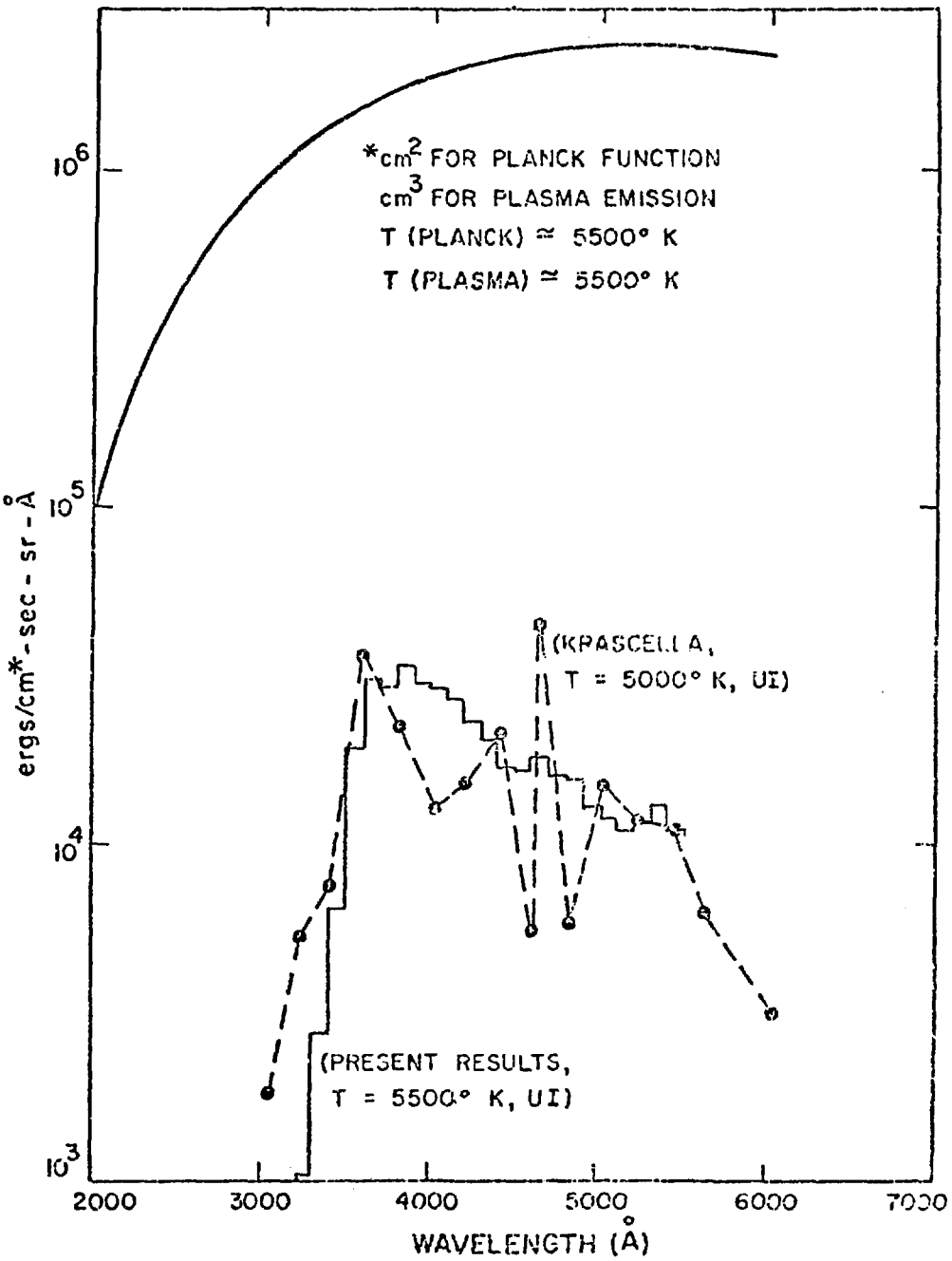

Fig. IV-7. Low-pressure uranium plasma emission coefficient comparison to Planck intensity.

two data sets are supportive. Thus, we have established corroborative evidence of the shape credibility of the low-pressure arc emission coefficient.

The work of Steinhaus et al.[18,19] also lends support to the major peak location around 4000 Å (for UI) and to the validity of the rapid emission decrease below 3500 Å. The range of experimentally observed UI levels extends to 40 000 cm^{-1} on the energy-level diagram ($\sim$ 5 eV). This implies there are no known UI transitions below approximately 2500 Å. Also, the bulk of known lines established by Steinhaus for UI falls within 3300 to 6000 Å, which also supports our information.

The Planck function for a blackbody temperature of $\simeq$ 5500 K is also plotted in Fig. IV-7 along with the emission data (different units). Since the magnitudes of the arc emission and Planck intensity are plotted logarithmically, the difference of these values at a specific wavelength is an indication of the absorption coefficient, κ_λ. The value of κ_λ is actually an average (over 100 Å) because the emission coefficient is also averaged over 100 Å. At all wavelengths $\kappa_\lambda \leq 0.034$, thus implying an optically thin plasma. Line-center absorption coefficients can be significantly greater for some lines as illustrated by the line-center κ_λ for the 3653 Å and 3659 Å UI lines.

V. *HELIUM-URANIUM ARC DATA REDUCTION*

The objective of this phase of research was the investigation of uranium plasma emission at higher temperature (than that of the low-pressure uranium arc) from the visible through portions of the vacuum ultraviolet wavelength region. The experimentally observed levels of UII (singly ionized uranium) extend up to 50 000 cm^{-1}, [18,19] and the ionization energy is about 100 000 cm^{-1}. Hence, UII line structure is likely to appear in the visible, uv, and vacuum uv wavelength regions. For this reason a uranium arc which produced strong UII radiation and operated under conditions similar to those observed by Randol[51] and Mack[52] was used.

The uranium plasma for the present study was generated with the identical configuration as the low-pressure arc (Figs. III-1 to 5). Helium cover-gas at 3 atm was added; the arc current and voltage were maintained at 30 A and 35V, respectively. Current-voltage and arc emission characteristics were controlled to duplicate those determined by Randol[51] to infer temperature and density from his photographic diagnostics. This was an important consideration because our uranium arc was too unstable for accurate photoelectric temperature and density diagnostics such as those performed on the low-pressure arc. This inference seemed reasonable, if spectral similarity (line location, half-width, and peak values) for arc plasmas generated by cascade and free burning systems at the same pressure-current-voltage conditions could be established within the error limits of Randol's temperature and density measurements.

V-1. Spectral Analysis

The line spectrum emitted from the helium-uranium arc was identified manually and cross-checked with the line identification computer analysis of Kylstra.[68] Identified lines were highly correlated with the known UII spectrum. Only a few helium line possibilities were observed, which indicated a relatively pure uranium plasma. This spectrum, as a whole, was significantly different in comparison with the low-pressure arc plasma, and provided some evidence that operation from a low- to a high-pressure arc was accompanied by a corresponding shift of radiation dominance to UII in addition to a shift from lower to higher temperature.

Comparison of helium-uranium arc spectra sets (ours and Randol's[51]) was first done on a wavelength basis. When superimposed, the two sets of spectra were virtually indistinguishable. Both line sets were composed of line spectra at the same wavelength locations and emitted by the same plasma constituent; namely, singly ionized uranium. This was necessary but not enough to justify the assumption of similar temperature and pressure ($T\text{-}P_{UII}$). The other necessary factor (provided most of the lines were sharp) to insure similar $T\text{-}P_{UII}$ conditions was consistency between the two sets of peak and half-width values. Detailed study showed little discrepancy for the lines examined at the arc centerline used in Randol's[51] diagnostic analysis. Further, peak and half-width values of these lines compared with those recorded at different current, voltage, and pressure conditions showed discernible differences which indicates the sensitivity of the comparison. Therefore, the centerline temperature and pressure of the constricted helium-uranium arc plasma was approximately characterized by Randol[51]

to be between 8000 and 9000 K and 0.01 atm UII partial pressure rounded to the nearest integral logarithmic pressure. Because of the inferred temperature and pressure, only a brief overview will be given (Sec. V.2 and V.3) of the methodology used by Randol[51] to determine these parameters.

V-2. Temperature Measurement

The central temperature of the helium-uranium arc plasma operated at 30 A, 36 V, and 3-atm total pressure was estimated by the Fowler-Milne method and measured by the relative Boltzmann plot method. The normal temperature for this plasma was estimated to range between 7000 and 9000 K for a corresponding pressure range of 0.001 to 0.1 atm total uranium pressure, using the 4171 Å UII transition. Slight off-axis maximums in the emission profile indicated the probability of close proximity to the normal temperature. To define temperature, the corresponding pressure must be known because temperature and pressure must be consistent. Because the spectrum taken from this plasma showed a clear majority of UII structure, and Saha analysis indicated (at 0.01 atm) a dominance of UII particles in the 7000 to 9000 K temperature range, the probability of close proximity to the normal temperature was increased. The centerline temperature was then measured for the above conditions using the Boltzmann plot method and found to be 8113 K ± 8%.[51] The centerline temperature of our helium-uranium arc plasma operated at similar conditions was therefore inferred to be ∿ 8000 K.

V-3. Density Measurement

The central UII partial pressure for the helium-uranium arc was measured by the absolute line method and cross-checked by the pressure-temperature correlation (PTC) technique (Sec. II.5B). This diagnostic was

similar to that applied to the low-pressure arc. Order-of-magnitude disagreement occurred between the absolute line values and those determined by vaporization and PTC studies.[51] In fact, the absolute line values were always lower than the others. These discrepancies were explained (to some degree) by assuming an inhomogeneous pressure profile radially across the arc and, as well, the characteristic uncertainties associated with most density measurements. In any event, the centerline UII density reported[51] for a 3-atm helium-uranium arc was $\simeq 3.8 \times 10^{16}$ cm^{-3} (0.042 atm) at a central temperature of $\simeq$ 8100 K. By Saha analysis this pressure and temperature imply a total uranium pressure of $\simeq$ 0.055 atm and an electron density of 4.3×10^{16} cm^{-3}.

The temperature measurement assumed partial LTE; however, the spectroscopic density determination required complete LTE. As described in Sec. IV.3, assuming complete LTE where only partial LTE was assured caused an underestimation of the ground-state densities; the magnitude of error was a function of the thermal limit. For the helium-uranium arc a rather high electron density was achieved, which easily satisfied the ladder, and possibly the hydrogenic LTE criterion as well. Based on these considerations, the ground-state underpopulation factor (if it could be calculated) would be small compared to the other uncertainties found in the density measurement. The collective error applied to this density measurement implied slightly better than an order-of-magnitude estimate.

V-4. Emission Coefficient Determination

Radiation from a helium-uranium arc operated at a total pressure of 3 atm and $\sim$ 1000 W arc power was detected without any collimating lenses. The arc chamber was continually purged with helium and the vacuum

spectrograph (McPherson Model 218) was maintained at $\sim 1\ \mu$. Separating the pressure-vacuum (arc cell-spectrograph) interface was a 3/8-in. Lif (lithium fluoride) window. The spectrograph grating contained 2400 grooves/mm and was blazed for 1500 Å in the first order. The sodium salicylate-phototube combination (described in Sec. III.3B) was used to detect photons transmitted by the spectrograph.

After initial detection of a vacuum uv signal, we tried to eliminate possible undesirable signals caused by internal reflections, stray light, etc. The McPherson spectrograph had a history of reflection problems, so optical blockouts (baffles) were used on the two spectrograph mirrors and the grating. The geometry of the baffles allowed only the central image of a light source to pass through the spectrograph to the exit slit, and the spectrographic internal reflections were eliminated.

Arc intensity data were collected in two wavelength segments, from 1050 Å to 1750 Å and from 1750 Å to 4300 Å. These bandwidths were used because the deuterium calibration standard had no valid calibration values lower than 1750 Å. Intensities at wavelengths above 1750 Å were calibrated as described by Eq. (III.1). The calibration standard used at wavelength $\geq$ 1750 Å was the Oriel deuterium discharge. This region was cross-checked at several wavelengths using the tungsten filament standard as a reference, and most of the uncertainty associated with the deuterium calibration values was removed.

Accurate calibration of intensity data found in the vacuum uv region below 1750 Å by ordinary methods was impossible. Many of the difficulties encountered are discussed in Sec. III.3C; application of back-extrapolation calibration (BEC) was necessary (see Sec. III.3C).

Because the intensity data were collected without a collimating lens, no detailed spatial resolution was performed on the observed intensities. However, a homogeneous plasma of 1-cm depth (the actual arc plasma diameter) was assumed. The intensity was converted to an approximation of the arc-centerline emission coefficient by simply weighting each intensity value by the inverse of the arc plasma depth (in this case 1/1). In general, this procedure yielded a conservative estimate of emission coefficient and a slight distortion of the true shape.

The calibrated and converted intensity values are shown in the approximate form of emission coefficient values in Fig. V-1. There is moderate emission in the 1000 to 2000 Å bandwidth mostly caused by overlapping line structure. This bandwidth has been rescaled in Fig. V-2 to expose more spectral detail. Figure V-2 indicates notable line structure and one distinct emission peak at $\sim$ 1550 Å, partly caused by grating response at the nominal blaze angle.

Grating scan uncertainty of +10 Å and rather large slit widths made precise wavelength location of the line structure unobtainable for comparison. Kelly,[80] however, lists a rather intense cluster of lines at 1575 Å, 1579 Å, and 1585 Å--consistent with our results. The emission data shown in Fig. V-2 are one of many sets taken (at similar arc conditions) which were cross-referenced to eliminate noise and insure that most of the residue be the desired signal.

Figure V-1 shows the remainder of the spectrum to 4300 Å. Many of the known UII and some of the stronger UI lines were potentially identified. Many unidentifiable lines could be of UII origin. There are

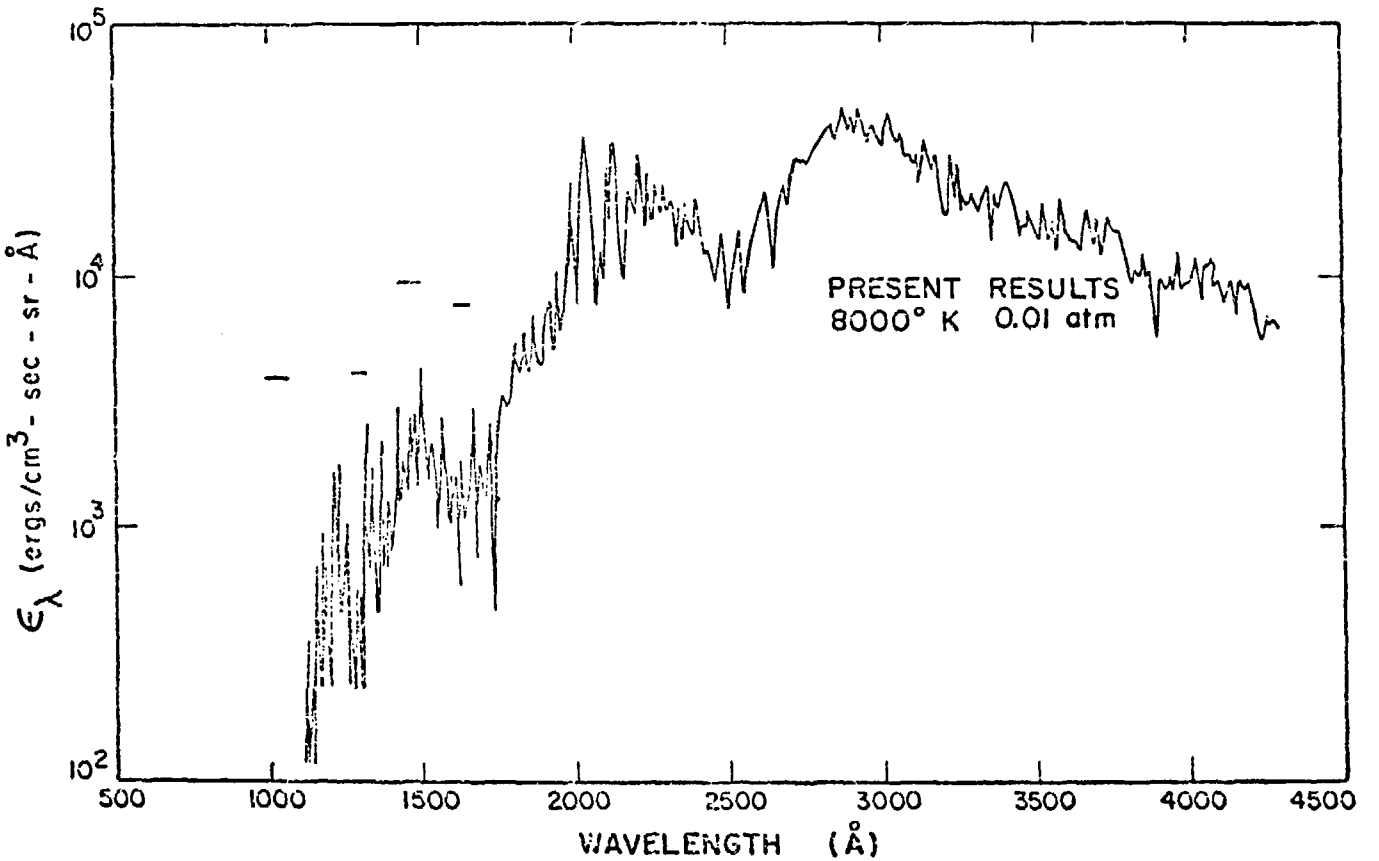

Fig. V-1. Uranium plasma emission coefficient from the helium-uranium arc.

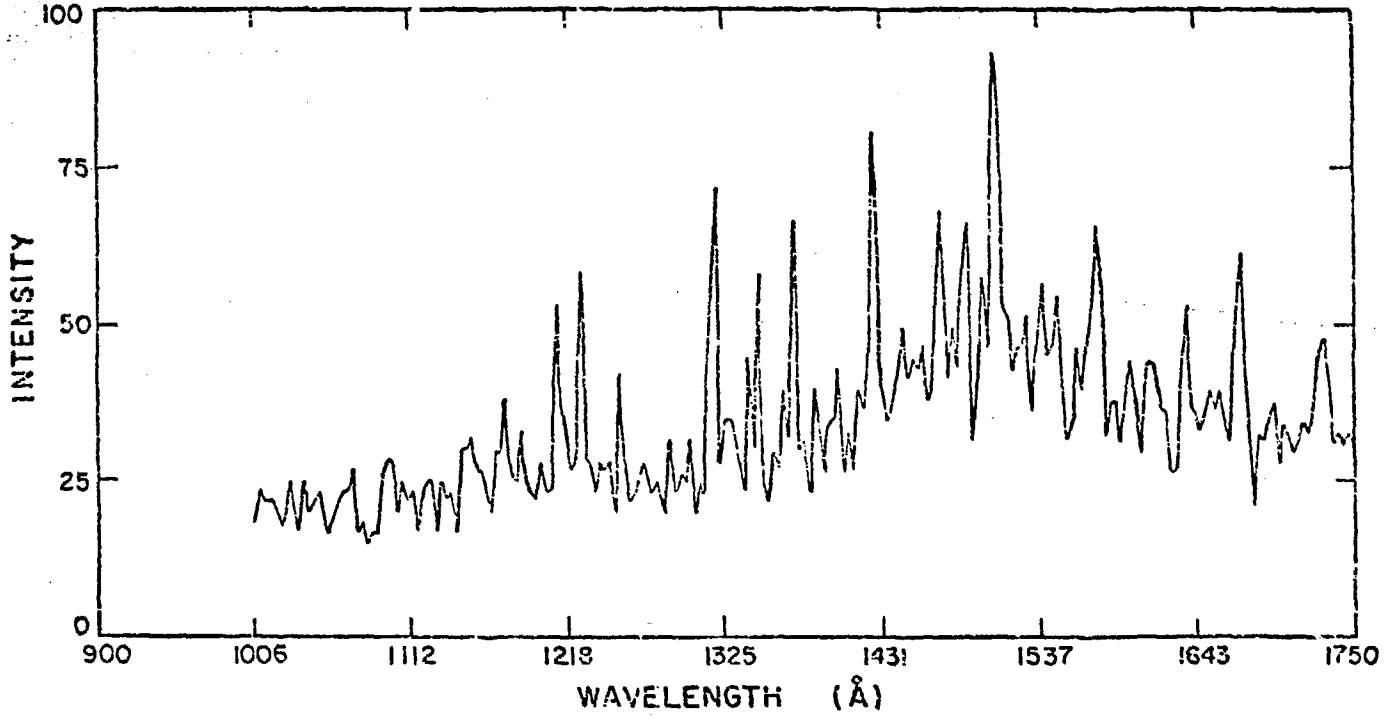

Fig. V-2. Uranium plasma intensity in the vacuum-ultraviolet.

distinct peaks at approximately 2300 Å and 2900 Å. The theoretical predictability of these peaks and the one at 1500 Å will be addressed in Chapter VI.

Vacuum uv signal authenticity and order contamination caused by overlapping orders were investigated. Light emitted by the uranium arc was passed through the vacuum spectrograph system and detected as usual with one exception--a test material composed of either Lif, quartz, or glass was placed just behind the entrance slit. Arc intensity data collected indicated that the system was detecting a true vacuum uv signal, and that contamination from other orders of the grating was negligible.

Uncertainty in the absolute value of the emission coefficient is a function of several sources, such as calibration of the standard radiation source, minimal spatial resolution, standard source positioning, digital processing, grating scan error, and arc fluctuation. For higher wavelength (>1750 Å) the emission coefficient value error is probably within ±30%. However, it is much more difficult to identify value error to wavelengths less than 1750 Å. Back-extrapolation calibration in this region assumed negligible system (optical) losses which is not the case. A good indicator of value uncertainty at these wavelengths is the system efficiency data in Table III-1. The dashes in Fig. V-1 represent the uncertainty limits on data at selected wavelengths in the vacuum uv. Clearly, as lower wavelengths are approached, the losses begin to dominate and are really indicative that all photons emitted below 1200 Å are unlikely to be detected. The error in emission coefficient values at wavelength > 1750 Å does not have this loss component because the calibration is more precise.

An extension of these data to 6000 Å was accomplished by comparison to uranium plasma emission coefficient data[81] taken using this arc system and is shown in Fig. V-3. The line structure in this figure refers to the latest measurements at 3-atm total pressure; the dashed-line curves represent previous results. The deviation in magnitude can be explained by our more sophisticated and accurate data-acquisition system. Even so, the comparative magnitudes remain within reason. Comparative shapes (along the wavelength scale) offer a high degree of correlation, as expected if past and present measurements were made properly. These factors validate the extrapolation of the present data to 6000 Å with substantial credibility. Thus, a spectral emission coefficient is now defined for a uranium plasma (8000 K, 0.01-atm uranium pressure, and 1-cm plasma depth) from 1200 to 6000 Å.

Figure V-4 shows the present results with the corresponding Planck function and other comparable measurements reported in the literature,[22,23,82] along with theoretical predictions made by Parks et al.[83] For the moment Parks' results will be accepted and their validity examined in Chapter VI. Because the graph is semilogarithmic, Kirchoff's Law provides a ready means to estimate directly the absorption coefficient by merely subtracting the value difference between plasma emission and the Planck function at a given wavelength.

For comparison it is necessary to remember that the Miller[22] and Marteney et al.[23] experiments used UF_6 as the discharge gas; the Florida experiment vaporized metallic uranium. Figure V-4 clearly indicates the differences in emission coefficient wavelength dependencies among experiments. At similar plasma conditions and compositions, differences in shape should be minimal. A distinct fall-off in emission coefficient is

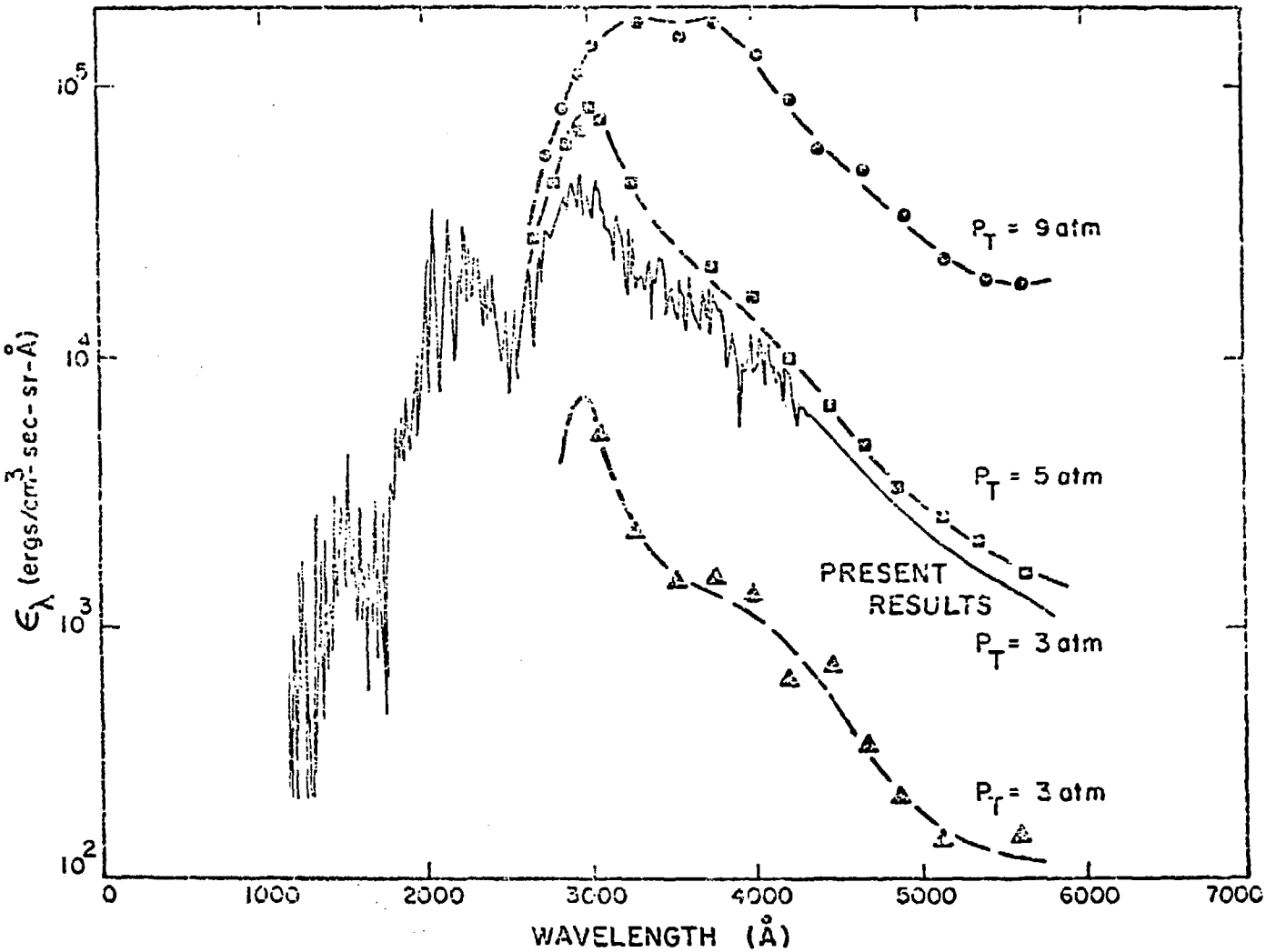

Fig. V-3. Past and present uranium plasma emission coefficients established with the University of Florida D. C. uranium arc.

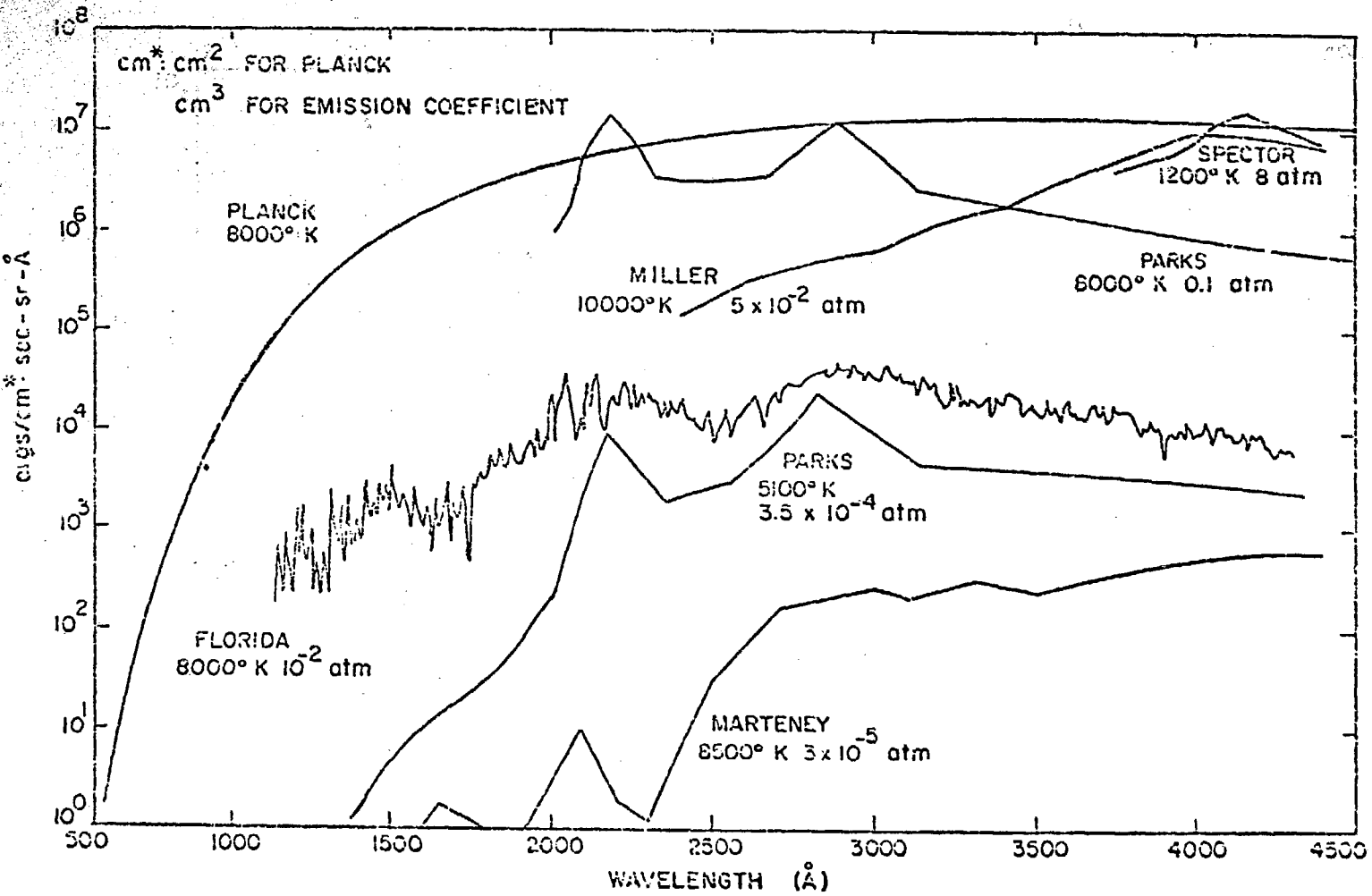

Fig. V-4. Uranium plasma emission coefficient survey.

apparent between 2500 and 4000 Å in both the Miller and Marteney results that is not evident in the Florida values. This discrepancy may be caused by strong UF_6 absorption in this wavelength region. This can be supported by Fig. V-5 which is a reproduction of some of the latest UF_6 photo absorption[84,85] and electron impact cross-section data[86,87,88] indicating significant UF_6 absorption at these wavelengths. It is unlikely that other candidates such as UF_5, UF_2, and F play a major role in light absorption within UF_6 discharges because their mean free paths are typically on the order of centimeters.[89,90]

Recent and fairly conclusive evidence shows that Miller's measurements may exhibit a substantial absorption effect from cold layers of UF_6, particularly in the 2000- to 4000-Å bandwidth. Spector[82] performed a low-temperature (700 to 1400 K) ballistic piston UF_6 absorption experiment with results remarkably similar in magnitude and shape to those of Miller whose temperature was a reported 10 000 K. The implication of this similarity is that while the uranium plasma in the Miller experiment may have been at 10 000 K, its emission/absorption characteristics were masked by such properties of UF_6.

Unfortunately, the Miller data do not extend below 2500 Å; however, the Marteney and Florida results do extend into the vacuum uv. Both indicate a small emission peak between 1400 and 1800 Å. The Florida peak appears at 1500 Å, while the Marteney peak is located at 1650 Å. The wavelength displacement between the two peaks cannot be explained by experimental error and, therefore, is attributed to the nature of each plasma and its associated emission/absorption mechanisms. The small peak shown by the Marteney curve at $\sim$ 1650 Å is inconsistent with the relatively large UF_6 absorption cross section in the 2000 to 4000 Å

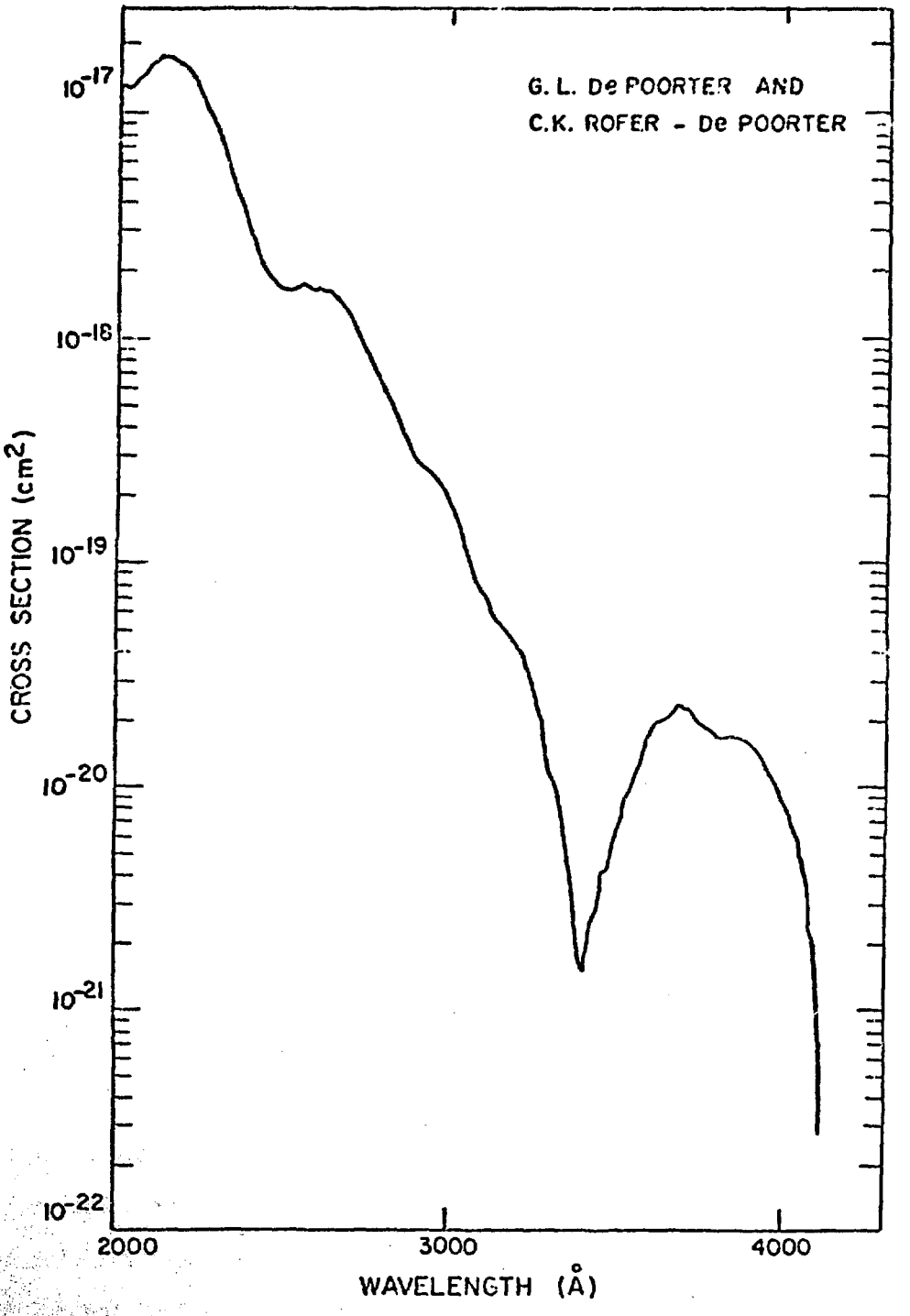

Fig. V-5. Photoabsorption spectrum of UF_6.

bandwidth. However, work by Srivastava et al.,[86] McDiarmid,[87] and Trajmar[88] has substantiated significant variation in the UF_6 absorption cross section in the 1500 to 2000 Å bandwidth as illustrated in Fig. V-6. (For absolute units the common point between Figs. V-5 and V-6 is at the peak value near 2255 Å.) In fact, there appears to be an absorption window at 1650 Å which may account for the emission peak at that wavelength from the Marteney measurement. This may also explain the vacuum uv peak shift between the Florida and Marteney results.

Now we examine UF_6 photoabsorption effects on the present arc data and the Marteney data because it may explain some of the discrepancies in shape. The Florida arc-emission coefficient data shown in Fig. V-1 were folded with several UF_6 photoabsorption strengths defined by layer thickness (as in the Marteney experiment) and molecular density. The concentrations correspond to UF_6 to approximately 0.01 to 0.1 atm at room temperature. (The details of the folding are found in Appendix E.) The results are shown in Fig. E-1 through E-4. They indicate a rather severe emission reduction in the 2100 to 2900 Å bandwidth, a possible peak emerging at 1750 Å, and the original peak at 1500 Å reduced and shifted toward the lower wavelengths. Attenuation is a function of the number of mean-free-paths traversed in all cases. This approximately agrees with the main features of the UF_6 Marteney emission data and strongly suggests that UF_6 photoabsorption is the common denominator between the Florida and Marteney results. Also included in Appendix E (Figs. E-5 through E-8) are results showing the original Marteney data with the same UF_6 photoabsorption strengths unfolded. These unfolded data exhibit characteristics in the unaltered arc emission data. However,

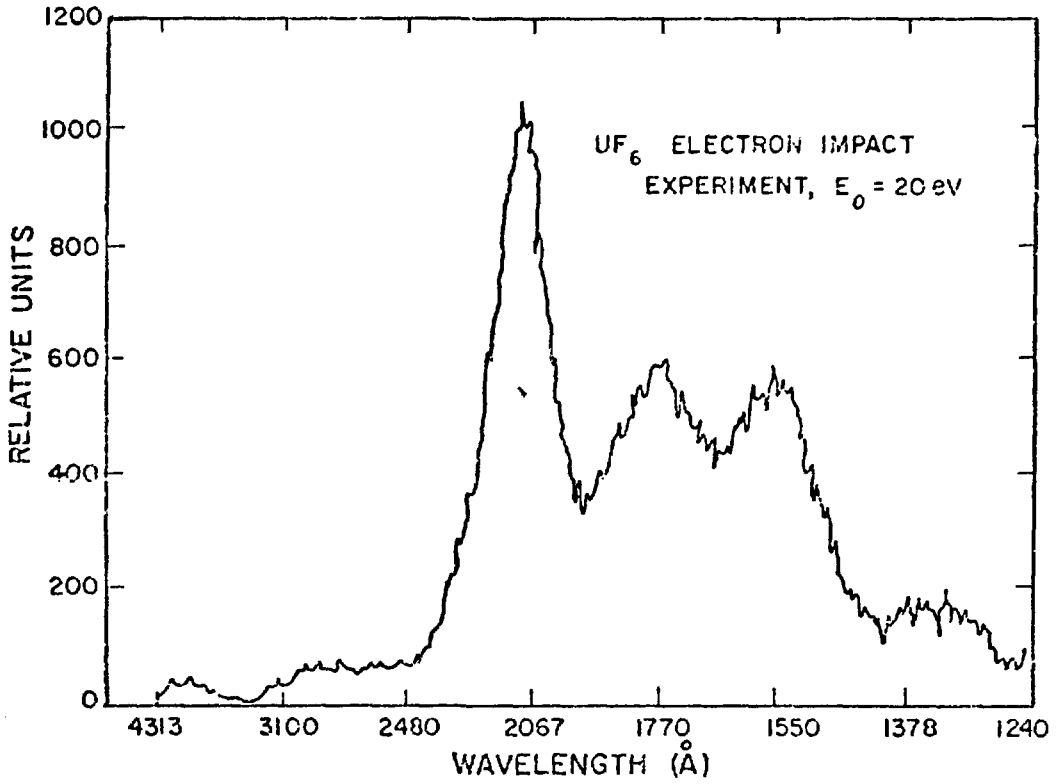

Fig. V-6. Photoabsortpion cross-section approximation into the vacuum-ultraviolet.

this analysis does not resolve the disparity in emission coefficient magnitudes as illustrated in Fig. V-4.

Shown in Fig. V-4 are differences in the absolute values of the emission coefficient measured at given wavelengths. This question has been addressed by Schneider, Campbell, and Mack,[91] where an optically thin plasma and an emission coefficient that is a direct function of particle density was assumed. It was then possible to use the perfect gas law to normalize the existing data to a common temperature and density. (The exponential temperature dependence of the emission coefficient was neglected.) The details of this comparison are an extension of this study and will only be summarized. The Marteney and Florida results agreed in the 1500 to 2200 Å bandwidth. Beyond 2200 Å the Marteney and Miller results agreed in shape and magnitude but differed from the Florida results by 1 to 3 orders of magnitude at 5000 Å. However, if the exponential temperature dependence were considered in the Miller (10 000 K) and Marteney (8500 K) data, their magnitudes would differ as well. These disparities among the three sets of measurements may, to some extent, be attributed to UF_6 masking processes. Substantial correlation in shape and magnitude resulted between Parks' theoretical data and the Florida experimental results when the two were normalized as previously described. The shape correlation can clearly be seen in Fig. V-4.

In summary, the emission coefficient of a uranium arc plasma ($T \simeq 8000$ K, $P \simeq 0.01$ atm) has been measured and compared with theory and other similar experimental data. The Florida emission data were measured from a relatively uncontaminated uranium plasma; the experimental comparison data were generated using UF_6 discharges exhibiting

UF_6 photoabsorption features that probably disguise the true emission picture. The emission coefficient curves taken from the UF_6 discharge experiments have been, to some extent, justified by relating their shape to that of the UF_6 photoabsorption cross sections. The predictability of emission coefficient shape and magnitude was addressed by a comparison between the Florida results and Parks' calculations. Favorable agreement exists in the 2000 to 4000 Å bandwidth. Since no calculations were made by Parks in the vacuum uv, this region will be investigated specifically in the next chapter by independent calculations.

VI. THEORETICAL CALCULATIONS

VI-1. Introduction

Theoretical justification for computing quantitatively accurate uranium plasma emission coefficients from first principles is nearly impossible because complete quantum-mechanical description of the uranium atom does not exist. There must also be theory (statistical mechanics) which determines the level population densities and ultimately, emission/absorption coefficients. However, it is possible to obtain useful information about relatively strong emission/absorption features as a function of wavelength without the approach described above. This information is in the oscillator strength calculations for those transitions in probable and strong transition arrays located in the wavelength region(s) of interest. Oscillator strength distribution can be a reasonable indicator to the emission characteristics of the system at those wavelengths.

For singly ionized uranium the task of calculating transition array oscillator strengths is still formidable--but possible. The procedure used to acquire this information for correlation to the UII experimental emission coefficients will be discussed.

VI-2. Terminology

Consistent terminology regarding atomic energy levels is necessary for unambiguous discussions about atomic structure calculations. The state of an atom is the condition caused by the collective motion of all the atomic electrons. The state is specified by four quantum numbers for each electron or a set of coupled quantum numbers for the entire atomic

system. The ground state is the lowest energy state. A level is represented by the total angular momentum, J. The lowest energy level is defined as the ground level. Several states can correspond to a given energy level. Terms are collections of levels tagged by multiplicity S and orbital angular momentum L. The statistical weight (distinct states) in a level is 2J + 1; in a term (2S + 1)(2J + 1). Definition of the n and ℓ quantum numbers for each electron orbital specifies a configuration. Electrons in equivalent orbitals are designated equivalent electrons. A transition of an electron between two levels generates a spectral line, whereas a multiplet is a group of transitions between two terms. Finally, a transition array is composed of transitions allowed between two configurations.

Coupling is the process whereby two or more electron angular momenta are combined into resultant angular momenta. Regarding LS, JJ, and intermediate coupling, the dominance of JJ over LS is expressed by the relative magnitudes of spin-orbit and electrostatic contributions to energy separation. Relative importance of spin-orbit interaction generally increases with increasing Z and n (principal quantum number); thus, for high-Z elements and large-electron orbits, JJ coupling would seem a logical choice. Conversely, for low-Z and small electron orbits, LS coupling would appear valid. However, at low- and high-Z there are many exceptions to these rules of thumb; intermediate coupling[92] is required for many atomic systems. A good example of the rule-of-thumb breakdown is in the highest energy level (J = 2) in the $2p^5 4f$ configuration of neutral neon. The electron eigenfunction given in a pure LS basis representation is composed of[93]

$$0.681|^3F_2> + 0.463|^3D_2> + 0.567|^1D_2>$$

whereas, if pure LS coupling really existed (as expected of neon with Z = 10) there would be no contribution from two of the three components and 100% contribution from the third.

VI-3. Configuration Selection

The credibility of the observed UII emission wavelength can be established (to some degree) by calculating transition arrays and their associated oscillator strength distribution of particular configuration pairs. Valuable information can be computed from first principles relating to the location, and in some cases, the strength of emission for a given transition array. Generating specific transition arrays is directly related to selection of configuration pairs that are likely to produce spectra at relevant wavelengths. The selection of particular configuration pairs requires knowledge of configuration average energies E_{av}. The difference ΔE_{av} between configurations is indicative of the average transition array wavelength between two specified configurations. Average energies are tabulated frequently in the literature for less complex atomic system but not for uranium; trial and error tactics were necessary.

We considered probable configurations where singly ionized uranium could find itself, beginning with the ground-state configuration $5f^3 7s^2$ and exciting an electron to another likely orbit. Table VI-I summarizes configuration pairs which were ultimately considered.

Table VI-1

UII CONFIGURATION PAIRS

$5f^3 7s^2 - 5f^3 7s7p$ [a]	$5f^2 6d7s^2 - 5f^2 6d^2 7s$
$5f^3 7s^2 - 5f^3 7s8p$ [a]	$5f^3 6d7s - 5f^3 6d7p$ [a]
$5f^3 7s^2 - 5f^2 6d7s^2$	$5f^3 7s7p - 5f^3 7s8d$ [a]
$5f^3 7s^2 - 5f^2 7s^2 7d$	$5f^3 6d7s - 5f^3 7s7p$ [a]
$5f^2 6d7s^2 - 5f^2 6d7s7p$	

[a] Configuration pairs which were very strong and/or lead to oscillator strength distribution at the desired wavelengths.

Once defined, likely configuration pairs were chosen (Table VI-1) for a quantum mechanical calculation to establish the transition array and oscillator strength distribution for a given pair. Appendix D illustrates the average energies of these configurations as well as average energies of some lower levels of UI and UII as reported by Radziemski and Blaise.[94]

VI-4. Calculation of Oscillator Strengths

We calculated oscillator strengths and distribution by choosing a coupling representation to determine the energy levels and wavefunctions for an atom in a specified configuration. For precision, energy levels and wavefunctions for all possible configurations must be found. These wavefunctions are used to calculate the electric dipole matrix that leads directly to oscillator strength for a given transition. The wavelength for each transition is given by the energy-state differential between levels of the transition.

To determine energy states and wavefunctions for the atom (ion) in a given configuration the Schrödinger equation, Eq. (VI-1) must be solved for the total wavefunction Ψ^k and energy eigenvalue E^k of each state k.

$$H \Psi^k = E^k \Psi^k \qquad \text{(VI-1)}$$

In this formalism H represents the complete Hamiltonian of the system. This problem reduces to finding the eigenvalues (E^k) and eigenvectors of the Hamiltonian energy matrix in a given basis representation. This is accomplished by the diagonalization of such a matrix into the following form:

$$< b|H|b' > = H_{bb'} D \quad . \qquad \text{(VI-2)}$$

In this case the columns of the diagonalization matrix, D, form the eigenvectors and the diagonal elements are the energy eigenvalues. The standard "bra" and "ket" notation used in many quantum mechanics texts[92,95] serves as shorthand for operator matrix elements H in this case. The proper definition of the energy matrix elements $H_{bb'}$ is the crucial step in obtaining the correct eigenvalues and eigenvectors. The complete Hamiltonian can be written as

$$H = -\frac{h^2}{2m}\sum_{i=1}^{N}\nabla_i^2 - \sum_i \frac{Ze^2}{r_i} + \sum_{j>1}\frac{e^2}{r_{ij}} + \sum_i \xi(r_i)(\vec{\ell}_i \cdot \vec{s}_i) + \cdots \quad \text{(VI-3)}$$

Kinetic energy of electron	Nuclear electro-static potential energy of electron i	Electrostatic potential energy between electrons i and j	Magnetic spin-orbit energy of electron i	Other terms of lesser importance

For uranium, Eq. (VI-1) cannot be solved in closed form with this Hamiltonian. Therefore, approximations are usually made which force a given electron to move in a central field of the nucleus and the N-1 other electrons. If spherical symmetry is assumed, the angular portions of the one-electron wavefunctions are hydrogenic and can be calculated. A self-consistent field (SCF) Hartree-Fock calculation[95] with a spherically symmetric potential is used for the radial wavefunctions. In many cases the Hartree-Fock approach is too complex for solution, and further approximation is necessary. These approximations are apparent as the form of radial potential that will account for the system's exchange properties. It is hoped that the potential used will have the important properties of the Hartree-Fock potential, will yield "correct" energy eigenvalues, and will establish properly orthogonal determinantal radial wavefunctions.

When wavefunctions and energy levels are established, atomic spectra information can be acquired. Several types of transitions are possible, but only electric dipole transitions will be considered here. Electric dipole transitions are allowed only when the matrix element in the dipole matrix is nonzero. The dipole matrix elements E are given by

$$E = \langle \Psi | r | \Psi' \rangle \quad , \tag{VI-4}$$

where Ψ and Ψ' represent the wavefunction for the upper and lower energy state, and $\langle \Psi | r | \Psi' \rangle$ indicates the average radius of an electron in a stationary state Ψ for the entire radiation process. The gf values (statistical weight times oscillator strength) are directly proportional to the square of the appropriate dipole matrix elements. The actual coupling can affect significantly the strength and overall location of a given transition array oscillator strength distribution. A simple example will illustrate this point.

Consider the case where the oscillator strength between the $^3P_1 \rightarrow {}^1S_0$ levels is desired, where $\leftrightarrow gf \propto |\langle \Psi | r | \Psi' \rangle|^2$. Suppose that eigenvector composition is

$$\text{Level 1} \text{ ———— } |^3P_1\rangle = 1.0\ |^3P_1\rangle$$

$$\text{Level 2} \text{ ———— } |^1S_0\rangle = 0.9\ |^1S_0\rangle + 0.439\ |^3P_0\rangle \ .$$

Level 1 is a pure* $^3P_0$ state and level 2 is a mixture of the $^1S_0$ and $^3P_0$ basis wavefunctions.

*For a development of the concept of purity, see G. H. Shortley's article, Ref. 96.

Clearly,

$$gf \propto | < 0.9\ ^1S_0 + 0.436\ ^3P_0 |r|\ ^3P_1 > |^2$$

$$= | 0.9 < ^1S_0 |r|\ ^3P_1 > + 0.436 < ^3P_0 |r|\ ^3P_1 > |^2$$

$$= 0.19 | < ^3P_0 |r|\ ^3P_1 > |^2 \quad .$$

In an assumed LS or JJ coupling scheme, mixing would not be manifest and the $^3P_1 \rightarrow {}^1S_0$ would be disallowed, resulting in gf = 0. Because the eigenfunction for the $^1S_0$ state is a linear combination of basis wavefunctions, the transition between levels 1 and 2 is allowed by the appearance of $^3P_0$ and $^3P_1$. Mixing frequently does occur and can play a major role in determining oscillator strength distribution and magnitude of transition arrays between two configurations. For a given energy matrix, transformation to JJ, LS, or intermediate basis representation will produce the same line pattern.

Oscillator strengths were calculated for the UII configuration pairs labeled in Table VI-1 with a computer code RCG created by Cowan.[97] Briefly, the code implements the relativistic Hartree exchange (RHX) approach[98] to calculate angular and radial wavefunctions in a basis representation defined by the appropriate coupling scheme. Established wavefunctions and energy eigenvalues are used to compute wavelengths and magnitudes of oscillator strength allowed between two configurations. Parks et al.[83] attempted a similar calculation using a statistical model for level distribution and the Thomas-Fermi approach for the one-electron wavefunctions. Table VI-2 illustrates the major considerations of the Parks relativistic scaled-Thomas-Fermi (RSTF)

Table VI-2

UII ATOMIC STRUCTURE CALCULATIONS --

A COMPARISON OF THE PARKS (STF) AND RHX APPROACH

SUBSTANTIAL ASPECTS OF CALCULATION	PARKS(STF)	RHX
Scaled-Thomas-Fermi (STF)	X	
Hartree-Exchange (HX)		X
Relativistic (Dirac)	X	X
Magnetic Spin-Orbit Interaction		X
Correlation Effects		X
Configuration Interaction		
Self-Consistent Field (SCF)	X	X
Scaled Thomas-Fermi Potential	X	
Hartree-Exchange Potential		X
Coupling Schemes		
1. None	X	(Statistical treatment)
2. Intermediate		X

calculations[83] and the RHX calculations. Results are discussed in Sec. VI-5. A flow diagram for RCG is given in Appendix B.

Parks used a relativistic Hartree-Fock-Slater self-consistent field treatment to calibrate the scaled Thomas-Fermi potential.[99] With this potential, he computes one-electron wavefunctions for the opacity calculations. The Thomas-Fermi model for heavy elements is adequate until encountering electrons in overlapping levels and when matching large and small radii boundary conditions. The scaled Thomas-Fermi potential does not account for the exchange contribution to the electron potential energy. The Hartree-exchange potential resembles the characteristics of the Hartree-Fock potential, and accounts for the exchange terms in the central-field approximation. This implies that wavefunctions developed with the Thomas-Fermi potential often will exhibit a greater uncertainty than those calculated with the Hartree-exchange potential. Even the energy eigenvalue calculations can be poor, as shown for the 5f uranium binding energy in Fig. 1 of Ref. 83. The exclusion of correlation effects in the Parks model is not a serious drawback and may be inconsequential;[98] however, omission of a detailed treatment of actual coupling could be its most serious shortcoming. Large inaccuracies are possible in line-pattern calculations and oscillator strengths, particularly if one configuration in the transition array is not well characterized by a pure coupling scheme. This situation arises often in the case of uranium.

VI-5. Comparison of Results

Figure VI-1 is a collective plot of the RHX oscillator strength distributions, the Parks theoretical emission coefficient STF calculation,[83] and the experimentally determined UII emission coefficient, all as a function of wavelength. Only the RHX oscillator strengths relate to the absolute values found on the ordinate, whereas the Florida and Parks emission coefficient curves are slightly distorted in the relative magnitude but the major inflection points have been preserved. This plot format shows only the significant features of the experimental emission coefficient curves for comparison to theory; magnitude was discussed in the previous chapter. For each transition array oscillator strength distribution (TAOSD) shown in Fig. VI-1, the TAOSD and the corresponding fractional number of spectral lines per wavelength interval are plotted in Appendix C. Plots showing the $5f^3 7s^2$ - $5f^3 7s8p$ and $5f^3 7s^2$ - $5f^3 7s7p$ transition arrays clearly show that many spectral lines in a cluster do not insure strong oscillator strength and strong emission.

In general, the Parks and RHX calculations support the variation in shape in the Florida experimental emission coefficient. Several positive points are made when comparing the RHX calculations with the Florida measurements.

(1) For our configurations, the strongest emission is likely to occur in the 2500 to 5000 Å bandwidth.

(2) An overall peak is likely in TAOSD at $2700 \begin{smallmatrix} + 250 \\ - 200 \end{smallmatrix}$ Å, with a relatively smaller peak at $2041 \begin{smallmatrix} + 132 \\ - 68 \end{smallmatrix}$ Å.

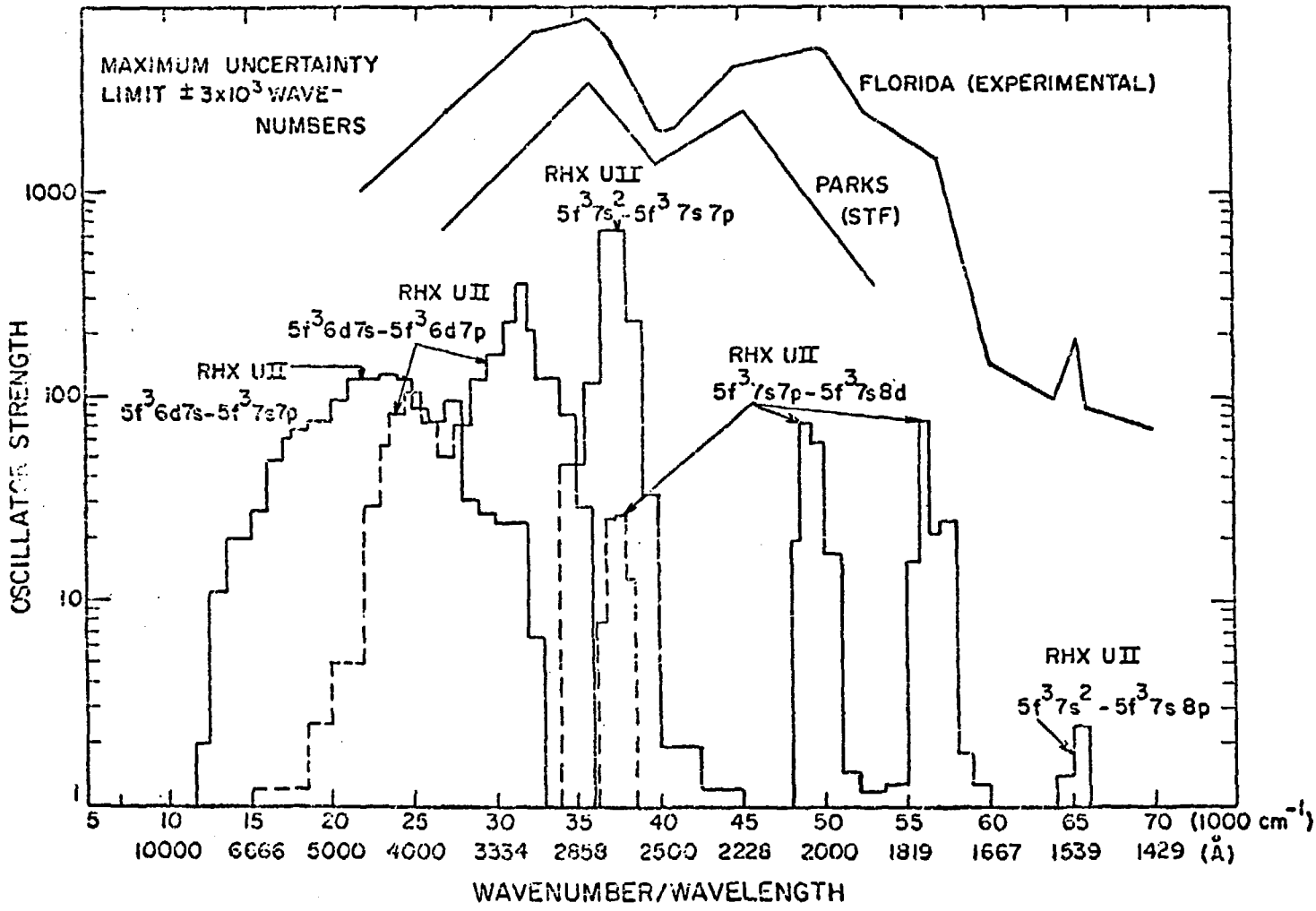

Fig. VI-1. Comparison of UII oscillator strength distribution to UII emission coefficient measurements.

(3) The experimental emission coefficient "shelf" between 1900 and 1750 Å can be supported by the fairly strong TAOSD from the $5f^3 8s7p$ - $5f^3 7s8d$ configuration pair.

(4) The emission coefficient decrease at ∿ 2500 Å is validated by a corresponding sparcity of oscillator strength between 2200 and 2500 Å.

(5) Similarly, an observed emission coefficient decrease in the 1600 to 1700 Å bandwidth is supported by a lack of oscillator strength with similar qualification as mentioned in point 4.

(6) The $5f^3 7s^2$ - $5f^3 7s8p$ TAOSD indicates good potential for a small but significant emission peak at ≈ $1539 \begin{smallmatrix} + 74 \\ - 68 \end{smallmatrix}$ Å, and it represents a theoretical-experimetnal verification of prominent UII emission in the vacuum ultraviolet wavelength region.

The Parks calculation, as far as it was taken in wavelength, reproduces the experimental results at the major peaks. He attributes the appearance of distinct emission/absorption peaks at 2800 and 2200 Å to the transition array formed between the $5f^3 7s^2$ - $5f^3 7s7p$ configuration-pair[83] for J = 1/2, 3/2 of the 7p electron. One can hypothesize a corresponding enhancement of the oscillator strength at these wavelengths for this transition array. However, the RHX calculation for the same transition array shows three clusters of lines (Appendix C, Fig. C-10) at 5890 Å, 4000 Å, and 2700 Å, but only <u>one</u> distinct oscillator strength peak at 2700 Å (Appendix C, Fig. C-9). It is evident that the distinct peaks predicted by the Parks model for J = 1/2, 3/2 of the 7p electron are not predicted by the more sophisticated model of Cowan. The experimental peak at 2100 Å is predicted by the RHX calculation of the transition array formed from the $5f^3 7s7p$ - $5f^3 7s8d$ configuration-pair.

The disparity in peak identification between the Parks and Cowan models lies in the theoretical approach. Emission peak location is determined by level splittings caused principally by spin-orbit and electrostatic (direct and exchange) interactions. For UII Parks neglects the exchange portion of the electrostatic interaction energy altogether; he also neglects the higher-order direct contributions associated with equivalent electrons in the 5f orbital. The RHX calculation indicates that not only are these interaction energies important, they are dominant, particularly with regard to transition array line-cluster location and oscillator strength distribution. The RHX coupled wavefunctions are certainly more accurate than those uncoupled wavefunctions used in the Parks treatment. Most quantities dependent upon wavefunction description (including oscillator strengths) reflect the accuracy (or inaccuracy) of the wavefunctions used. Further, Parks includes level populations in his calculations, but the main effect of ignoring this feature is to produce changes in relative peak magnitude when calculating emission coefficients, but not in the locations of such peaks. However, the Parks calculations indicate strong emission trends between 2300 and 4000 Å, and in that sense, are supported by experiment and RHX theory. In fact, it is remarkable that, for the most part, the Parks calculations came out as well as they did considering the approximations used and the complexity of the problem.

VII. CLOSING REMARKS

Emission coefficients of uranium plasma at two distinct temperatures and pressures over an unusually broad wavelength region have been measured. These new data represent an extension of previous information published by Krascella,[79] Miller,[22] Marteney et al.,[23] Randol,[51] and Kylstra.[68] The results are significant additions to available information, and the major points are summarized below.

Specific emission coefficients for a low-pressure uranium arc at 5500 K, 0.001-atm uranium pressure were measured from 2500 to 5500 Å. These data were in reasonable agreement with the semi-empirical work of Krascella[79] and the spectral line catalogue of the first spectrum of uranium reported by Steinhaus et al.[18,19] For this arc there was no emission detected below 2500 Å, probably because of the relatively low temperature and the importance of radiation from neutral uranium. Plasma temperature, pressure, and emission coefficient were obtained simultaneously, thus reducing fluctuation problems usually associated with photoelectric diagnostics. The temperature and pressure diagnostics depended upon assuming LTE, and although not proven, LTE was reasonably substantiated with cross-checks and comparison to NBS work by Voigt.[75]

Specific emission coefficients of a high-pressure helium-uranium arc at approximately 8000 K, 0.01-atm uranium pressure were measured from 1050 to 6000 Å. These results represent a rare successful attempt to obtain emission coefficient data for singly ionized uranium in the vacuum ultraviolet. Intensity calibration in the visible and vacuum

ultraviolet was done with a tungsten standard and hydrogen discharge for each respective wavelength region. Calibration below the wavelength cutoff (1750 Å) of the hydrogen standard was inferred by extrapolation. Direct comparisons with similar experimental results by Marteney et al.[23] were understandably poor because of differing discharge systems and plasma characteristics. The Marteney data were consistent in shape with our results because of probable UF_6 photoabsorption in the Marteney experiment. The emission coefficient values of the Florida and Marteney efforts agreed to within an order of magnitude if scaled to a common temperature and density.[91]

Comparison of our experimental results for singly ionized uranium with Parks et al.[83] theoretical calculations using a relativistic scaled Thomas-Fermi model, and those using the relativistic Hartree exchange approach, provided insight into the origin of the vacuum uv emission and strong emission at other wavelengths. The Parks calculation included a statistical mechanical treatment of the calculated energy level population. The RHX computations defined only the oscillator strength distribution for selected transition arrays, which are useful for predicting significant emission location as a function of wavelength. The Parks and RHX calculations supported the experimental results to varying degrees. The peak locations at 2100 and 2900 Å were predicted by both approaches, but for different reasons. The disagreement is explained by the distinctions between the two models. Although the Parks calculations did not extend through the vacuum uv, RHX calculations conclusively predict the peak in UII emission coefficient observed at about 1540 Å. These theoretical-experimental comparisons indicate that substantial success can be anticipated in predictions of qualitative features in the wavelength dependence of emission from plasmas of very complex systems.

This effort has resulted in a credible definition of uranium plasma emission properties over an extended wavelength range near the reported temperature/pressure regimes. Presumably, the success of the theoretical predictions will increase the confidence in atomic structure calculations for heavy elements and will indicate possible areas for model improvement. Although there were numerous difficulties in this research, and many compromises were made, the overall result is clearly progressive in the experimental and theoretical aspects of the problem.

APPENDIX A

SAHA NUMBER DENSITIES AND NORMAL TEMPERATURES

Saha analysis was used to calculate LTE number densities of uranium for two stages of ionization at several total pressures of interest. The Saha equations are given by

$$S_i(T) = \frac{n_{i+1}\, n_e}{n_i} = \frac{2U_{i+1}(T)}{U_i(T)} \frac{(2\pi\, m_o k)^{2/3}}{h^3} T^{3/2}\, e^{-E_i/KT} \quad , \qquad \text{(A-1)}$$

where

i = the ionization stage,

n_i = number density (cm^{-3}) for all i-fold ionized particles,

n_e = electron number density (cm^{-3}),

$U_i(T)$ = partition function of i-fold ionized atom,

m_o = electron rest mass (= 9.108×10^{-28} gm),

h = Planck's constant (= 6.626×10^{-27} ergs-seconds),

k = Boltzmann's Constant (= 1.381×10^{-16} ergs/K),

E_i = ionization energy for ionization from $i \rightarrow i+1$,

T = absolute temperature (K).

The number density solutions were obtained using Eq. (A-1) coupled with the equation of charge neutrality:

$$n_e = \sum_{i=0}^{i} i n_i \quad , \qquad \text{(A-2)}$$

and the equation of state:

$$P = kT \{n_e + \sum_{i=0}^{i} n_i\} \quad . \qquad \text{(A-3)}$$

These number densities are plotted in Figs. A-1 through A-6 as a function of plasma temperature. Uranium ionization potentials used were those reported by Williamson et al.[100] and partition function temperature dependence was included by incorporating semiempirical curves defined by Krascella et al.[79] Lowering the ionization potentials was not considered.

The Saha number densities at various total pressures were then used to define normal temperatures for representative UI and UII transitions. The mathematical formalism is discussed in Secs. II-4B and 4C--this information is in Fig. A-7.

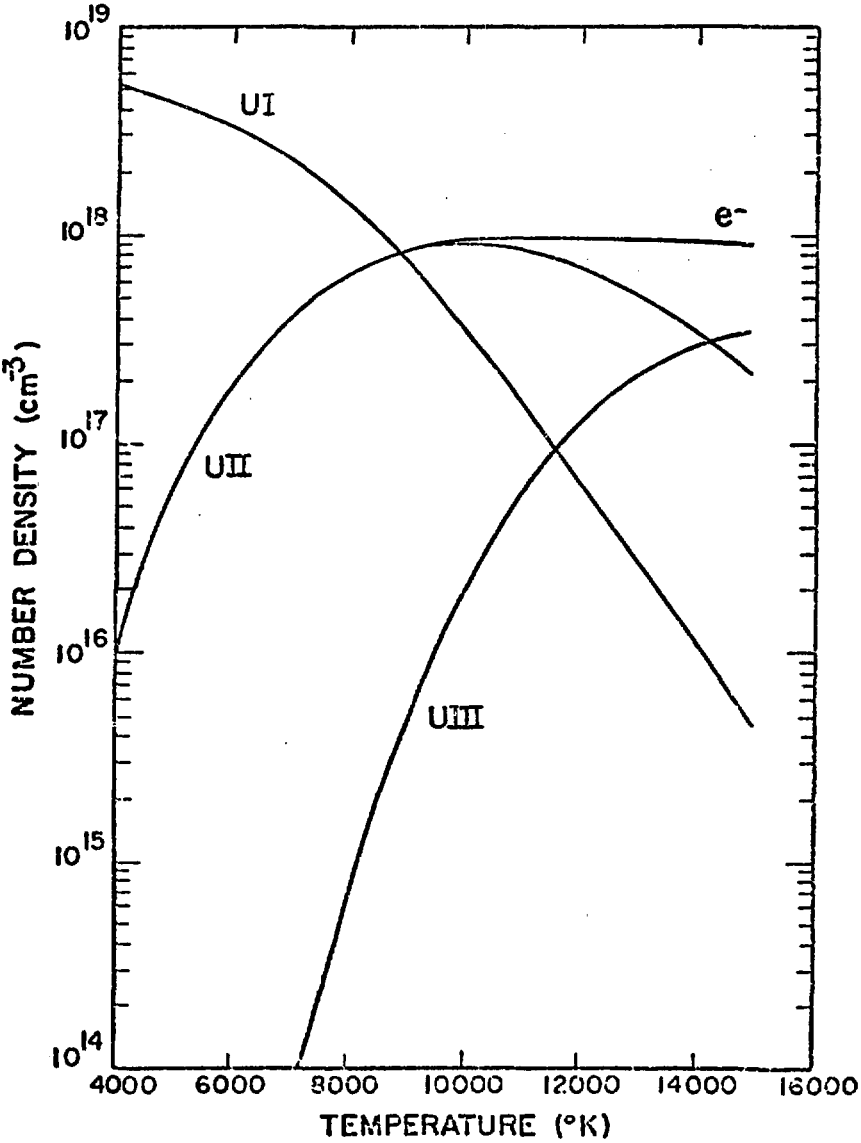

Fig. A-1. Uranium plasma Saha number densities, P=3 atm.

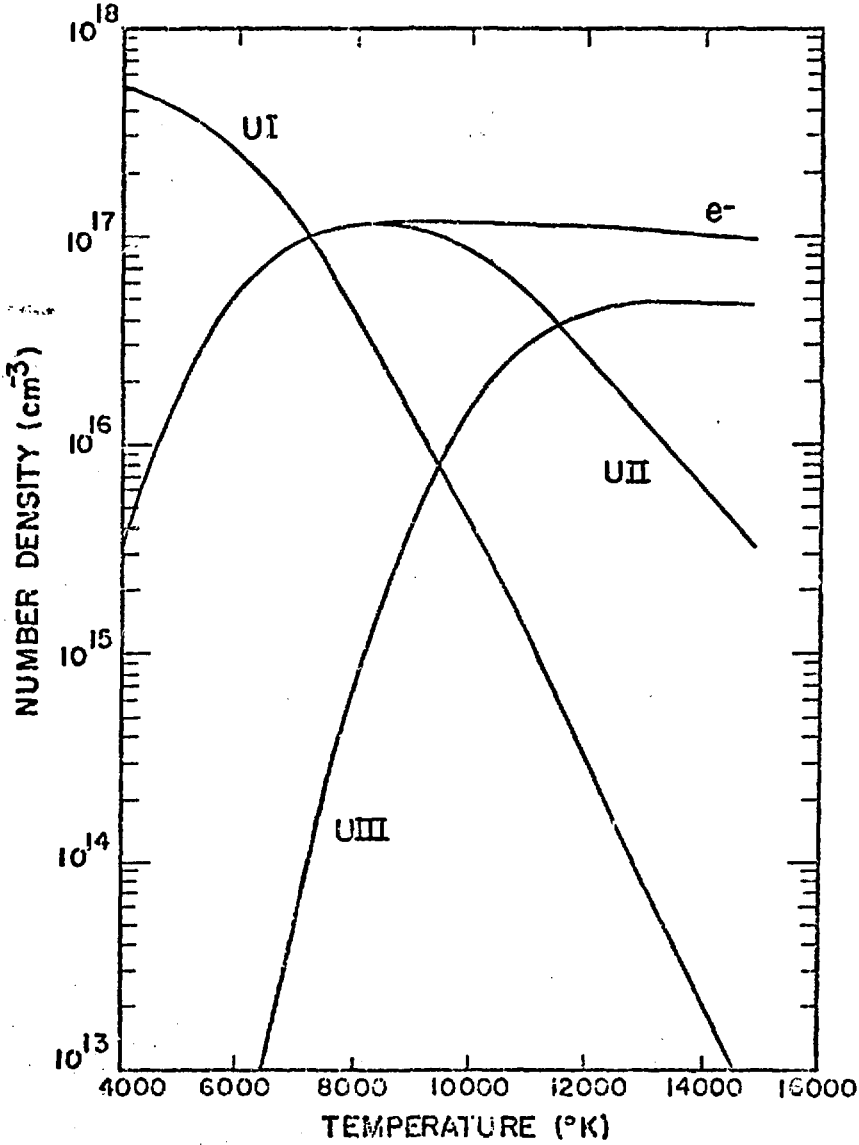

Fig. A-2. Uranium plasma Saha number densities, P=0.3 atm.

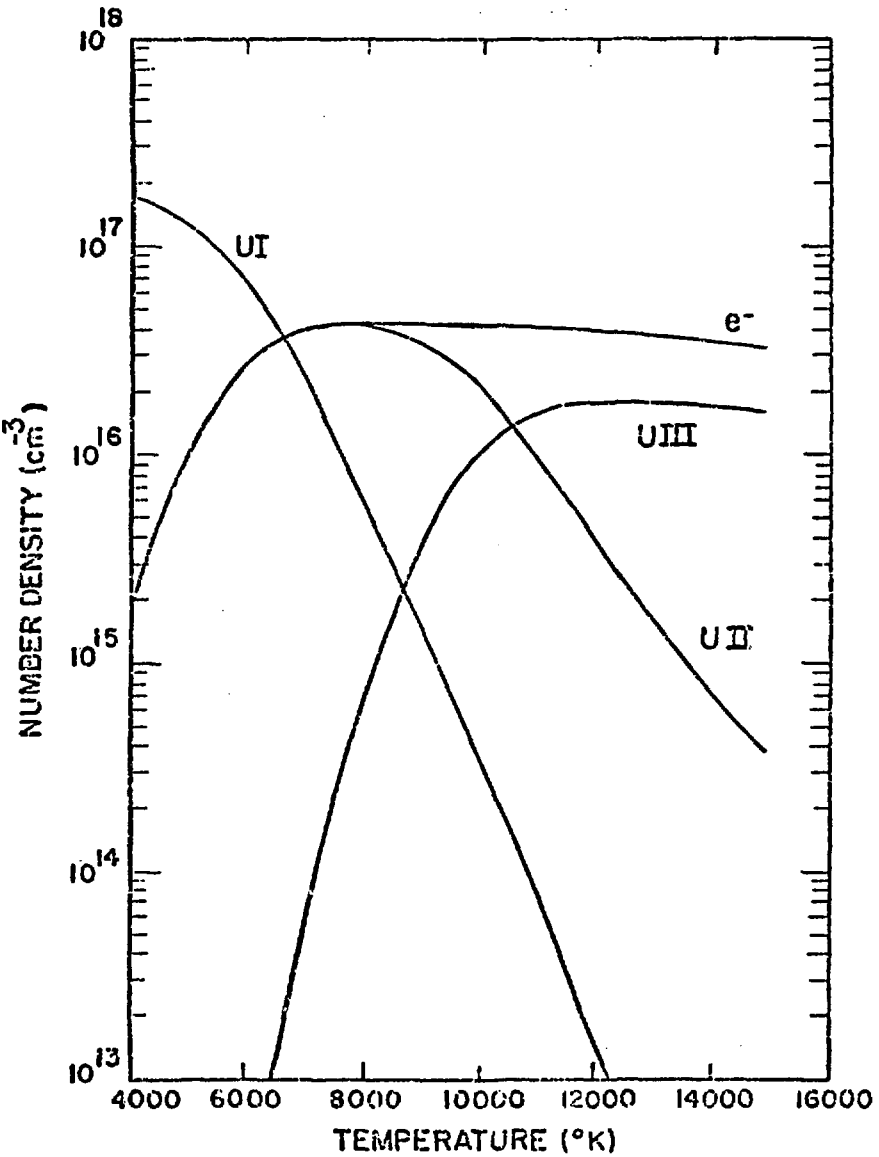

Fig. A-3. Uranium plasma Saha number densities, P=0.1 atm.

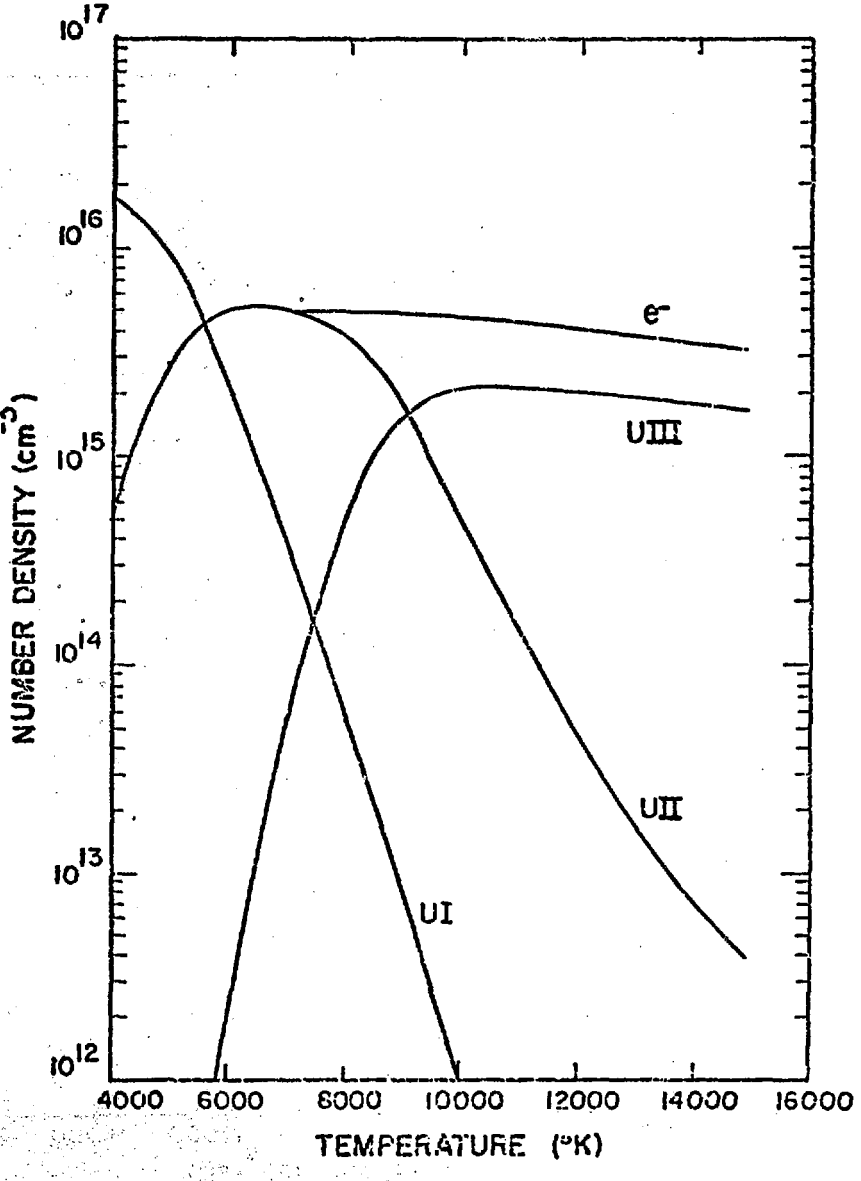

Fig. A-4. Uranium plasma Saha number densities, P=0.01 atm.

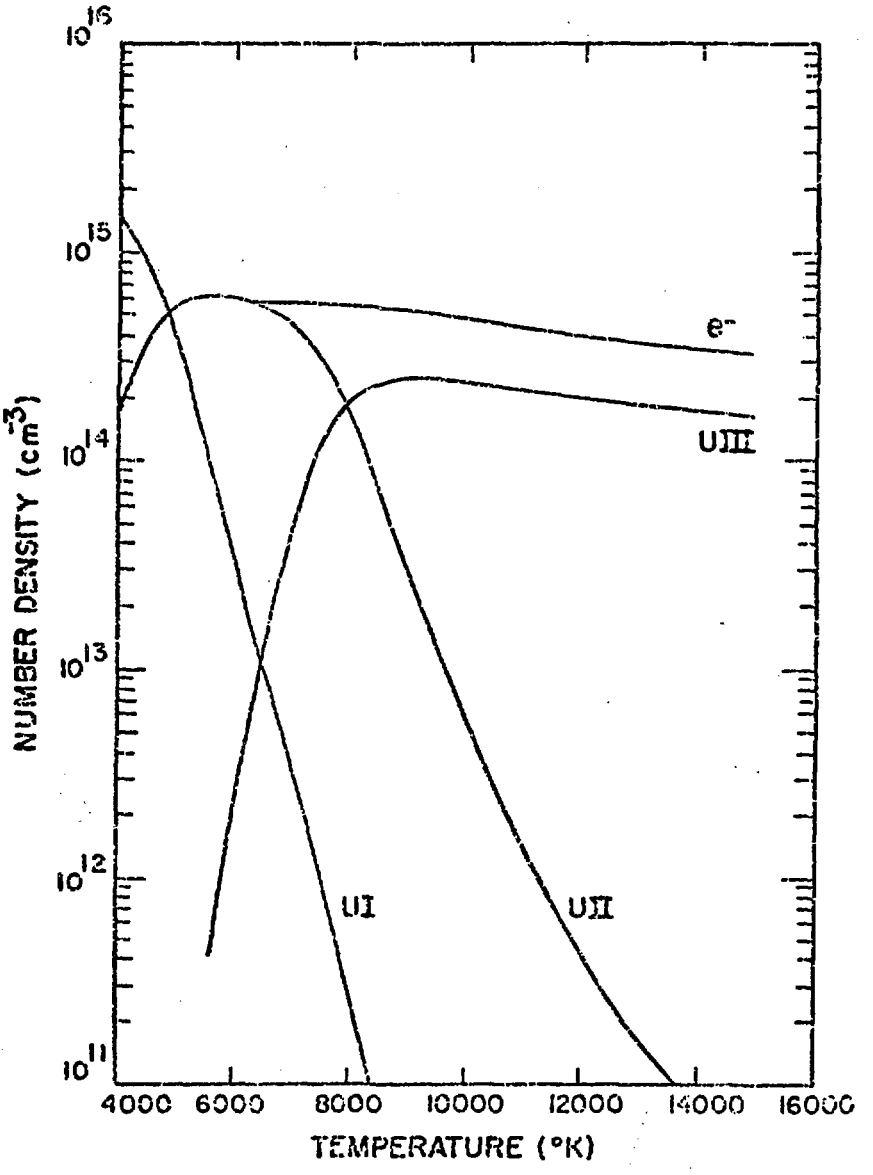

Fig. A-5. Uranium plasma Saha number densities, P=0.001 atm.

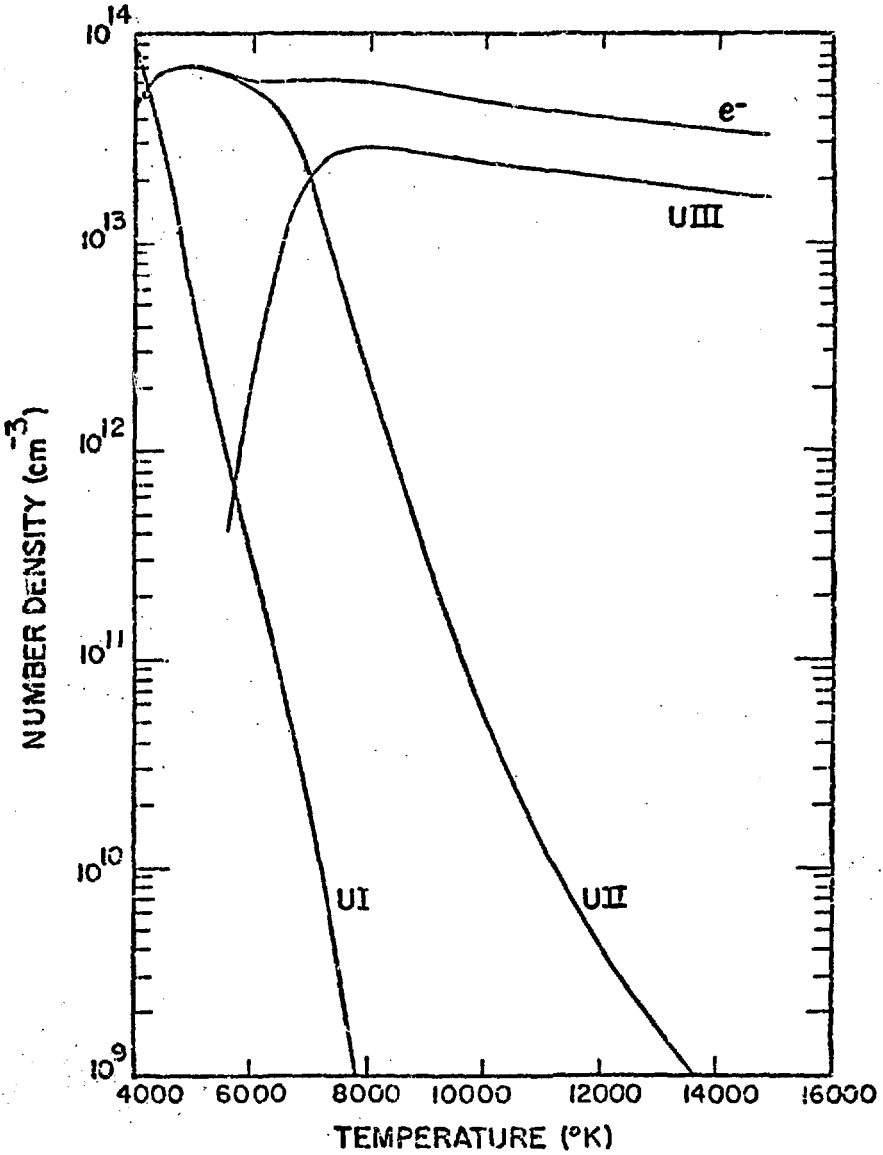

Fig. A-6. Uranium plasma Saha number densities, P=0.0001 atm.

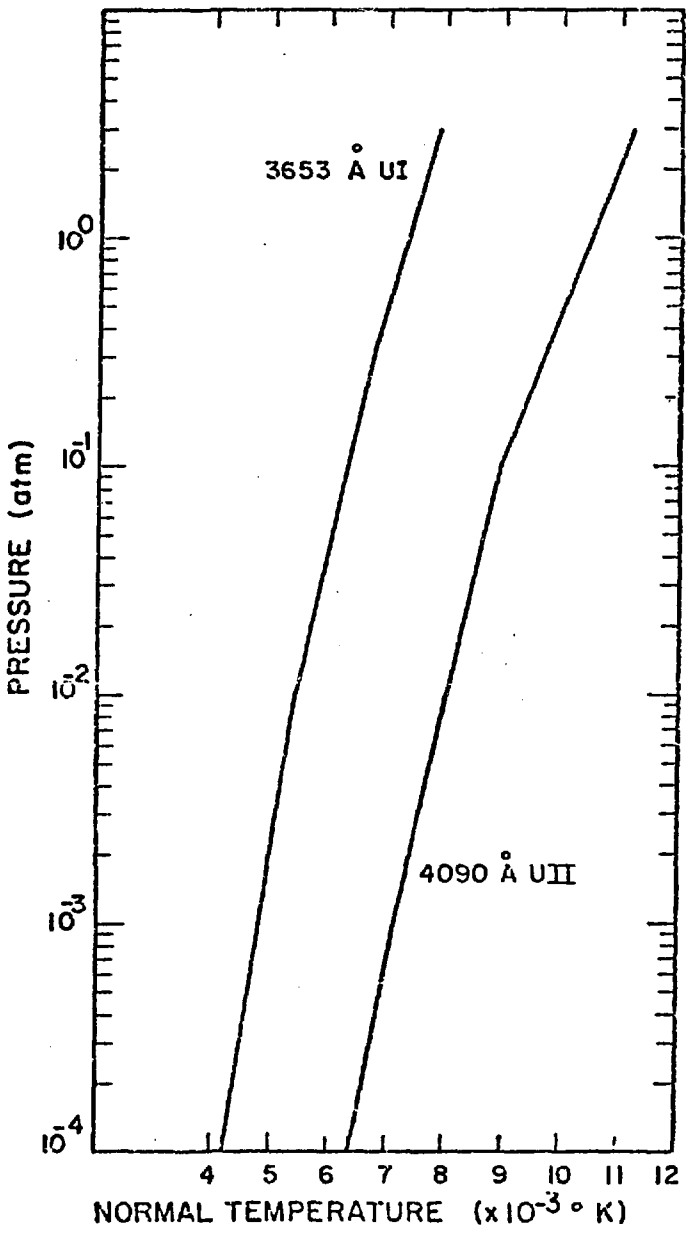

Fig. A-7. Pressure vs normal temperature of neutral and singly-ionized uranium in LTE.

APPENDIX B

COMPUTER SCHEMATIC FOR THE COWAN RCG CODE

The information in Fig. B-1 was taken from two sources[97,100] and represents the major steps in the RCG code for calculating oscillator strength distributions used in this study. It is not meant to expose the intricacies of the entire calculation but to present an overview of the calculations reported in this study. Electrostatic interaction parameters in the form of Slater radial integrals[95] are denoted by F^k and G^i for the direct and exchange contributions, respectively. The spin-orbit interaction term is indicated by ζ and E_{av} is the average energy of all states of a configuration.

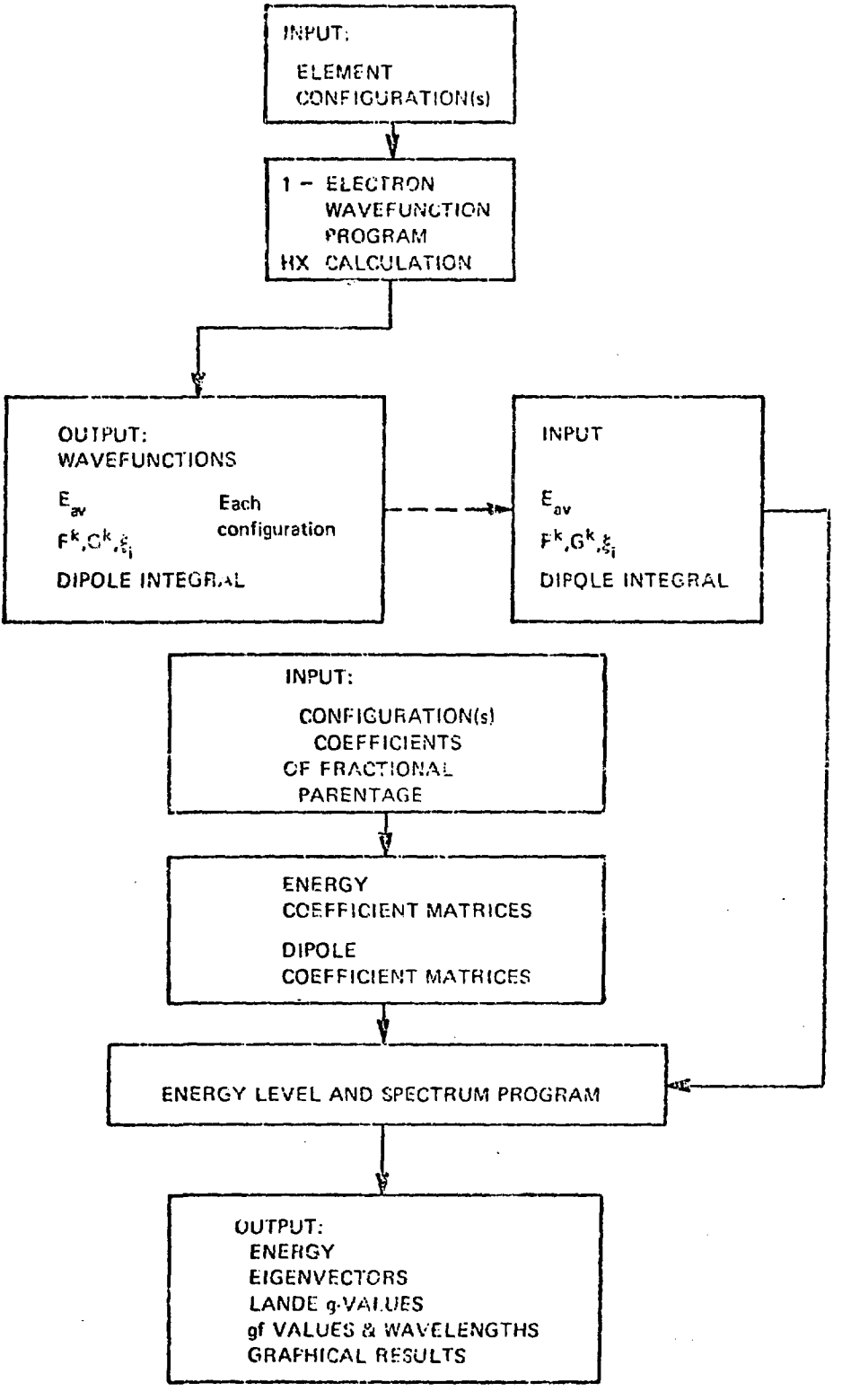

Fig. B-1. Code schematic for RCG calculation of oscillator strength distributions.

APPENDIX C

SPECTRAL LINE AND OSCILLATOR STRENGTH DISTRIBUTIONS

FOR SELECTED UII CONFIGURATION PAIRS

The following figures illustrate UII spectral line and oscillator strength distributions as a function of wavenumber. They compose the majority of graphical output from the RCG calculation. Figures C-1, C-3, C-5, C-7, and C-9 are the oscillator strength distributions for a specified UII configuration pair and have already been presented in Fig. VI-2. Figures C-2, C-4, C-6, C-8, and C-10 illustrate the calculated fractional spectral line distributions for corresponding configuration pairs. The number of spectral lines calculated for the five configuration pairs reported approached 203 000. Only those lines which had strengths above a user-set cutoff were plotted.

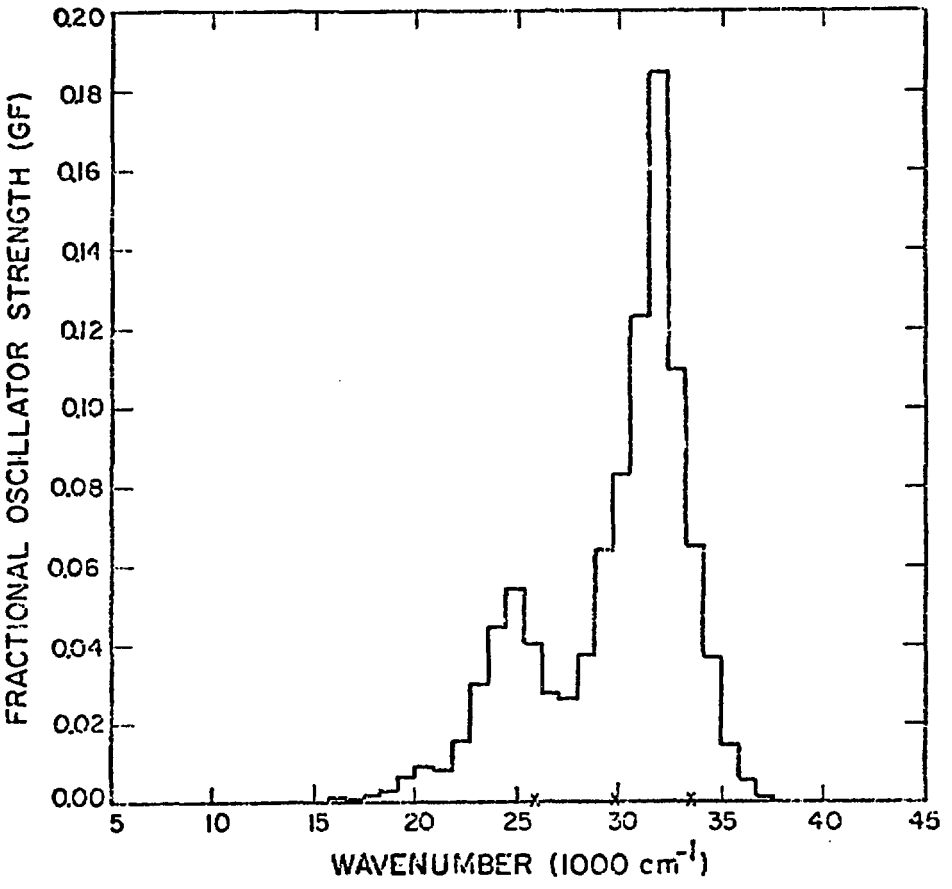

Fig. C-1. RHX transition array oscillator strength distribution for UII f3 6d7s--f3 6d7p.

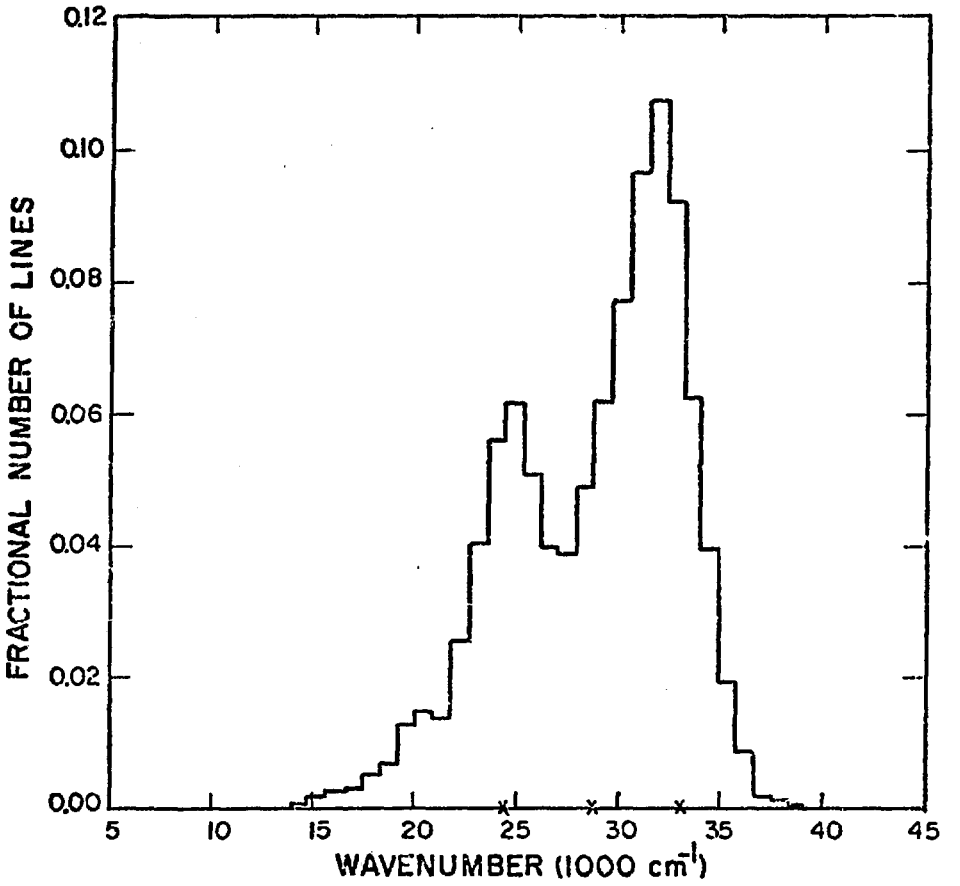

Fig. C-2. Fractional spectral line distribution in Δwavenumber interval for the f3 6d7s--f3 6d7p UII transition array.

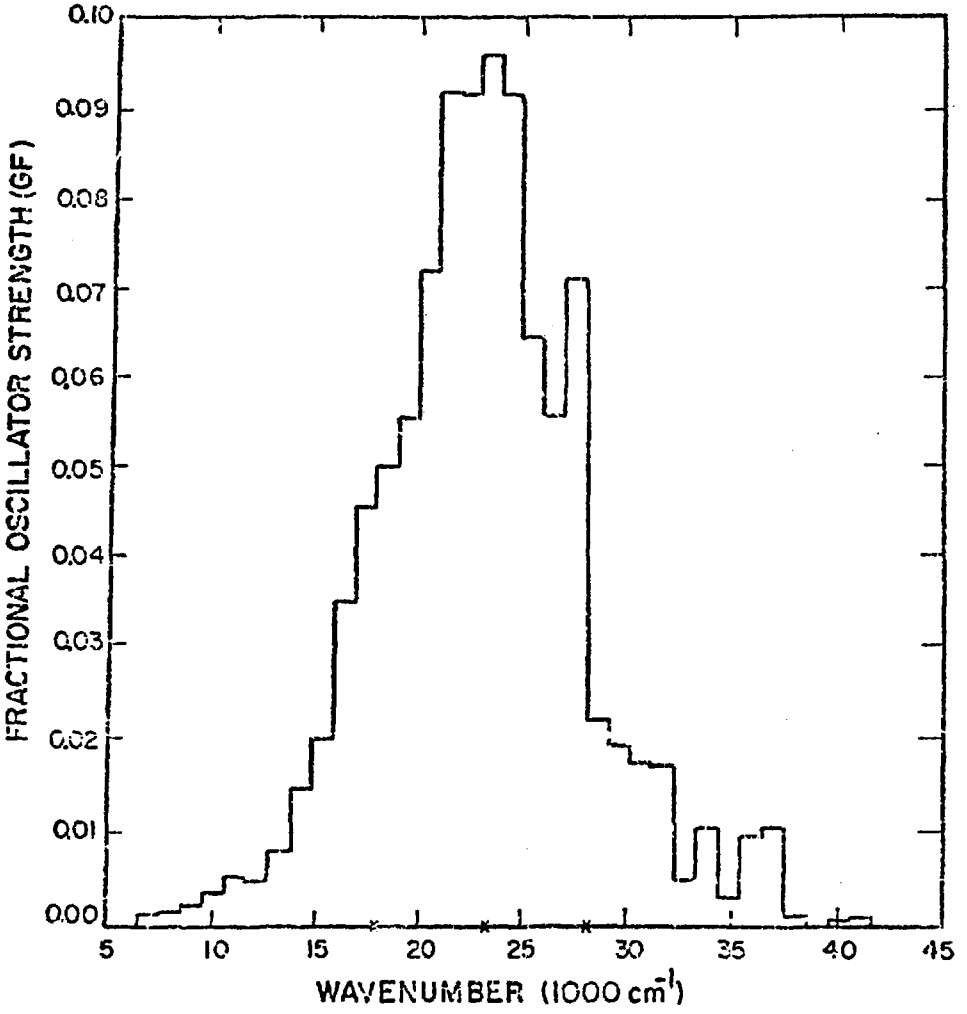

Fig. C-3. RHX transition array oscillator strength distribution for UII f3 6d7s--f3 7s7p.

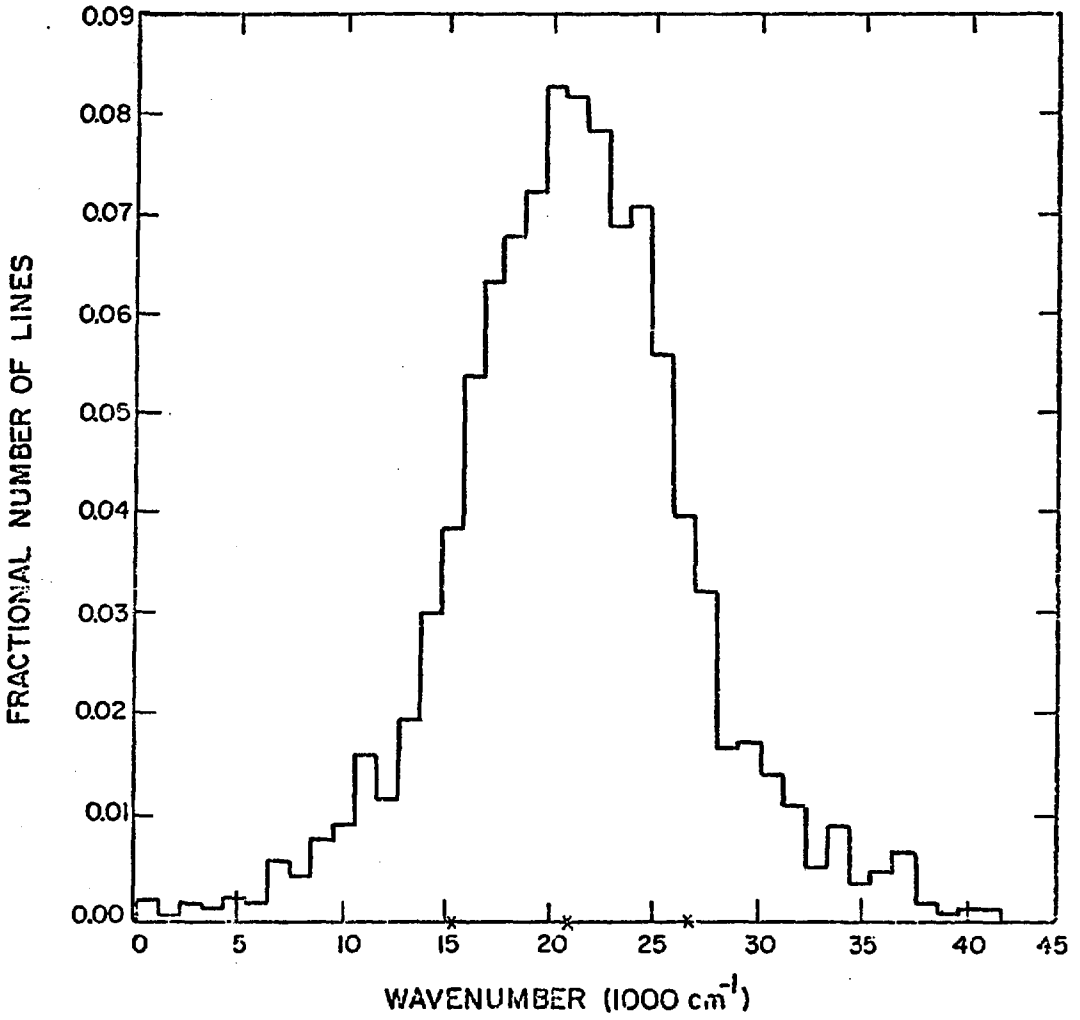

Fig. C-4. Fractional spectral line distribution in Δwavenumber interval for the f3 6d7s--f3 7s7p UII transition array.

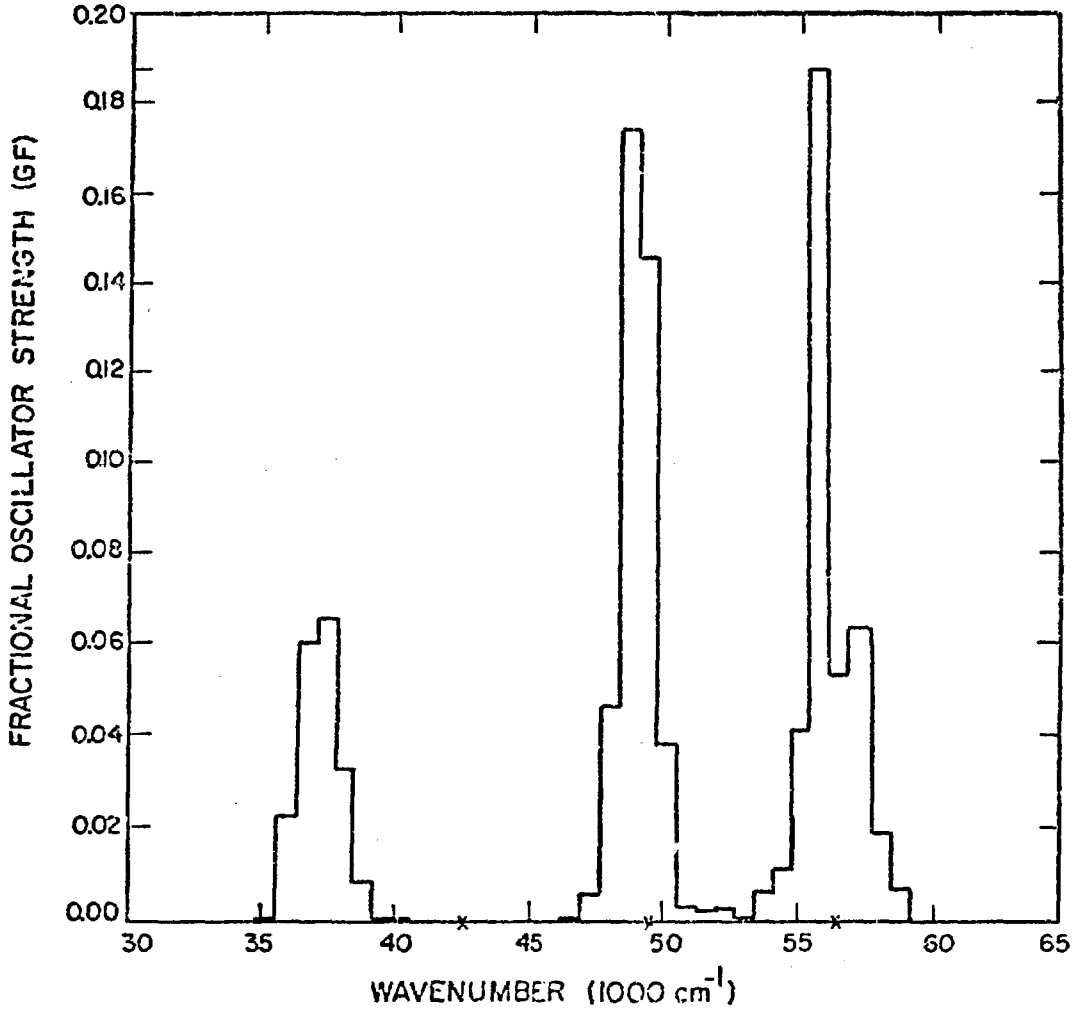

Fig. C-5. RHX transition array oscillator strength distribution for UII f3 7s7p--f3 7s8d.

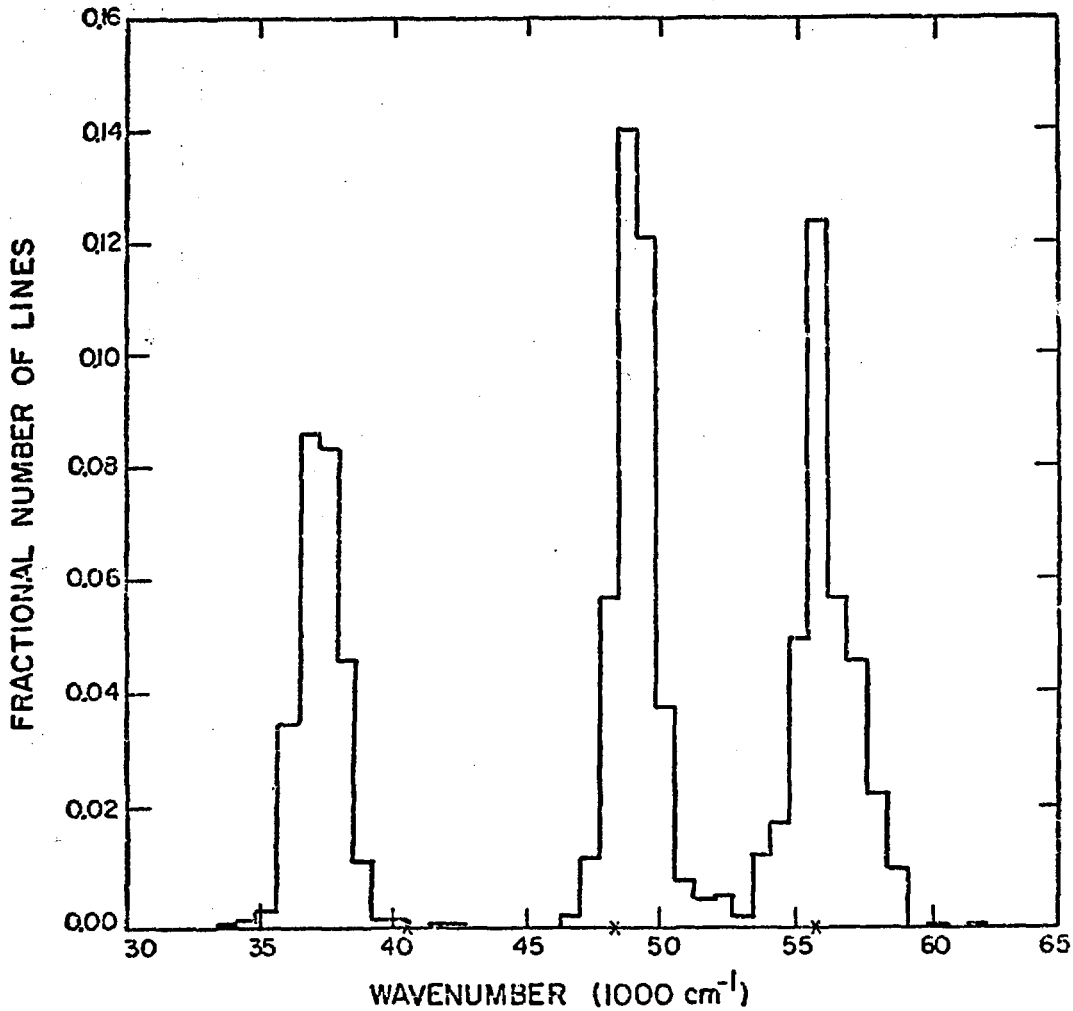

Fig. C-6. Fractional spectral line distribution in Δwavenumber interval for the f3 7s7p--f3 7s8d UII transition array.

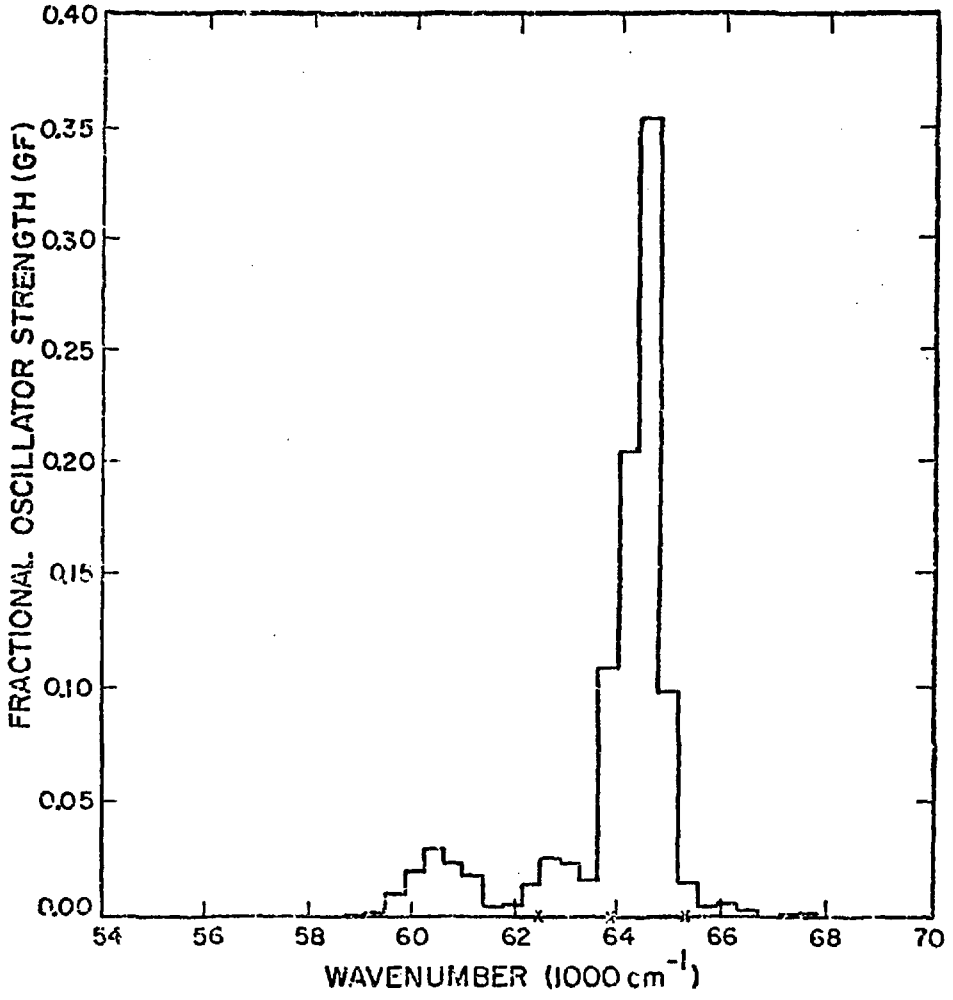

Fig. C-7. RHX transition array oscillator strength distribution for UII 5f3 7s2--5f3 7s8p.

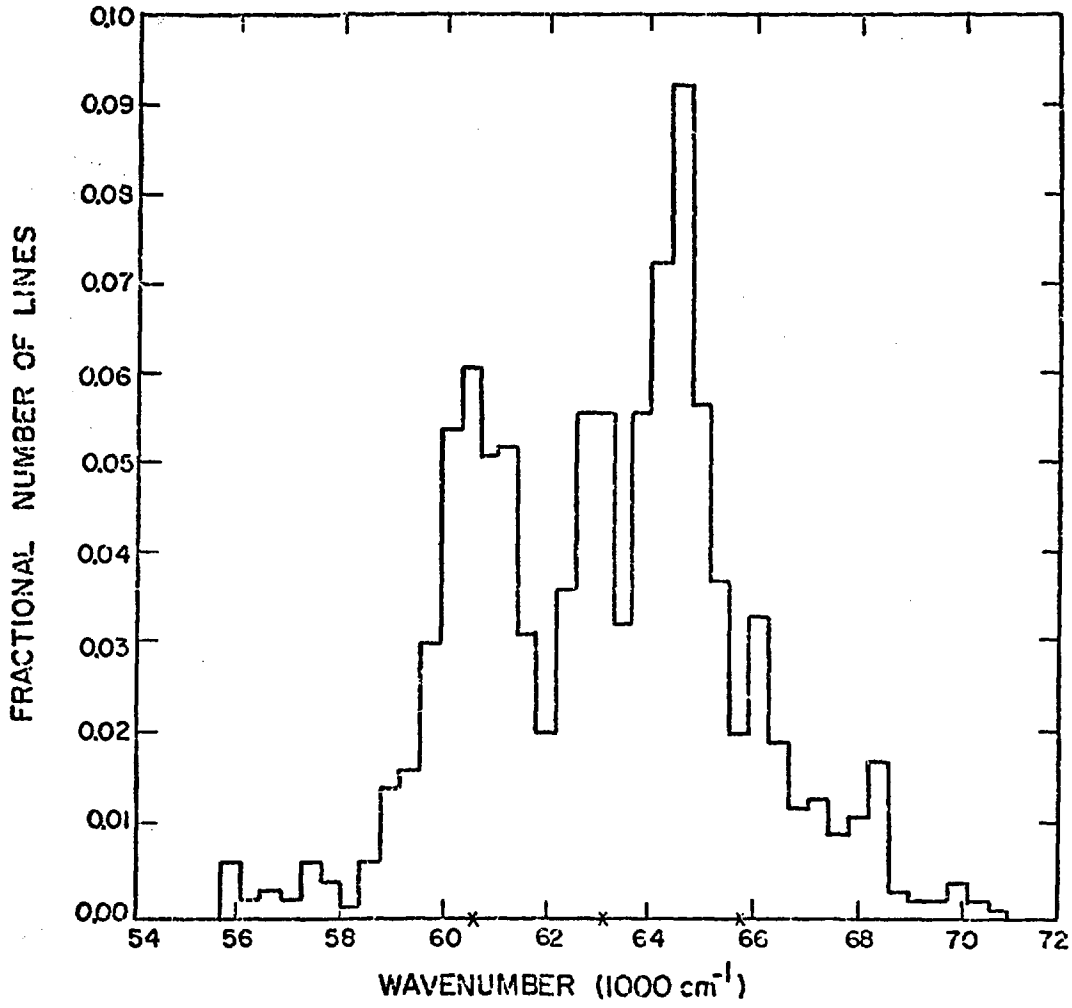

Fig. C-8. Fractional spectral line distribution in Δwavenumber interval for the 5f3 7s2--5f3 7s8p UII transition array.

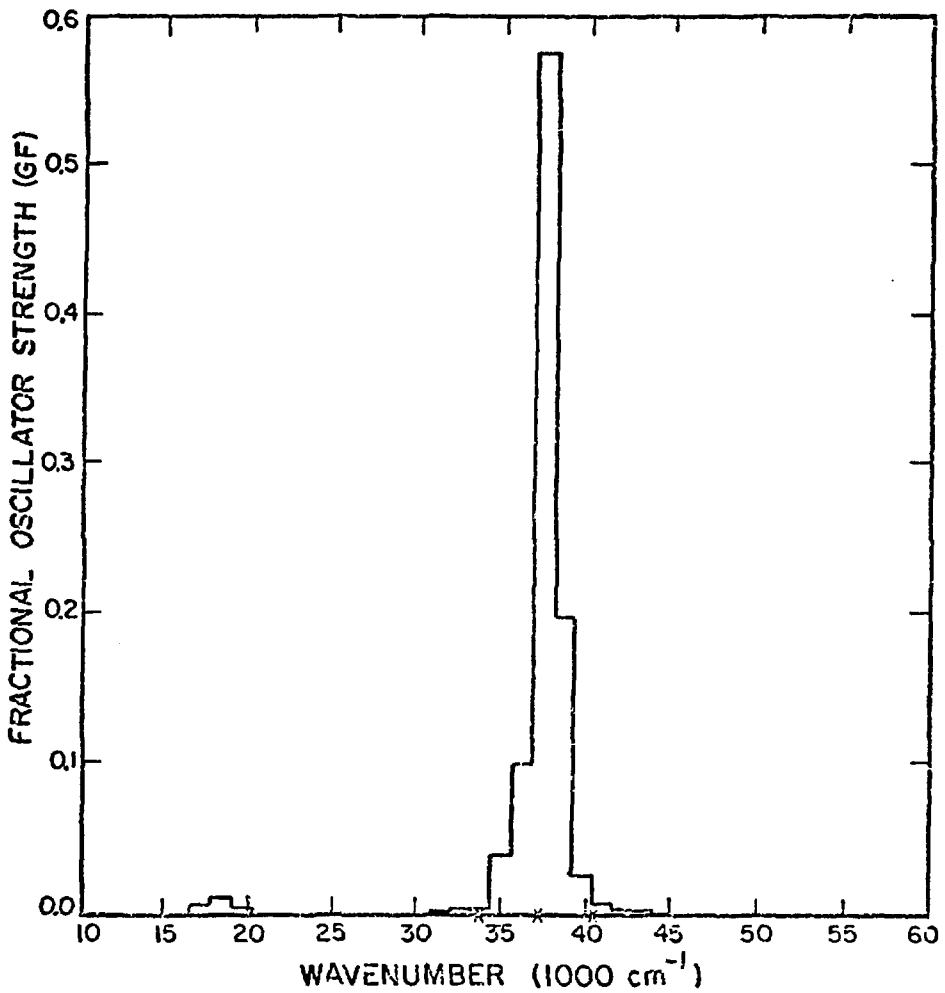

Fig. C-9. RHX transition array oscillator strength distribution for UII 5f3 7s2--5f3 7s7p.

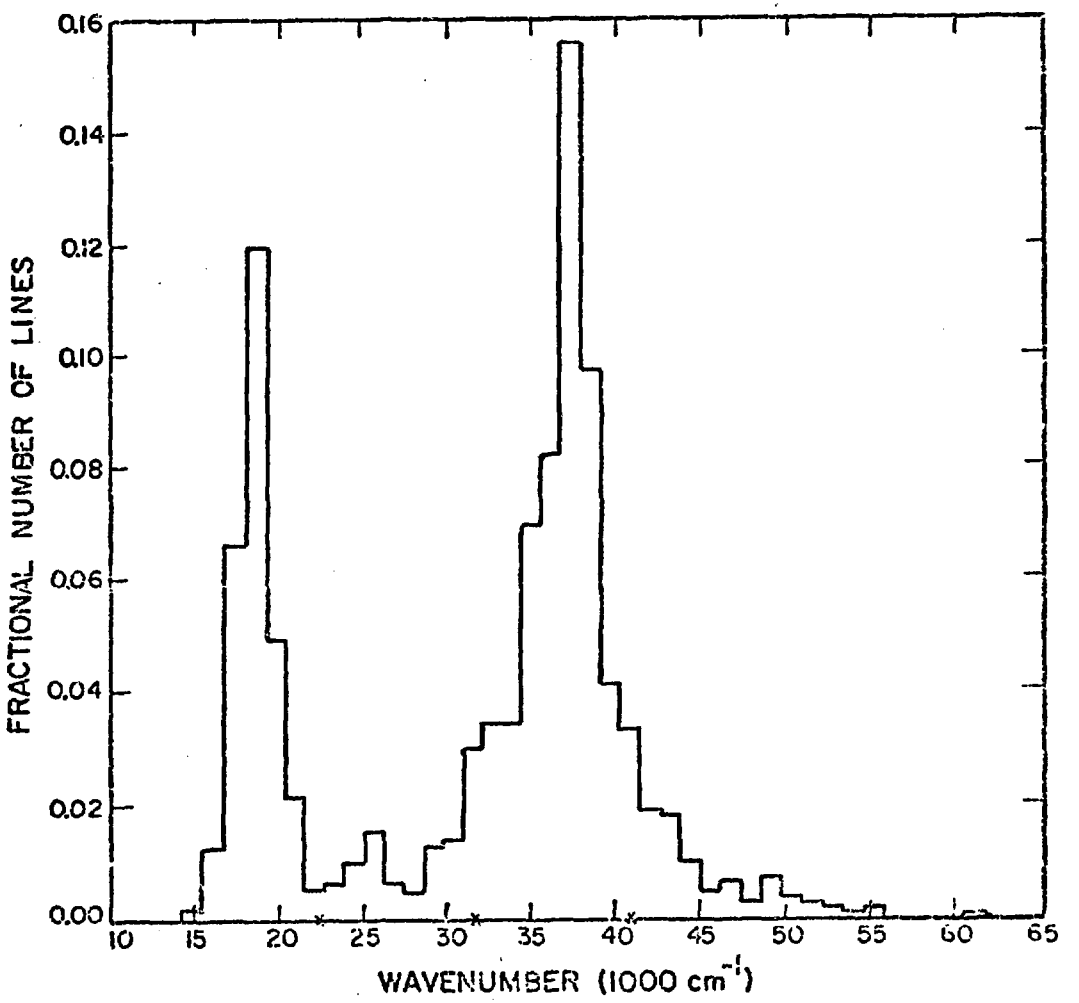

Fig. C-10. Fractional spectral line distribution in Δwavenumber interval for the 5f3 7s2--5f3 7s7p UII transition array.

APPENDIX D

REPRESENTATIVE ENERGIES OF SELECTED

UI AND UII CONFIGURATIONS

When estimating probable wavelength locations of transitions between configuration pairs, the difference in average configuration energies is useful. Radziemski and Blaise[94] have tabulated energies of the lowest known levels of ten configurations of UI and UII and this information is shown in Figs. D-1 and D-2. While the lowest level energy is not the true average configuration energy, it is usually a good approximation. Also in Fig. D-3 are the average configuration energies, calculated by the RHX method, of the UII configurations used in this study.

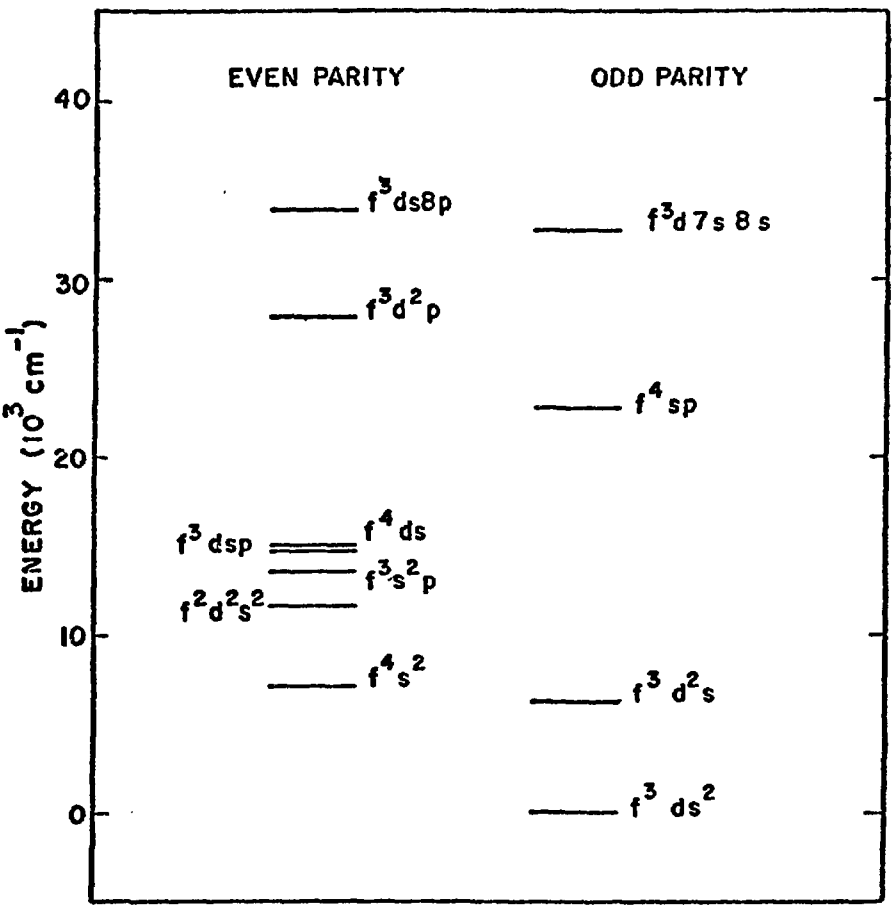

Fig. D-1. Energy of lowest levels of known UI configurations.

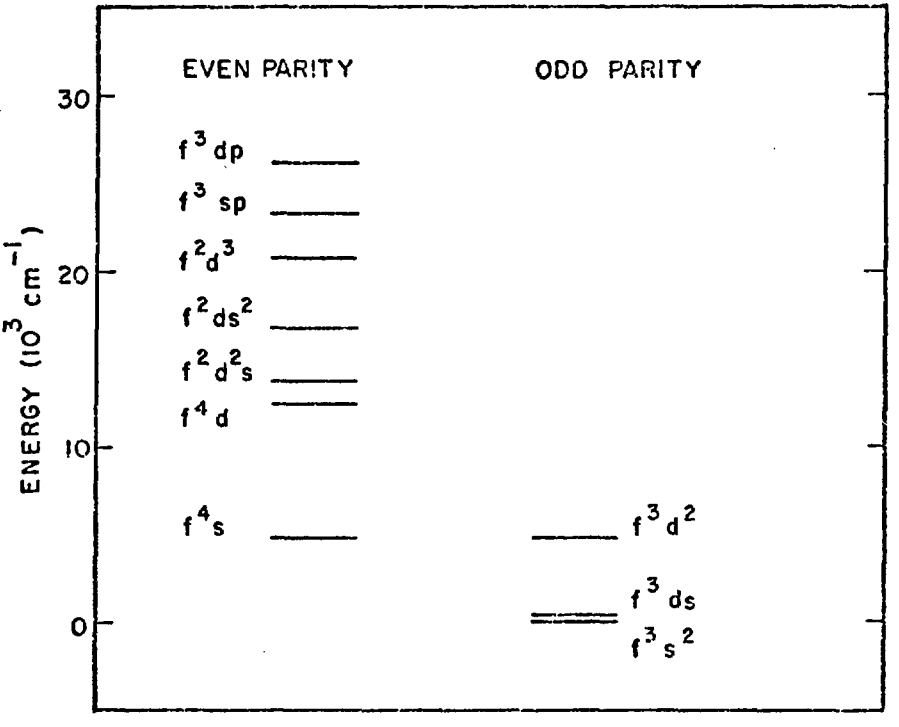

Fig. D-2. Energy of lowest levels of known UII configurations.

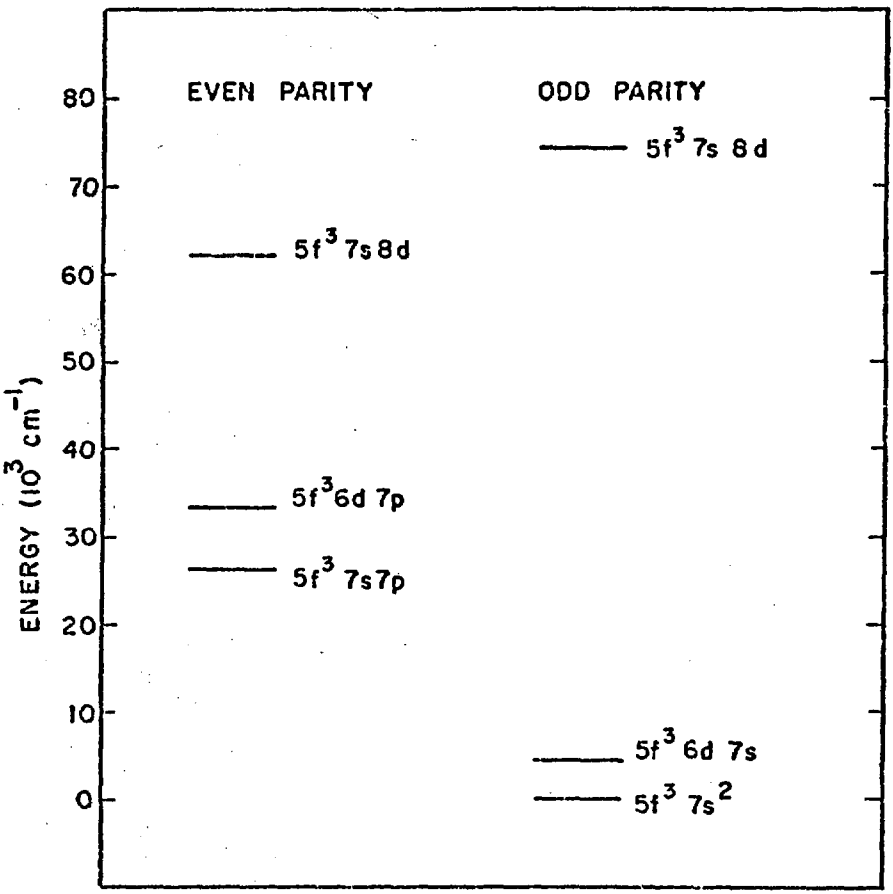

Fig. D-3. Relativistic Hartree exchange average configuration energies for selected UII configurations.

APPENDIX E

UF_6 PHOTOABSORPTION EFFECTS OF THE MARTENEY AND FLORIDA EMISSION COEFFICIENT DATA

UF_6 photoabsorption strengths as a function of wavelength were calculated using the cross-section data of DePoorter,[84,85] Srivastava,[86] McDiarmid,[87] Trajmar,[88] and Hay[89] (Figs. V-5 and V-6). The intensity of transmitted light I_T that has passed through a defined depth of UF_6 of given molecular concentration is related to the incident light I_0 by the equation

$$\frac{I_T(\lambda)}{I_0(\lambda)} = e^{-n\ell\sigma(\lambda)} \quad , \tag{E-1}$$

where ℓ = UF_6 cell or layer thickness in cm,

n = molecular concentration in UF_6 molecules/cm^3, and

$\sigma(\lambda)$ = wavelenght dependent UF_6 photoabsorption cross-section in cm^2.

These absorption factors (I_T/I_0) were used to illustrate the possible effect of UF_6 photoabsorption on the arc emission coefficient data of the present experiment. This was done by folding absorption strenghts calculated using Eq. (E-1) with the arc emission coefficient values at regularly defined wavelengths. The folding was preformed at UF_6 layer thicknesses of 1.5, 2.0, 3.0, and 5.0 cm with molecular concentrations ranging from $1 \times 10^{16} \rightarrow 1 \times 10^{17}$ cm^{-3}. The results of these calculations are shown in Figs. E-1 through E-8.

Presumably, the Marteney data have UF_6 photoabsorption contamination at the strenghs defined by UF_6 layers of 1.5 to 5.0 cm and molecular concentrations of 1×10^{16} to 1×10^{17} cm^{-3}. The reciprocal absorption strength factors were also folded into the matreney data to remove the potential UF_6 photoabsorption effects, thus yielding an uncontaminated uranium emission coeffienent. These results are displayed in Figs. E-5 through E-8.

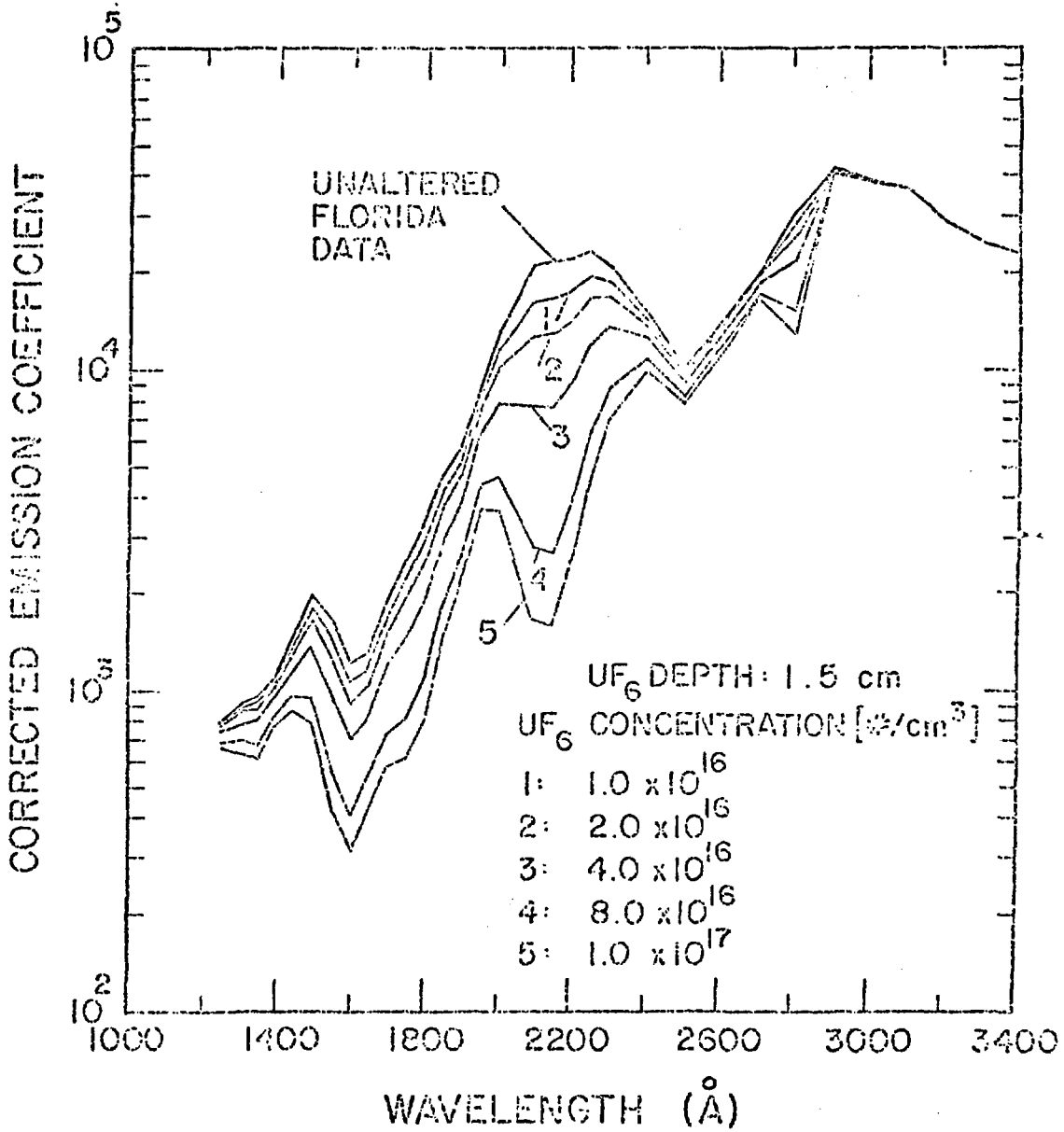

Fig. E-1. Florida uranium emission coefficient data as altered by photoabsorption through 1.5 centimeters of UF_6.

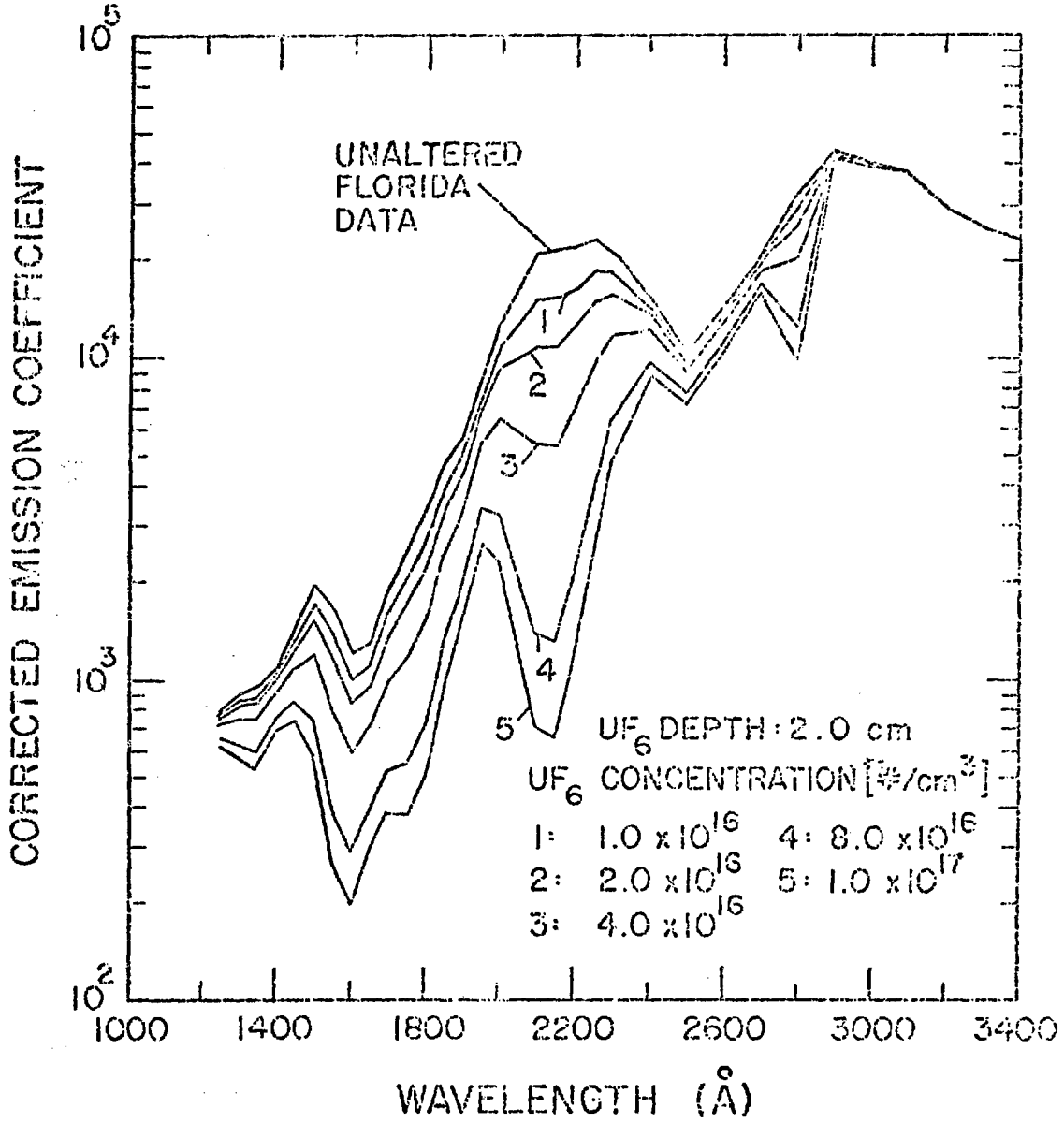

Fig. E-2. Florida uranium emission coefficient data as altered by photoabsorption through 2.0 centimeters of UF_6.

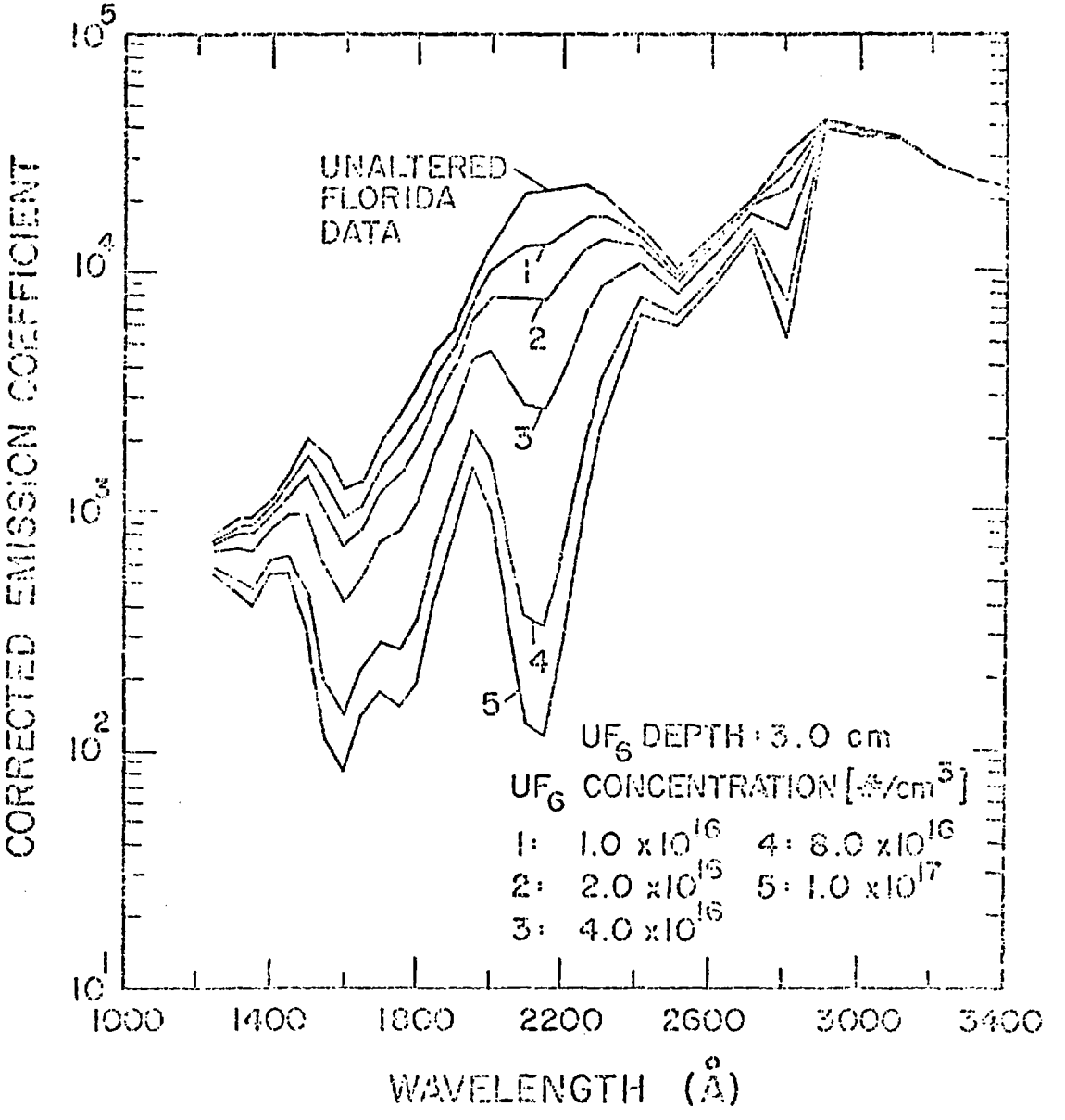

Fig. E-3. Florida uranium emission coefficient data as altered by photoabsorption through 3.0 centimeters of UF_6.

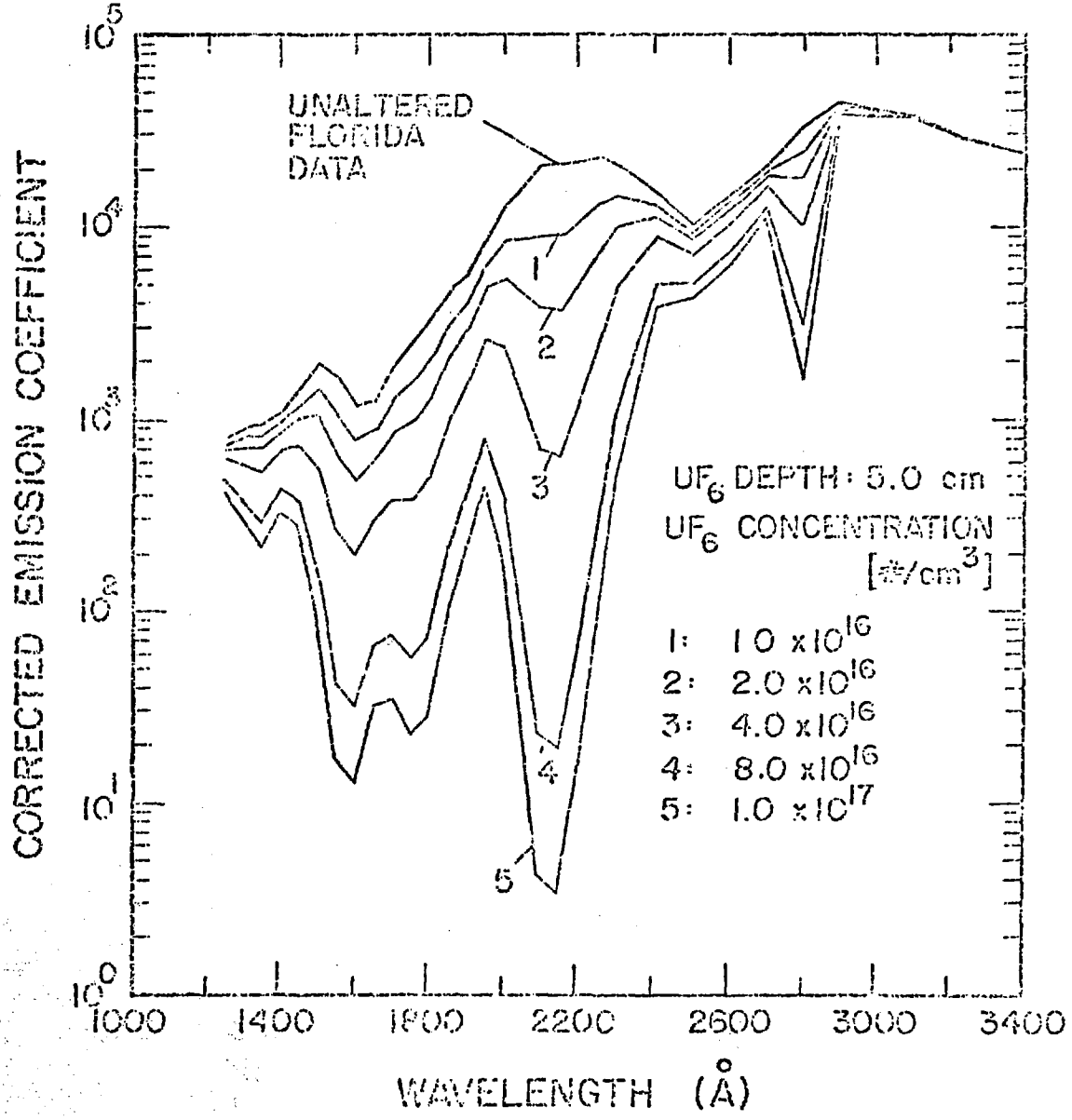

Fig. E-4. Florida uranium emission coefficient data as altered by photoabsorption through 5.0 centimeters of UF_6.

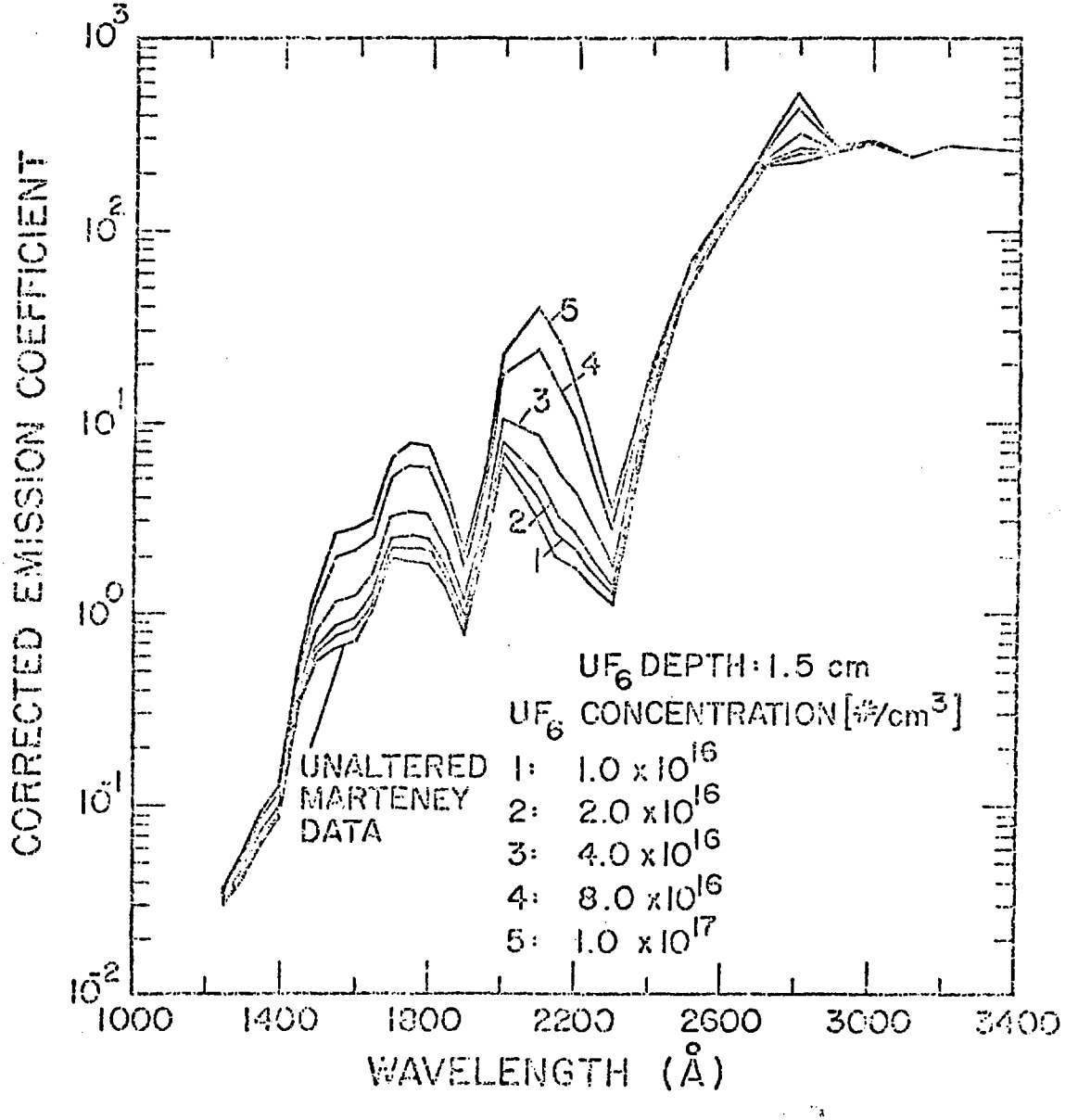

Fig. E-5. Marteney Ar-UF_6 emission coefficient data as altered by photoabsorption unfolding for 1.5 cm of UF_6.

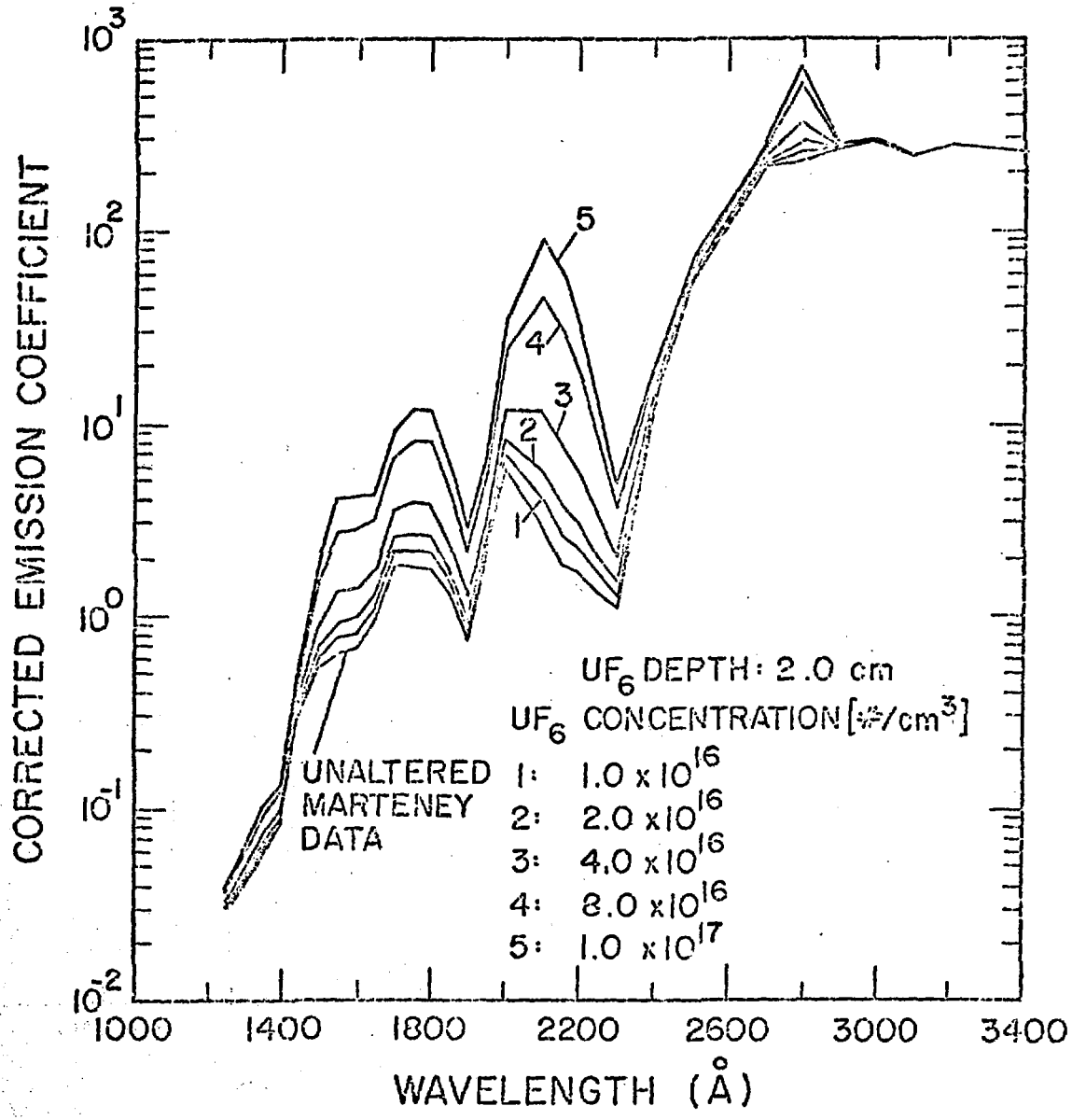

Fig. E-6. Marteney AR-UF_6 emission coefficient data as altered by photoabsorption unfolding for 2.0 cm of UF_6.

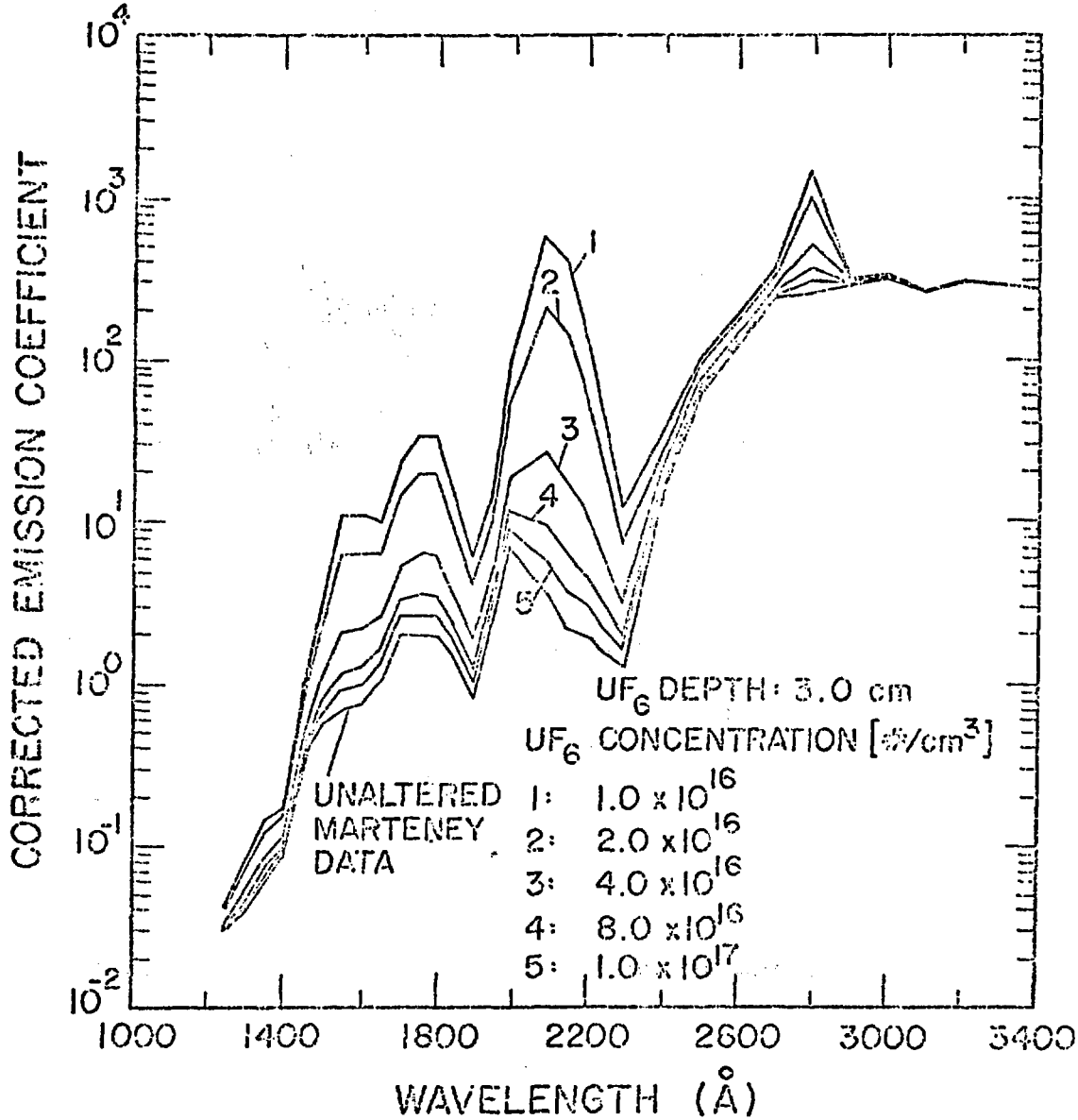

Fig. E-7. Marteney Ar-UF_6 emission coefficient data as altered by photoabsorption unfolding for 3.0 cm of UF_6.

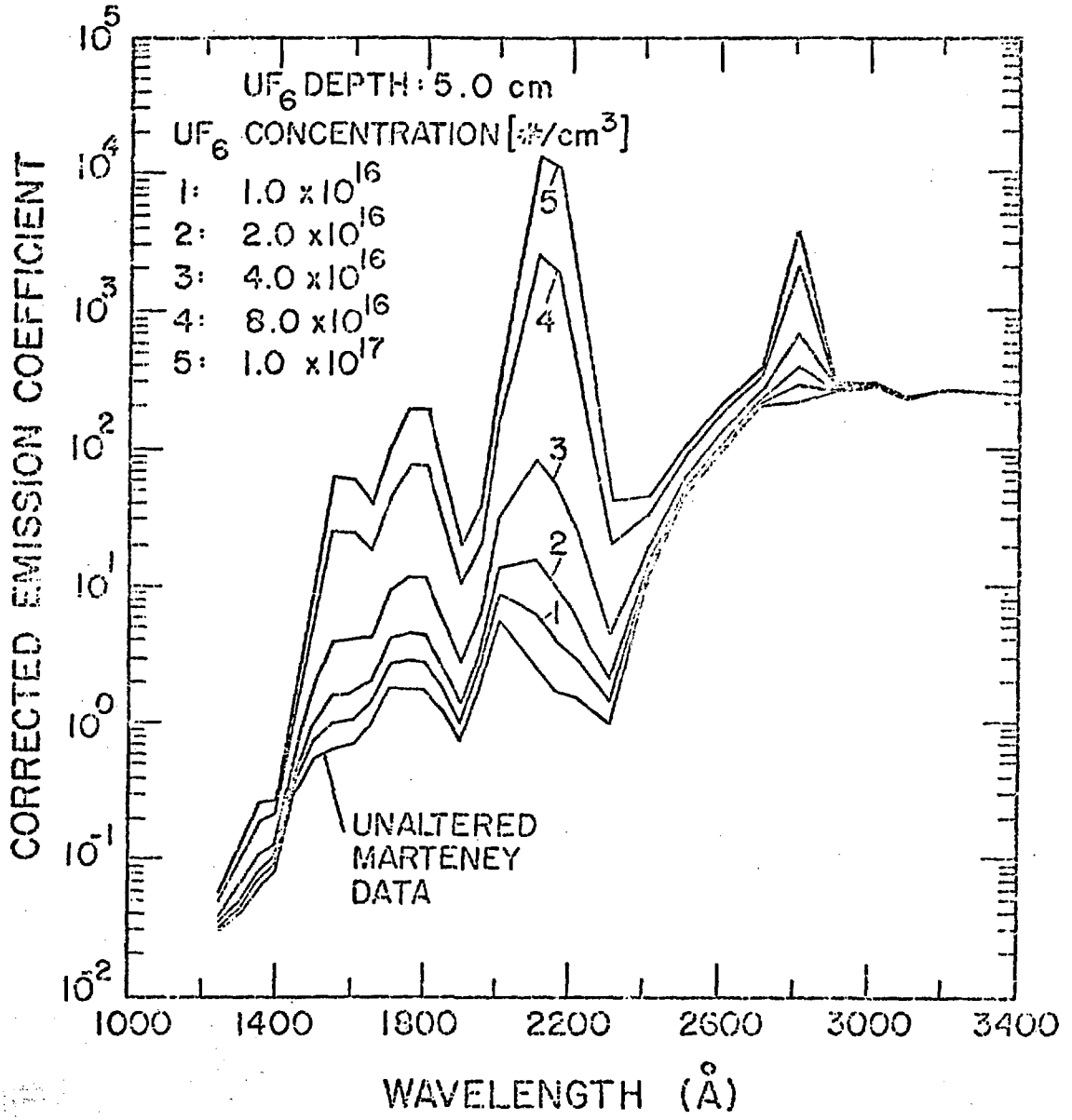

Fig. E-8. Marteney Ar-UF_6 emission coefficient data as altered by photoabsorption unfolding for 5.0 cm of UF_6.

REFERENCES

1. Jacobson, B. A., "The Opacity of Uranium at High Temperature," Ph.D. Dissertation, Univ. of Chicago, 1947.

2. Thom, K., "Introduction and Review of Research on Uranium Plasmas and their Technical Applications," 1st Symposium on Uranium Plasmas, University of Florida, Gainesville, January 7-8, 1970.

3. Schneider, R. T., Thom, K., "Research on Uranium Plasmas and their Technological Applications," Proceedings of 1st Uranium Plasma Symposium, University of Florida, Gainesville, January 7-8, 1970

4. Clement, J. D., Ragsdale, R. G., Williams, J. R., A Collection of Technical Papers, Proceedings of 2nd Uranium Plasma Symposium, Georgia Institute of Technology, Atlanta, November 15-17, 1971.

5. Robinson, C. P., "Laser Isotope Separation," Annals New York Academy of Science, 267, 81-92 (1976).

6. Dubrin, J. W., "Laser Isotope Separation," Lawrence Livermore Laboratories report UCRL-75886 (November 1974).

7. Gillette, R., "Uranium Enrichment: Rumors of Israeli Progress with Lagers," Science 183, 1172 (22 March 1974).

8. "The News in Focus," Laser Focus Magazine, Vol. 10, 10 (March 1974).

9. Moore, C. B., "Isotope Separation with Lasers," adapted from Moore's article in Accounts of Chemical Research in Laser Focus Magazine, Vol. 10, 65 (April 1974).

10. Metz. W. D., "Uranium Enrichment: Laser Methods Nearing Full Scale Test," Science 185, 602 (16 August 1974).

11. "Highest Rate of Isotope Enrichment is Attained with Radiation Pressure," in "News Update," Laser Focus Magazine, Vol. 10, 18 (October 1974).

12. Forsen, Harold EXXON Nuclear Company, personal communication, July 1974.

13. Schneider, R. T., Thom, J., "Fissioning Uranium Plasmas and Nuclear-Pumped Lasers," Nuclear Technology 27, 34-50 (September 1975).

14. McArthur, D. A., Tollefsurd, P. B., "Observation of Laser Action in CO as Excited Only by Fission Fragments," Sandia Laboratories report SAND-74-01 (July 1974).

15. Slater, J. C., Quantum Theory of Atomic Structure, Volumes I and II, (McGraw-Hill, Inc., New York 1960).

16. Herman, F., Skillman, S., Atomic Structure Calculations (Prentice-Hall, Inc., Englewood Cliffs, N.J. 1963).

17. Cowan, R. D., Los Alamos Scientific Laboratory, unpublished notes, 1971.

18. Steinhaus, D. W., Phillips, M. V., Moody, J. B., Radziemski, L. J., Fisher, J. J., Hahn, D. R., "The Emission Spectrum of Uranium Between 19080 and 30261 cm^{-1}," Los Alamos Scientific Laboratory report LA-4944 (August 1972).

19. Steinhaus, D. W., Radziemski, L. J., Cowan, R. D., Blaise, J., Guelachvili, G., Osman, F. B., Verges, J., "Present Status of the Analyses of the First and Second Spectra of Uranium (UI and UII) as Derived from Measurements of Optical Spectra," Los Alamos Scientific Laboratory report LA-4501 (October 1971).

20. Schuurmans, P. H., "On the Spectra of Neodymium and Uranium," Physica 11, 419 (February 1946).

21. Kiess, C. C., Curtis, J. H., Laun, D. D., "Preliminary Description and Analysis of the First Spectrum of Uranium." J. Res. Natl. Bur. Stand. 37, No. 57 (July 1946).

22. Miller, M. H., "Measured Emissivities of Uranium and Tungsten Plasmas," Proceedings of 2nd Uranium Plasma Symposium: Technology, Atlanta, Georgia (November 15-17, 1971).

23. Marteney, P., Mensing, A. E., and Krascella, N. L., "Experimental Investigation of Spectral Emission Characteristics of Argon-Tungsten and Argon-Uranium Induction Heated Plasmas," United Aircraft Corporation NASA report CR-1314 (1969).

24. Drawin, F., Felenbok, P., Data for Plasmas in Local Thermodynamic Equilibrium (Gauthier-Villars, Paris, 1965).

25. Griem, H. R., Plasma Spectroscopy (McGraw-Hill, Inc., New York 1964).

26. Griem, H. R., "Validity of Local Thermal Equilibrium in Plasma Spectroscopy," Phys. Rev. 131, 1170 (1963).

27. McWhirter, R. W. P., "Spectral Intensities," in Plasma Diagnostic Techniques, R. H. Huddlestone and S. L. Leonard, Eds. (Academic Press, New York, 1965), Ch. 5, 206.

28. Wilson, R., "The Spectroscopy of Non-Therman Plasmas," J. Quant. Spectrosc. Radiat. Transfer, 2, 447-490 (1962).

29. Blaise, J., Radziemski, L. J., "Energy Levels of Neutral Atomic Uranium (UI)," J. Opt. Soc. Am. 66, No. 7, 644 (July 1976).

30. Radziemski, L. J., Los Alamos Scientific Laboratory, personal communication, December 1976.

31. Cooper, J., "Plasma Spectroscopy," Reprint from Reports in Physics, 29, Part I, 35 (1966).

32. Emmons, H. W., "Arc Measurements of High-Temperature Gas Transport Properties," Phys. Fluids 9, No. 6, 1125 (June 1967).

33. Bott, J. F., "Spectroscopic Measurement of Temperatures in an Argon Plasma Arc," Phys. Fluids 9, No. 8, 1540 (August 1966).

34. Lowke, J. J., Capriotti, E. R., "Calculation of Temperature Profiles of High Pressure Electric Arcs Using the Diffusion Approximation for Radiative Transfer," J. Quant. Spectrosc. Radiat. Transfer 9, 207 (1969).

35. Lowke, J. J., "Predictions of Arc Temperature Profiles Using Approximate Emission Coefficients for Radiation Losses," J. Quant. Spectrosc. Radiat. Transfer 14, 111 (1964).

36. Lowke, J. J., "A Relaxation Method of Calculating Arc Temperature Profiles Applied to Discharges in Sodium Vapor," J. Quant. Spectrosc. Radiat. Transfer 9, 839-854 (1969).

37. Giannaris, R. J., Incropera, F. P., "Radiative and Collisional Effects in a Cylindrically Confined Plasma - I. Optically Thin Considerations, II - Absorption Effects," J. Quant. Spectrosc. Radiat. Transfer 13, 167-195 (1973).

38. Horman, H., "Temperaturverteilung und Electronendichte in Freibrennenden Lichtbogen," Z. Physik 97, 539 (1935).

39. Park, C., Moore, D., "A Polynomial Method for Determining Local Emission Intensity by Abel Inversion," National Aero-Nautics and Space Administration (Ames Research Center) TN-A3444 (October 1969).

40. Berge, O. E., Richter, J., "Measurement of Local Spectral Intensities in Case of a Nonuniform Light Source of Radial Symmetry," Wright-Patterson Air Force Base, Ohio, AFML-TR-66-165 (October 1966).

41. Barr, W. L., "Method for Computing the Radial Distribution of Emitters in a Cylindrical Source," J. Opt. Soc. Am. 52, No. 8, 885-888 (August 1962).

42. Nestor, O. H., Olsen, H. N., "Numerical Methods for Reducing Line and Surface Probe Data," Sci. Am. Rev. 2, No. 3, 200-206 (July 1960).

43. Bockasten, K., "Transformation of Observed Radiances into Radial Distribution of the Emission of a Plasma," J. Opt. Soc. Am. 51, No. 9, 943-947 (September 1961).

44. Kock, M., Richter, J., "The Influence of Statistical Errors on the Abel Inversion," Wright-Patterson Air Force Base, Office of Aerospace Research, AF61(052)-797 (November 1967).

45. Hefferlin, R., "Diagnostics in Field-Free Plasmas with Medium-Dispersion Optical-Spectrographic and Source Monitoring Equipment," Pergamon Press, Oxford and New York, reprinted from Progress in High Temperature Physics and Chemistry, C. W. Rouse, Eds. (Pergamon Press, Oxford and New York, 1969) 149-229.

46. Lochte-Holtgreven, W., Plasma Diagnostics (North-Holland-Amsterdam, Inc., New York 1964).

47. Usher, J. L., "Temperature Profile Determination in an Absorbing Plasma," M.S. Thesis, University of Florida, Gainesville (August 1971).

48. Usher, J. L., Campbell, H. D., "Temperature Profile Determination in an Absorbing Plasma," J. Quant. Spectrosc. Radiat. Transfer 12, 1157-1160 (1972).

49. Van De Hulst, H. C., Reesinck, J. J. M., "Line Breadths and Voigt Profiles," Astrosphy. J. 106, 121-127 (April 1947).

50. Randol, A. G., III, Schneider, R. T., Shipman, G. R., "Measurement of the Temperature and Partial Pressure of a Uranium Plasma," J. Appl. Spectrosc. 24, No. 2, 253-258 (March/April 1970).

51. Randol, A. G., III, "A Determination of High Pressure, High Temperature Uranium Plasma Properties," Ph.D. Dissertation, University of Florida, Gainesville (August 1969).

52. Mack, J. M., Jr., "Temperature Profile Determination of a Uranium Plasma in a Helium Atmosphere," M.S. Thesis, University of Florida, Gainesville (June 1969).

53. Dejardin, G., Herman, L., "Remarques sur la Fluorescence du Salicglate de Sodium," Seance 24, 651-654 (1936).

54. Fowler, M., Marion, J. B., Fast Neutron Physics (Interscience Publishers, Inc., New York, Part I, 1960) 705.

55. Pitz, E., "Spectral Radiance of the Carbon Arc Between 2500 Å and 1900 Å," Appl. Opt. 10, 813 (April 1971).

56. Ott, W. R., National Bureau of Standards, Washington, DC, personal communication (September 1975).

57. Ott, W. R., Plasma Spectroscopy Section, Optical Physics Division, National Bureau of Standards, personal communication, (July 1972).

58. Griffen, W. G., McWhirter, R. W. P., "An Absolute Intensity Calibration in the Vacuum Ultra-Violet," in Proceedings of the Conference on Optical Instruments and Technology, K. J. Habell, Ed., (John Wiley & Sons, Inc., New York, 1963) 14-21.

59. Hinniov, E., Hopmann, F. W., "Measurement of Intensities in the Vacuum Ultraviolet," J. Opt. Soc. Am. 53, 1259-1265 (1963).

60. Berning, P. H., Hass, G., Madden, R. P., "Reflectance-Increasing Coatings for the Vacuum Ultraviolet and Their Application," J. Opt. Soc. Am. 50, No. 6, 586-597 (June 1960).

61. Hunter, W. R., "High Reflectance Coatings for the Extreme Ultraviolet," Optica Acta 9, 255-268 (January 1962).

62. "Harshaw Chemical Company Catalogue," Harshaw Chemical Co., Ohio (1967).

63. Hass, G., Tousey, R., "Reflective Coatings for the Extreme Ultraviolet," J. Opt. Soc. Am. 49, No. 6, 593-602 (June 1959).

64. Quartz, J., Bausch & Lomb Optical Company, personal communication, (November 1975).

65. Allison, R., Burns, J., Tuzzolino, A. J., "Absolute Fluorescent Quantum Efficiency of Sodium Salicylate," J. Opt. Soc. Am. 54, 747-751 (1964).

66. Watanbe, K., Inn, E. C. Y., "Intensity Measurements in the Vacuum Ultraviolet," J. Opt. Soc. Am. 43, 32-35 (1953).

67. Smith, N. A., Jr., "Xenon Flashtube Brightness Temperature Calibration," Special Report, University of Florida, Department of Nuclear Engineering Sciences (January 1970),

68. Kylstra, C. D., Schneider, R. T., "Computerized Spectrum Analysis," Appl. Spectrosc. 24, No. 1, 115-120 (Jan/Feb 1970).

69. Corliss, C. H., Bozman, W. K., Experimental Transition Probabilities for Spectral Lines of Seventy Elements, U. S. Department of Commerce, National Bureau of Standards Monograph 53 (1962).

70. Lowke, J. J., "Characteristics of Radiation Dominated Electric Arcs," J. Appl. Phys. 41, No. 6, 2588-2600 (May 1970).

71. Shawyer, R. E., "Theoretical Prediction of Temperature Profiles in a Wall-Stabilized Arc," European Conference on Temperature Measurement, National Physical Laboratory, Teddington, G. B., April 1975, 368-374.

72. Lowke, J. J., Westinghouse Research Laboratories, Pittsburg, personal communications (November 1975).

73. Shumaker, J. B., Jr., "Arc Source for High Temperature Gas Studies," The Review of Scientific Instruments 32, No. 1, 65-67 (January 1960).

74. Gurevich, D. B., Podmoshenski, I. V., "The Relationship Between the Gas Temperature in the Positive Column of an Arc Discharge," Opt. Spectrosc. 15, No. 5, 319-322 (November 1963).

75. Voigt, P. A., "Measurement of UI and UII Relative Oscillator Strengths," Phys. Rev. A 11, No. 6, 1845-1853 (June 1975).

76. Griem, H. R., Los Alamos Scientific Laboratory, personal communication, June 1975.

77. Merts, A., Los Alamos Scientific Laboratory, personal communication July 1976.

78. Mack, J. M., Jr., "Plasma Source Calibration Program," Special Report, Dept. of Nuclear Engineering Sciences, University of Florida, Gainesville (August 1972).

79. Krascella, N. L., "Theoretical Investigation of the Composition and Line Emission Characteristics of Argon-Tungsten and Argon-Uranium Plasmas," United Aircraft Research Laboratories, NASA report CR-NASW-847, East Hartford, Connecticut (September 1968).

80. Kelly, R. L., "A Table of Emission Lines in the Vacuum Ultraviolet for all Elements," Lawrence Radiation Laboratory report UCRL-5612 (1965).

81. Kylstra, C. D., Schneider, R. T., Campbell, H. D., "Uranium Plasma Emission Coefficients," AIAA 6th Propulsion Joint Specialist Conference, San Diego, California, June 15-19, 1976, AIAA Paper 70-692.

82. Spector, J., "Absorption Coefficient of Uranium Hexafluoride Measured by a Ballistic Piston Compressor," M.S. Thesis, University of Florida, Gainesville (1973).

83. Parks, D. E., Lane, G., Stewart, J. C., Peyton, S., "Optical Constants of a Uranium Plasma," Gulf General Atomic Incorporated report GA-8244 (NASA-CR-72348), (February 1967).

84. DePoortter, G. L., Rofer-DePoorter, C. K., "The Absorption Spectrum of UF_6 from 2000 Å to 4200 Å; Digitized Form," Internal Memorandum, Los Alamos Scientific Laboratory (May 1976).

85. DePoorter, G. L., Rofer-DePoorter, C. K., "The Absorption Spectrum of UF_6 from 2000 Å to 4200 Å," Spectroscopy Letters, 8, No. 3, 521-524 (1975).

86. Srivastava, S. K., Cartwright, D. C., Trajmar, S., Chutjian, A., Williams, W. H., "Photoabsorption Spectrum of UF_6 by Electron Impact," J. Chem. Phys. 65, 208 (1976).

87. McDiarmid, R., "Assignments in the Electronic Spectrum of UF_6 J. Chem. Phys. 65, 168 (1976).

88. Trajmar, S., Jet Propulsion Laboratory, Pasadena, California, unpublished research, 1976.

89. Hay, P. J., Cartwright, D. C., "Rydberg, Conic, and Valence Instructions in the Excited States of F_2," Los Alamos Scientific Laboratory report LA-7639 (1976).

90. Steurenberg, K. K., Vogel, R. C., "The absorption Spectrum of Fluorine," Journal of American Chemical Society 78, 901 (March 1956).

91. Schneider, R. T., Campbell, H. D., Mack, J. M., "On the Emission Coefficient of Uranium Plasmas," Nuclear Technology 20, 25 (October 1973).

92. Shore, B. W., Menzel, D. H., Principles of Atomic Spectra, (John Wiley and Sons, Inc., New York 1968), 370.

93. Cowan, R. D., Los Alamos Scientific Laboratory, personal communication, October 1976.

94. Radziemski, L. J., Jr., Blaise, J., "Current Status of the Spectrum of Uranium UI and UII," Atomic Spectroscopy Symposium, U.S. Dept. of Commerce, Ed., Proceedings of Atomic Spectroscopy Symposium, National Bureau of Standards, Gaithersburg, MD, September 23-26, 1975, 124-125.

95. Slater, J. C., The Quantum Theory of Matter, (McGraw-Hill, Inc., New York, 1968), 326-349.

96. Shortley, G. H., "The Energy Levels of Rare-Gas Configurations," Phys. Rev. 44, 666 (October 1933).

97. Cowan, R. D., "Theoretical Calculation of Atomic Spectra Using Digital Computers," J. Opt. Soc. Am. 58, No. 6, 808 (1968).

98. Cowan, R. D., "Atomic Self-Consistent-Field Calculations Using Statistical Approximations for Exchange and Correlation," Phys. Rev. 163, No. 1, 163 (November 1967).

99. Stewart, J. C., Rotenberg, M., "Wavefunctions and Transaction Probabilities in Scaled Thomas-Fermi Ion Potentials," Phys. Rev. 140, A1508 (November 1965).

100. Cowan, R. D., "Theoretical Study of $p^m - p^{m-1}$ ℓ Spectra." J. Opt. Soc. Am. 58, No. 7, 924 (July 1968).

ACKNOWLEDGEMENTS

This work describes research performed within the Department of Nuclear Engineering Sciences at the University of Florida and also at the Los Alamos Scientific Laboratory in New Mexico. The effort was financially supported by the National Aeronautics and Space Administration (Contract NGR 10-0050089) and directed by a committee composed of Dr. Richard T. Schneider, Chairman, Dr. Hugh D. Campbell, Dr. Edward E. Carroll, Dr. Dennis R. Keefer, Dr. John W. Flowers, and Dr. Leon J. Radziemski.

The author is grateful to Dr. Schneider for his constant encouragement and suggestions throughout the duration of this investigation. Dr. Campbell was of valuable assistance in maintaining a realistic perspective as to the theoretical and practical limitations. Special thanks is given to Dr. Radziemski for his persistence in encouraging the author to complete this work and also for the many timely discussions regarding dissertation content.

The author wishes to show exceptional appreciation to Dr. Robert D. Cowan for his willingness to allow the use of his atomic structure code and the sharing of his insight related to these computations. It was indeed a great honor to have worked with Dr. Cowan in this regard.

Because of the extensive nature of the effort required for the successful completion of this research, many people became involved, both students and faculty alike. The author wishes to convey his

recognition of the assistance given by the following:
Dr. Chester D. Kylstra, Arthur G. Randol, Noval A. Smith, John L. Usher, Bruce G. Schnitzler, George R. Shipman, Jeff Dixon, George Fogel, Kenneth Fawcett, Peter Schmidt, Ralph Nelson, and Willie B. Nelson.

The author is further indebted to his secretaries at the Los Alamos Scientific Laboratory, Ofelia M. Diaz and Delores M. Mottaz, for their persistence in the painstaking labor which went into the typing of the manuscript.

Financial support through the University of Florida Assistantship Program and the Atomic Energy Commission Traineeship plan is acknowledged.

☆ U.S. GOVERNMENT PRINTING OFFICE: 1978—777-089/2